Purdue University
Purdue e-Pubs

Open Access Dissertations | Theses and Dissertations

January 2015

Application of microperforated elements in axial fan noise control and silencer design

Seungkyu Lee
Purdue University

Follow this and additional works at: https://docs.lib.purdue.edu/open_access_dissertations

Recommended Citation
Lee, Seungkyu, "Application of microperforated elements in axial fan noise control and silencer design" (2015). *Open Access Dissertations*. 1308.
https://docs.lib.purdue.edu/open_access_dissertations/1308

This document has been made available through Purdue e-Pubs, a service of the Purdue University Libraries. Please contact epubs@purdue.edu for additional information.

Graduate School Form 30
Updated 1/15/2015

PURDUE UNIVERSITY
GRADUATE SCHOOL
Thesis/Dissertation Acceptance

This is to certify that the thesis/dissertation prepared

By Seungkyu Lee

Entitled

Application of microperforated elements in axial fan noise control and silencer design

For the degree of Doctor of Philosophy

Is approved by the final examining committee:

J. Stuart Bolton
Chair

Charles M. Krousgrill

Kai Ming Li

Stephen D. Heister

To the best of my knowledge and as understood by the student in the Thesis/Dissertation Agreement, Publication Delay, and Certification Disclaimer (Graduate School Form 32), this thesis/dissertation adheres to the provisions of Purdue University's "Policy of Integrity in Research" and the use of copyright material.

Approved by Major Professor(s): J. Stuart Bolton

Approved by: Jay P. Gore 10/5/2015

Head of the Departmental Graduate Program Date

APPLICATION OF MICROPERFORATED ELEMENTS IN AXIAL FAN NOISE CONTROL AND SILENCER DESIGN

A Dissertation

Submitted to the Faculty

of

Purdue University

by

Seungkyu Lee

In Partial Fulfillment of the

Requirements for the Degree

of

Doctor of Philosophy

December 2015

Purdue University

West Lafayette, Indiana

ACKNOWLEDGMENTS

Firstly, I would like to express my sincere gratitude to my advisor Professor J. Stuart Bolton for his continuous support and perfect advice on my Ph.D. study, for his patience, motivation and knowledge. His guidance and kind consideration helped me all the time through out my study. I learned from him that the research is fun and exciting. I would also like to thank my committee members, Professor Krousgrill, Professor Li, Professor Sun and Professor Heister for their valuable guidance and support.

I would like to make an acknowledgment to the financial support of the 3M Company, MN, USA as well as the provision of materials for this research. Especially, I would like to thank Thomas Herdtle, Ron W. Gerdes, Jonathan H. Alexander, and Tom Hanschen at 3M Company for their helpful supports and comments on this research.

I am indebted to my colleagues at Ray W. Herrick Laboratories. I am especially thank to Nicholas Kim, Janghyun Kim and Hyunjun Shin for sharing their precious times, experiences and knowledges, which allowed me to enjoy my life at Purdue. I would also like to thank to Rui Cao, Yanfan Liu and Tongyang Shi for their helps and kind words.

Last but not the least, I wish to thank my family. I would like to express my love and thank to my wife, Jaeyoung Kim for her endless support and my daughter, Elizabeth Woohyun Lee. I would like to express sincere and deep gratitude to my mother for her support and love, and father, who I respect the most. I will try do my best to make you proud. I would also like to thank you my parents-in-law for their devotional support and love. Most importantly, thank you my lord who gives me strength.

TABLE OF CONTENTS

LIST OF FIGURES

Figure Page

Figure Page

LIST OF TABLES

ABSTRACT

Lee, Seungkyu. PhD, Purdue University, December 2015. Application of Microperforated Elements in Axial Fan Noise Control and Silencer Design. Major Professor: J. Stuart Bolton, School of Mechanical Engineering.

The microperforated panel (MPP) is considered to be an alternative sound absorbing material, which could replace the traditional glass fibers and other porous materials because of its sound absorbing characteristics in a wide frequency range. The MPP is also very useful in various human involved environments because it is less harmful to human respiratory system than traditional sound absorbing materials, meaning more hygienic. Therefore in this study, microperforated panels were used in fan noise control and in acoustic silencers, where both of the devices are easily accessible by humans.

Axial fans are widely used to cool electronic devices, and the fans typically generate noticable amounts of noise during their operation. Among the various sources responsible for fan noise, tip clearance noise is one of the more critical components. It has been demonstrated, in gas turbine applications, that tip clearance noise can be reduced by installing a finite flow resistance, circumferential strip in the housing of the fan immediately adjacent to the turbine blade tips. It is possible, for example, that the finite level of flow resistance created by the slightly permeable housing may reduce turbulence levels in the tip region, thus decreasing the noise generation. In the present work, a similar approach was taken to the control of noise generated by a 120 mm axial fan. In this case, a microperforated film material was used as the finite flow resistance strip built into the scroll housing of the fan, spanning the axial region through which the blade tips sweep. Measurements of both sound radiation and of flow performance of a number of prototype fans having microperforated strips of varying flow resistances were conducted using an ISO plenum. A hemispherical

array of ten microphones was used to measure the sound power of the fan as a function of fan operating point. The fan noise was quantified primarily on the basis of the blade passage sound power level. It was found that there were areas in the fan performance map within which tonal and/or overall noise levels could be consistently reduced by the use of the microperforated housing element. It was also found that the flow resistance needed to obtain an optimal noise reduction was a function of the fan operating point.

Further, it was found that the inclusion of the microperforated strip in the fan housing had a negligible impact on the fan performance: that is, there was no performance penalty associated with the fan noise reduction. The MPP treatment in the housing area of the fan was extended to the upstream and downstream sides of the fan so that the housing could make itself as the duct. Therefore the MPP treatment effects in the upstream and the downstream side of the fan were also considered. In addition to the sound power measurement, the differences in the sound field around the fan due to different housing treatments were visualized and investigated by adopting Nearfield Acoustic Holography (NAH).

The objective of the study on the acoustic muffler was to develop a compact, multi-chamber silencer incorporating dissipative microperforated elements that could be used to reduce transmitted noise in a flow system. Two expansion mufflers in series were used to create a relatively compact system that attenuated sound effectively over the speech interference range. The microperforated elements were used both to increase the acoustic performance of the silencer and to reduce the system pressure drop with respect to a muffler without a microperforated lining. Both Finite Element Modeling (FEM) simulation and experimental methods were employed in the detailed design of the multi-chamber silencer. In the FEM simulations, the microperforated lining was modeled as a fluid layer having complex properties, and the model was used, for example, to identify the optimal flow resistance of the microperforated lining. The predicted results were successfully compared with full-scale experimental results that were obtained by using a four-microphone standing wave tube. Additionally, mean

flow effect inside the silencer and different structural internal designs of silencers such as inlet and outlet extensions, were considered.

1. INTRODUCTION

1.1 Motivation in Application of the Microperforated Panel in Acoustic Solution

Noise in the world can be controlled by many ways. For example, some of the noise can be controlled at the noise source itself and some can be control by anti-noise signals, which is also known as noise cancellation or active noise control. Application of sound absorbing materials, can be called passive noise control techniques, and is also the most commonly used methodology to control the noise.

The widely known sound absorbing materials such as glass fiber, mineral wool, etc. have been used in many application of noise control. The sound absorption occurs when the sound absorbing materials interact with the sound field: some of the sound wave is reflected or dissipated by the material and some of the wave is transmitted through the material. These absorption characteristics of fibrous materials can be determined by porosity and flow resistivity. The porosity is the ratio of the porous volume to the total volume of the material. The air flow resistivity calculation was suggested by Delany and Bazley [1]. However, these fibrous materials are hardly applicable in certain acoustic environments. For instances, harsh environments such as engine rooms of vehicles and environments directly related with human respiratory systems are those environments where the application of the traditional sound absorbing materials are not suitable. Therefore microperforated materials, which is the perforated material that has the diameter of the perforation in the sub-millimeter range, has been considered in the field of noise control engineering as an alternative sound absorbing material.

The sound attenuation of perforated materials occurs similarly with other porous materials. When the acoustic wave faces the perforated panel, some of the energy

will either be reflected or dissipated by the panel and the rest of the energy will be transmitted. The energy dissipation occurs due to viscous effects, which are created when the waves pass through the perforated holes in the perforated panel. However, if the diameter of the perforated panels is in the size of millimeter or centimeter, it is hard to obtain wide frequency range of sound absorption with those perforated panels. In order to obtain the sound attenuation over the wide frequency range, the sound absorbing material must have low acoustic mass but the regular perforated panel can only have low acoustic mass when its acoustic resistance is very low. Therefore additional sound absorbing materials such as glass fiber, mineral wool, etc. must be added to improve the acoustic resistance that was reduced by using the regular perforated panel. However, this deficiency of regular perforated panels could be overcome by reducing the diameter of the perforated holes to the sub-millimeter range. By doing this, the energy dissipation that occurs when the acoustic wave passes through the perforates in the panel can be enhanced. These perforated materials, with the size of diameter of holes in the sub-millimeter range, are called microperforated panels (MPP).

Maa [2], introduced the concept of the MPP, which can produce a wider frequency range of sound absorbing performance by the perforated panel itself. The sound absorption of the MPP can be gradually increased from the acoustic energy dissipation, which occurs as the acoustic wave passes though the micro perforation of the panel. Maa suggested a theory considering important parameters in the sound absorption characteristics of MPP that are acoustic resistance, the resonance frequency of maximum absorption, and the perforation constant [2–4]. His theory was adopted in many studies of MPP modeling and applications.

Other modeling techniques of microperforated panel were also studied by many researchers. The pourus model suggested from the studies made by Johnson et al. [5], Champoux and Allard [6] and Atalla and Sgard [7], which is also called the JCA model. In the JCA model, the perforated panel was modeled as a rigid-frame porous medium considering related parameters such as thermal and viscous characteristic

lengths, which are determined from the shape of the perforation, the tortuosity, the porosity and the static air flow resistivity of the panel. This JCA model was experimentally validated with application to the MPP by Jaouen and Becot. [8]

Along with those reliable theoretical models of MPP's and the various advantages of the MPP, its application in the field of passive noise control nowadays has grown gradually. In this study, the MPP was used in two different applications, one is an axial fan noise control and the other is to acoustic silencer design. These fans and ducts are often used in human environments, for example, computer, electric devices, and vehicle and building HVAC systems. Therefore the MPP, which is more hygienic material than other sound absorbing materials such as glass fibers and mineral wools, can be appropriate material to be applied in these areas.

1.2 Microperforated Panel Application in Fan Noise Control

The axial fan is one of the most widely used devices to cool electronic devices such as computers, home appliances, etc. During operation, the axial fan creates significant amount of noise which generated by various flow interaction made by the circumstances of where the fan is located. For example, flow interaction between the housing and the blades, inlet and outlet flow interferences due to the operation circumstances, flow separation, vortex shedding, etc. All of these effects cause unavoidable tonal and broadband noise.

Therefore many studies have been conducted aimed at reducing fan noise by using various approaches. For example, Gresho [9], Wang and Huang [10], and Lee et al. [11], focused on the structural design of the fan, such as the struts supporting the fan hub which could generate noise by interacting with the flow exiting from the rotor. Gregor et al. [12] conducted research on the impact of the guard grille design of the axial fan. Active noise control approaches to reduce axial fan noise have also been studied. Such studies were performed by Quinlan [13], Gee and Sommerfeldt [14], and Schulz et al. [15]

In this thesis, experimental research aimed at reducing the noise generated in the tip clearance region of a fan will be discussed. The tip clearance region is the narrow space between the blade tips and the housing of the fan. A number of researchers have already conducted research on controlling the noise generated in the tip clearance region. Jin et al. focused on the design of the blades of the fan [16] while Gorny and Koopmann [17] conducted research on blade passage tone cancellation by implanting a perforated resonator within the housing of the fan. The present work follows most closely that of Sutliff and Jones who investigated the beneficial effect of a foam-metal liner in close proximity to turbine blade-tips [18]. So, the purpose of the present research was to find the potential effect of a finite flow resistance microperforated housing in reducing the fan noise generated in the tip clearance region. To gauge the effectiveness of various materials, the total sound power radiated by the fan was measured, along with the sound power of the blade passage tone.

In addition to the MPP housing treatment around the blade-tip region of the axial fan, an extended inlet-end and outlet-end of the MPP treated housing of the axial fan will be considered. This extension of the housing causes the fan to be in the middle of a circular duct. Then the blade passage tone attenuation performance of the MPP duct casings will be studied.

Once the sound power radiated from different types of axial fans has been discussed, the effects of MPP elements in the fan noise application will be thoroughly discussed by investigating the sound field of the fan reconstructed by using Nearfield Acoustic Holography (NAH). NAH is a widely known and used technique to visualize the sound source. Maynard summarized and introduced conventional NAH methodologies using array microphones. [19, 20] Kim et al. suggested partial sound field decomposition method using multi-reference signals in NAH [21]. Many researchers used NAH to visualize the noise field around the fan and moving flow medium. For example, Lee et al. used NAH to visualize the fan noise radiates from the electronic enclosure [22] and Niu and Kim adopted NAH in three-dimensional visualization of open fan and adopted statistically optimal NAH in visualizing the moving fluid with

relatively small hologram surfaces [23, 24]. However, in this study, the noise source is small enough to be measured with the array microphone. Therefore conventional planar NAH along with multi-reference signals will be used to visualize and investigate the fan noise from the side-view of the fan.

1.3 Microperforated Panel Application in the Acoustic Silencer Design

Many studies of silencer design have been made with the objective of obtaining particular levels of acoustical performance. Studies on the effect of designing the inlet and outlet of the expansion muffler have been conducted by Selamet and Ji [25, 26], and by Wu et al. [27]. Some researchers have focused on the effects of creating multiple chambers within the silencer. For example, Denia et al. studied multi-chamber hybrid mufflers consisting of a folded resonator [28], Liu et al. studied the flow resistance of a double expansion muffler with various designs of inlets and outlets [29], and Selamet et al. employed several different designs for inlets and outlets of the ducts and for the hole sizes of the baffles that separated the chambers of the silencer [30]. In addition to multi-chamber silencer designs, perforated materials have been employed in silencers to achieve specific acoustic performance targets. Ji and Selamet studied the use of a perforated duct within the muffler by using the Boundary Element Method (BEM) [31], Lee et al. studied the acoustic impedance of perforated panels placed next to fiborous layers, as used in mufflers [32].

Microperforated panels are also known to be useful when seeking to improve the acoustic performance of silencers. For example, Tan and Ripin looked at the effect of attaching microperforated panels on the inlet and outlet ends of an expansion muffler [33], and Allam and Abom used microperforated material as a tube in a circular expansion muffler with multiple chambers [34].

In the current study, a silencer was developed, which was intended to provide good acoustic attenuation performance over the speech range: approximately 400 Hz to 4000 Hz. A dual-chamber silencer was used in combination with microperforated

tubes that connected the inlet and outlet of the silencer. The Finite Element Method (FEM) was employed to create predictive models for different designs of the silencer by using the commercial software, ABAQUS^{TM}. Then, a prototype of the muffler was built, following the simulation results, and a comparison was made between the predicted and measured acoustic attenuation performance. The measurement results for the designed silencer were obtained by mounting the silencer on a standing wave tube and by using a 4-microphone measurement. In the FEM simulations, the microperforated film was modeled as a rigid porous medium as suggested by Jaouen and Bécot [8]. The work of Jaouen and Bécot followed the approach suggested by Atalla and Sgard [7] and entails the use of the Johnson-Champoux-Allard (JCA) model for rigid porous media [5,6]. Bolton and Hou also showed that the performance of rigid MPP's can be predicted with good accuracy by using the Johnson-Champoux-Allard model for rigid porous media with an appropriate equivalent tortuosity [35].

In addition to FEM simulation of the silencer, the grazing flow effect on the MPP will be considered. Silencers can also be applied to HVAC ducts in vehicles and buildings. Therefore the designs of silencers using the MPP that can be applied to HVAC systems will be studied. Many researches have been conducted on the grazing flow effect of the MPP by adding flow term in the impedance equation of Maa [34,36]. However, it is known that the grazing flow effect on the MPP is relatively small compare to the grazing flow effect on the regular perforated panels [37]. Moreover, the required flow velocity in HVAC system is usually less than 20 m/s (Mach number of 0.058), which is relatively low flow velocity. Therefore, in this study, the grazing flow effect on the MPP will be considered by using FEM simulation adopting the steady-state acoustic pressure field around the MPP and validated with the standing wave tube measurement results.

1.4 Structure of the Thesis

This thesis covers two main parts, which are the applications of MPP in fan noise control and acoustic silencer design and each part consists of two chapters. First chapter of fan noise control (Chapter 2) covers the sound power radiated from fans with various casings including ducts. Chapter 3, which is second chapter of fan noise, covers the visualization of sound field of fans with different casings by using multi-reference Nearfield Acoustic Holography (NAH). Chapter 4, the first chapter of acoustic silencer design, covers the design of silencer having MPP treatments without considering mean flow effects. In chapter 5, acoustic silencer design considering mean flow effects will be considered. Finally, summary of the thesis and future work will be provided in chapter 6.

2. FAN NOISE CONTROL: SOUND POWER RADIATED FROM THE FAN

2.1 Experimental Set-up

The experimental set up required to test the noise generated by a 120 mm axial fan was created by following the procedures and equipment described in ISO 3744 [38], ISO 3745 [39] and ISO 10302 [40]. ISO 10302 contains the construction manual for building the mylar plenum that was designed to allow estimation of radiated fan noise as well as the performance of the fan. The same ISO document also describes procedures to measure the sound power that is radiated from the noise source. ISO 3744 and ISO 3745 provide methodologies for setting up a microphone array around the noise source in a semi-anechoic chamber and for measuring the sound power level.

2.1.1 Sound Power Level Measurement

The mylar plenum for the fan noise experiment was built exactly following the specification provided in ISO 10302. The plenum was designed to give accurate measurements of the flow rate and static pressure generated by the specimen fan. Therefore by operating the fan on the plenum, both the noise level and the performance of the fan can be estimated. The flow rate and internal pressure of the plenum generated by the fan can be adjusted by changing the outlet opening area of the plenum. Figure 2.1 shows the drawing of the plenum as provided in ISO 10302.

A hemispherical microphone array was built for sound power level measurement. The hemispherical frame dimensions and the locations of the microphones on the frame were decided by following ISO 3744. The configuration of the frame and the location of each microphone are specified in Figure 2.2. ISO 10302 and ISO 3745 as well as ISO 3744 provide a procedure to determine sound power level from sound pressure level measurements, so the measurement procedure of sound power level for

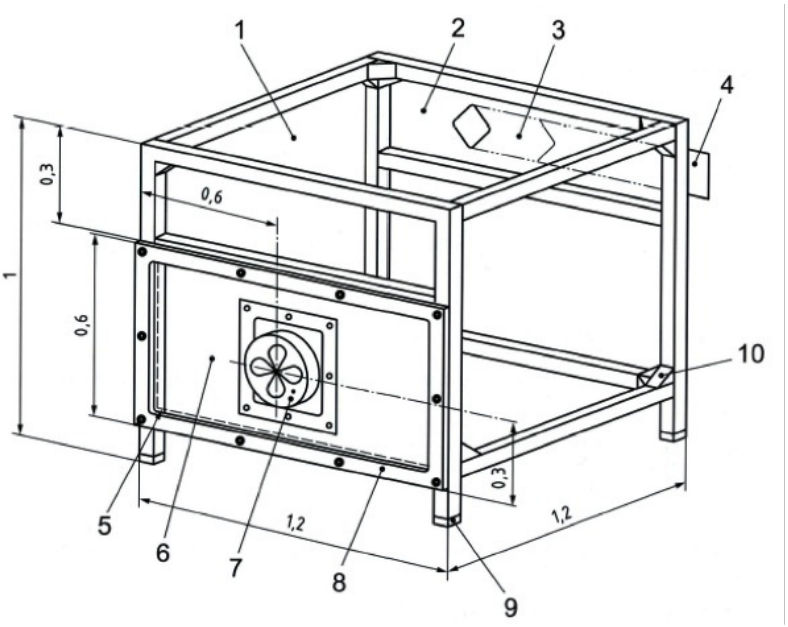

Figure 2.1. ISO 10302 mylar plenum design for accurate measurement of fan noise level and performance.

the experiment followed these standard documents. The experimental equipment was set up in the anechoic chamber at the Ray W. Herrick Laboratories at Purdue University, as shown in Figure 2.3.

The sound power level measurement followed the procedure described in the ISO documents. The sound power level is ten times the logarithm to the base 10 of the ratio of the sound power, P , to a reference value, P_0, expressed in decibels as shown in Equation (2.1)

$$L_w = 10log\frac{P}{P_0} \tag{2.1}$$

where, the reference value, P_0, is 1pW. However, the sound power level can also be estimated from the sound pressure level as:

$$L_w = \bar{L}_p + 10log_{10}\frac{S}{S_{ref}} \tag{2.2}$$

Position #	z-dir.	Position #	z-dir.
1	0.15 R	**6**	0.45 R
2	0.15 R	**7**	0.75 R
3	0.15 R	**8**	0.75 R
4	0.45 R	**9**	0.75 R
5	0.45 R	**10**	1 R

R: Radius of Hemispherical frame

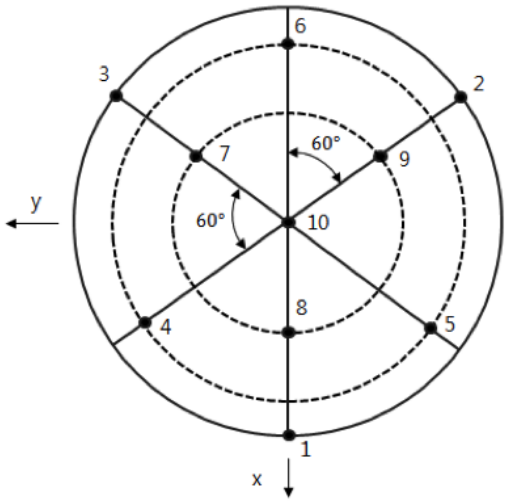

Figure 2.2. ISO 3744 10-microphone positions in the array.

where, $\bar{L}_p$ is the space-averaged sound pressure level, S is surface area of the hemisphere and S_{ref} the reference area, 1 m^2. The second approach, in which the sound power level was calculated from the averaged sound pressure level, was used in the present research along with the measurement method following the ISO standards.

2.1.2 Description of the Fan used in this Study

The 120 mm axial fan that was used in this fan noise study is DC axial fan manufactured by Minebea and the model of the fan is 4710KL-05W-B20. The rated volatage is 24V and the operating volatage range is from 10.0 V to 27.6 V. Figure 2.4 shows the dimension of the fan provided by the manufacturer [41]. The rest of the specifications provided by the manufacturer of the fan are tabulated in Table 2.1.

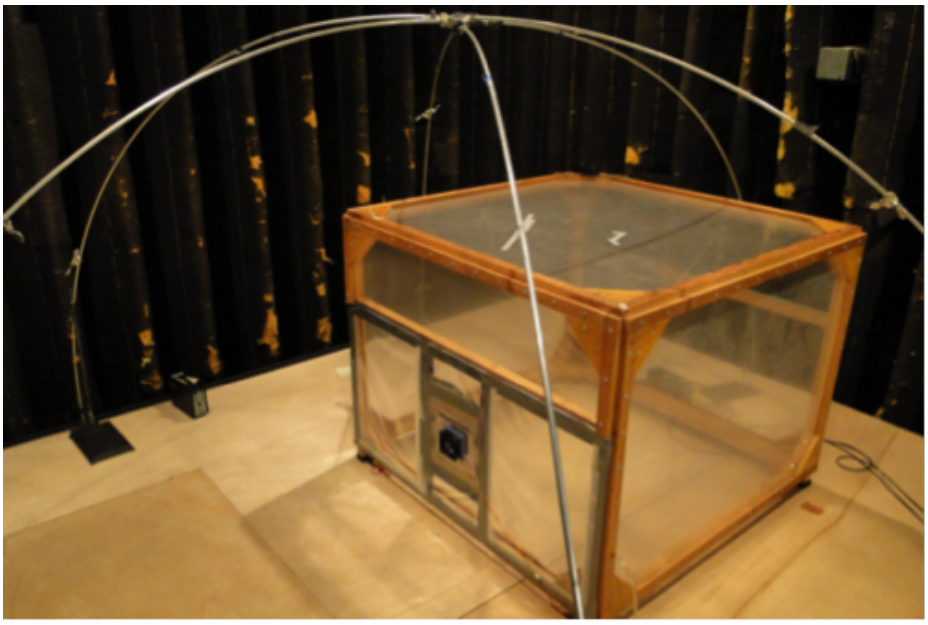

Figure 2.3. Test setup in the anechoic chamber at Ray W. Herrick Laboratories, Purdue University.

Table 2.1. Specification of the fan.

Model	Rated Voltage [V]	Operating Voltage [V]	Current [A]	Input Power [W]	Speed [RPM]	Max. Air Flow [m^3/min]	Max. Static Pressure [Pa]	Noise [dB]	Mass [g]
4710KL-05W-B20	24	10.0 27.6	0.10	2.40	1900	2.15	24.8	31.0	180

2.1.3 Data Acquisition and Signal Processing

Brüel and Kjaer type 4189 and type 4190 free-field microphones were used to measure the sound radiated by the fan and an Agilent VXI 8403A was used to acquire the signals which were obtained by the microphones array. Sound pressure signals for acoustical measurements were obtained while running the fan at each operating condition: 120 seconds of data were recorded at a sampling rate of 25.6 kHz. The recorded signal obtained by each microphone was divided into segments with 50 percent overlap and a Hann window was applied to each segment. Then the power spectral density of the signal was estimated using Welch's method by using MATLAB

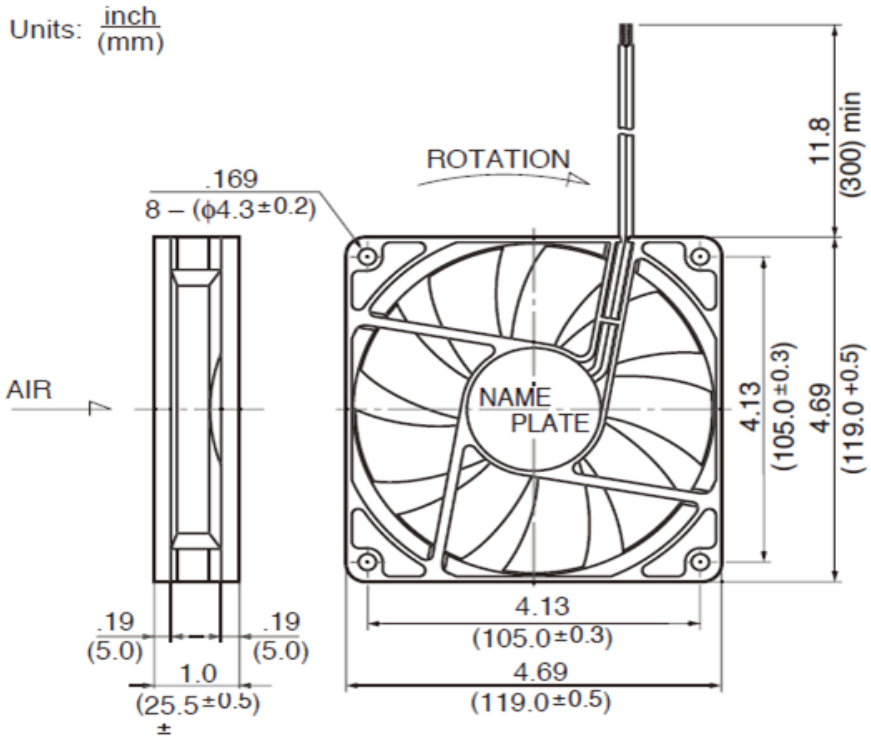

Figure 2.4. The dimension of the fan that was used in this study.

function "pwelch." The result after the power spectral density calculation was then applied to Equation (2.2) to calculate the sound power level generated by the axial fan.

2.2 Microperforated Panel Application

2.2.1 Microperforated Materials and Fan Casing

Three different microperforated panels (MPPs) were used as housings of the fan and the sound power level of each case was measured using the experimental set-up described in the previous section. Then the measured results using MPP housings were compared with a non-perforated housing by focusing at the level of blade passage frequency tones. Figure 2.5 shows the materials that were used for the fan housing. The non-perforated material, which is denoted as "Impermeable (regular)" in the

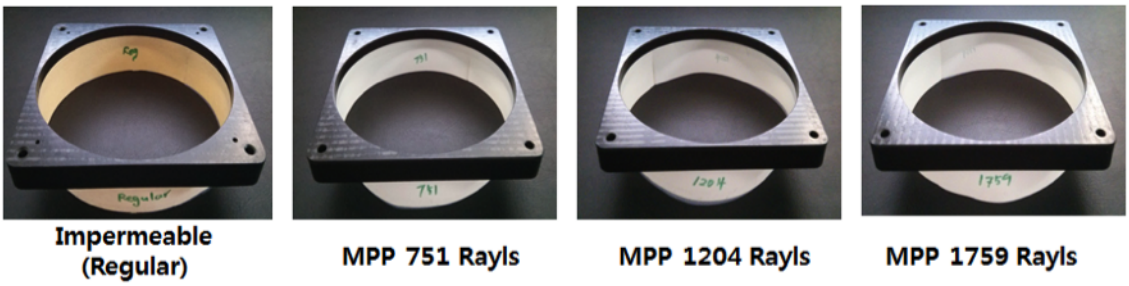

Figure 2.5. Microperforated materials used for the housing of the fan.

figure will be called the Regular casing from now on. The other three materials, named as MPP 751, MPP 1204 and MPP 1759 in the figure, are different MPPs that were used in the experiments. The numbers after MPP indicate the flow resistance of each material in Rayls.

The specimen 120 mm axial fan was modified to insert microperforated housings; the assembly of the fan and the MPP is shown in Figure 2.6.

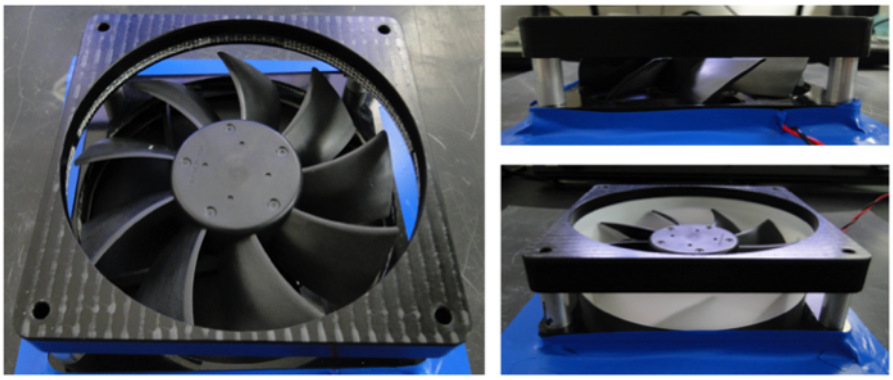

Figure 2.6. Modified fan to insert the microperforated materials in the housing area.

2.2.2 Performance Curve of the Fan

The acoustical measurements explained in the previous section were used for the comparison study of the different MPPs. The axial fans with the different casings were compared by operating the fans with the same operating condition to perform reliable comparison studies. In the determination of the operating conditions, the pressure-flow rate performance curve (P-Q curve) of the fan, shown in Figure 2.7, was used. The P-Q curve was obtained by following the procedure described in ISO 10302 using the plenum shown in Figure 2.1. The P-Q curves of the fan with the MPP 751 housing and the regular fan casing were plotted, respectively, in the Figure 2.7. The solid lines represent the P-Q curves of the regular fan housing case and the dashed lines represent the P-Q curves of the MPP fan housing case. It can be seen that substituting the fan casing with the microperforated material with the flow resistance of 751 Rayls did not reduce the flow performance of the fan compared with the regular housing. Therefore it is reasonable that the MPPs with higher flow resistances such as 1204 Rayls and 1759 Rayls, which were also selected in this study, would also maintain the same flow performance of the fan with the unperforated housing. Therefore determination of the operating conditions of different fan casing types with this P-Q curve for the comparison study can be considered as reasonable approach. Red dots in Figure 2.8 indicate fifteen different operating conditions that were selected by varying pressures and flow rate generated by the fan. Table 2.2 shows the blade passage frequency of each point and the outlet opening area of the plenum when the fan produces the desired static pressure and flow rate. The acoustic measurement results of the fan noise at these operating conditions will be discussed in the following section.

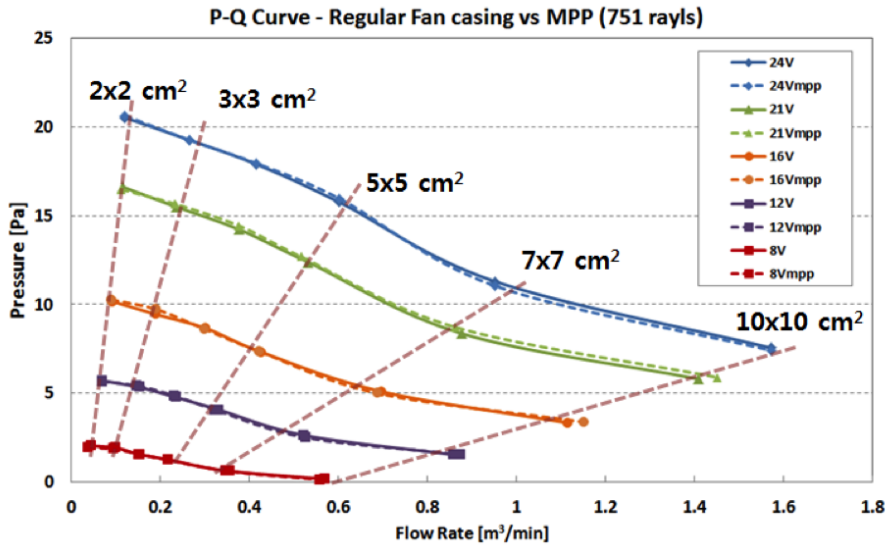

Figure 2.7. Performance curve of the fan (Pressure-Flow rate curve).

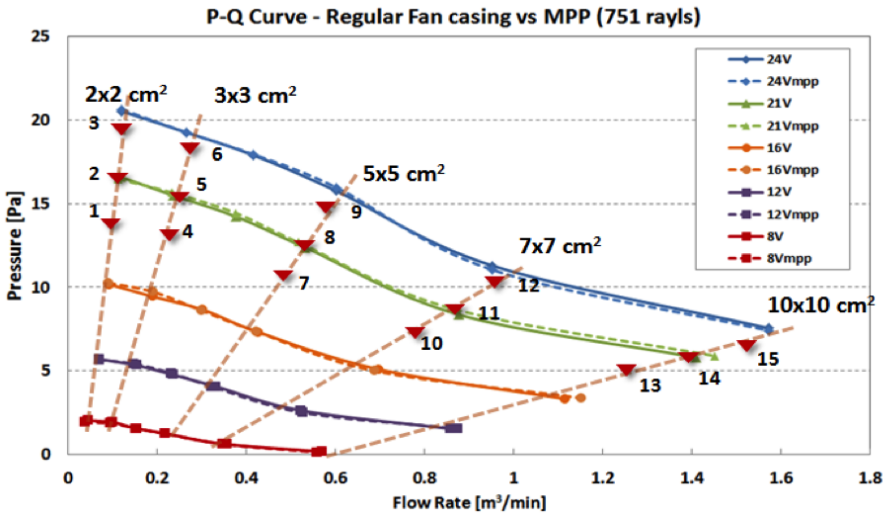

Figure 2.8. 15 operating condition points of the fan over the performance curve.

2.3 Experimental Results for Regular MPP Fan Casing

2.3.1 MPP Housing Application in the Fan

A discussion of the measurement results for the materials described in the previous sections will be provided here. The fan with different casings was tested under fifteen

Table 2.2. Blade Passage Frequency for each operating condition.

Operating Points	Opening Area [cm²]	BPF [Hz]	Operating Points	Opening Area [cm²]	BPF [Hz]	Operating Points	Opening Area [cm²]	BPF [Hz]
1	2 x 2	221.2	6		260.5	11		262.2
2		239.9	7	5 x 5	231.5	12		282.3
3		257.5	8		242.8	13	10 x 10	237.1
4	3 x 3	223.9	9		260.5	14		256.8
5		242.8	10	7 x 7	240.9	15		277.5

BPF - Blade Passage Frequency

different operating conditions indicated in Figure 2.8 as well as Table 2.2. In this chapter, five out of the fifteen operating points will be discussed in details; the result figures and for, the rest of the operating conditions will also be provided in the table at the end of this section. The five points that were selected are tabulated in Table 2.3. These five points were carefully selected so as to represent the different pressure and flow rate regions in the P-Q curve of the fan. For example, condition 1 in the table represents the high pressure and low flow rate region and condition 5 in the table represent the low pressure and high flow rate region of the fan.

Table 2.3. Selected operating conditions.

	Condition 1 (Pt. #2)	Condition 2 (Pt. #6)	Condition 3 (Pt. #7)	Condition 4 (Pt. #11)	Condition 5 (Pt. #14)
Pressure (Pa)	16.5	18.2	10.5	8.68	5.91
Flow rate (m^3/min)	0.11	0.27	0.48	0.88	1.39

Figure 2.9 shows the sound power level and the cumulative sound power spectra of fans with different housing materials at the first blade passage frequency region. The cumulative sound power level is the spectrum that can be obtained by simply integrates the area under the sound power level curves and each frequency point of the cumulative spectrum represent the overall sound power level up to that frequency.

These particular plots will be given along with the sound power level curves in this section because the cumulative spectrum provides a clear visualization of the blade passage tone level differences that are caused by different housing materials of the fan.

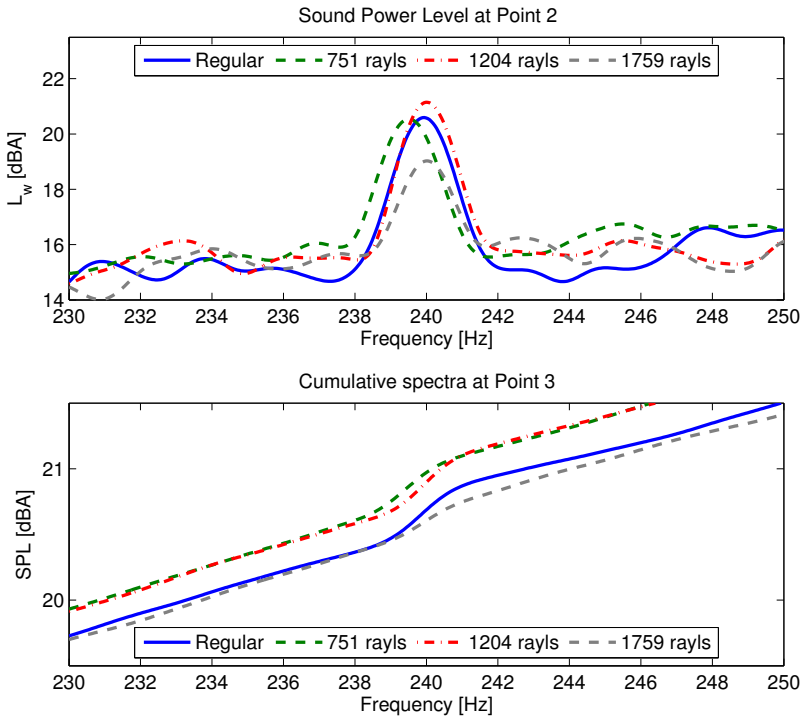

Figure 2.9. Sound power level and cumulative spectra at P=16.0Pa, Q=0.11m^3/min.

The operating condition of the fan was point 2 in the P-Q curve in the Figure 2.8. When the fan operates under this condition, it generates low flow rate and high static pressure. It can be seen that the microperforated panel that has the flow resistance of 1759 Rayls, which is the highest flow resistance, shows the best performance in reducing the blade passage tone. Note that the "step" in the cumulative spectrum at the blade passage frequency in bottom figure of Figure 2.8, also shows that the MPP with 1759 Rayls of flow resistance MPP results in the lowest overall sound power level. However, MPPs with lower flow resistances such as 751 Rayls and 1204 Rayls

increased the blade passage tone of the fan in comparison with the regular housing. Therefore it can be noticed that relatively high flow resistance is required for the microperforated housing of the axial fan with 120 mm diameter in this performance range.

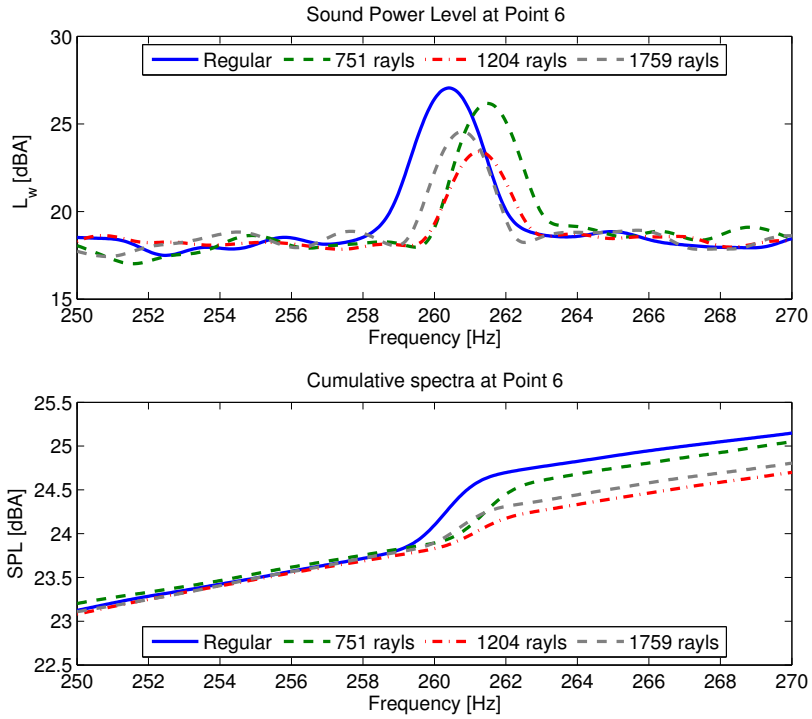

Figure 2.10. Sound power level and cumulative spectra at P=18.2Pa, Q=0.27m^3/min.

Figure 2.10 shows the results when the fans with different housing materials was run under the operating condition 6 in Figure 2.8. This condition represents a low flow rate (0.27 m^3/min) and very high pressure region (18.2 Pa) in the performance curve. The operating condition 6 circumstance can be achieved by adjusting the opening area of the plenum in Figure 2.1 to 2 x 2 cm^2. It can be seen from the figure that the MPP with 1204 Rayls of flow resistance reduced the blade passage frequency tone the most and by looking at the cumulative spectra, the overall sound power level at the blade passage frequency tone was the lowest as well among the fans with other

housing materials. Therefore in this particular operating condition, the MPP with 1204 Rayls for flow resistance is suitable for the housing material.

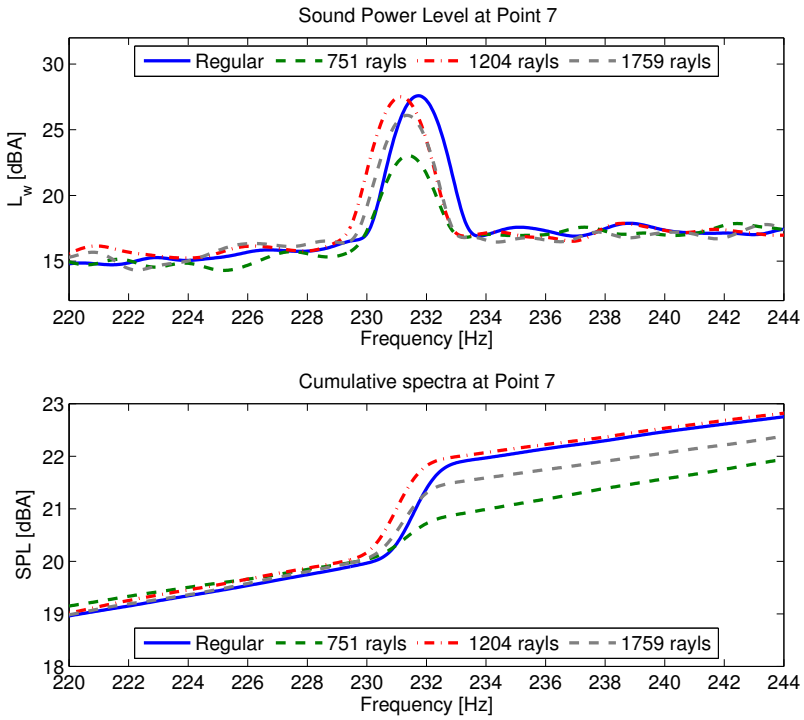

Figure 2.11. Sound power level and cumulative spectra at P=10.5Pa, Q=0.48m^3/min.

Figure 2.11 shows the result of the fan running under the operating condition 7, which is a low flow rate (0.48 m^3/min) and medium pressure region (10.5 Pa). This condition can be achieved by adjusting the opening area of the plenum to 5 x 5 cm^2. Unlike Figure 2.9 and 2.10, the MPP with flow resistance of 751 Rayls resulted in the lowest blade passage tone. Moreover, the overall sound power level is also the lowest with the microperforated panel with 751 Rayls of flow resistance.

The acoustical measurement results obtained by running the fan under operating condition 11 in Figure 2.8 is shown in Figure 2.12. This operating condition represents a medium pressure (8.68 Pa) and a little bit higher flow rate (0.88 m^3/min) compared to operating condition 7. It can be seen from the sound power level result in the figure

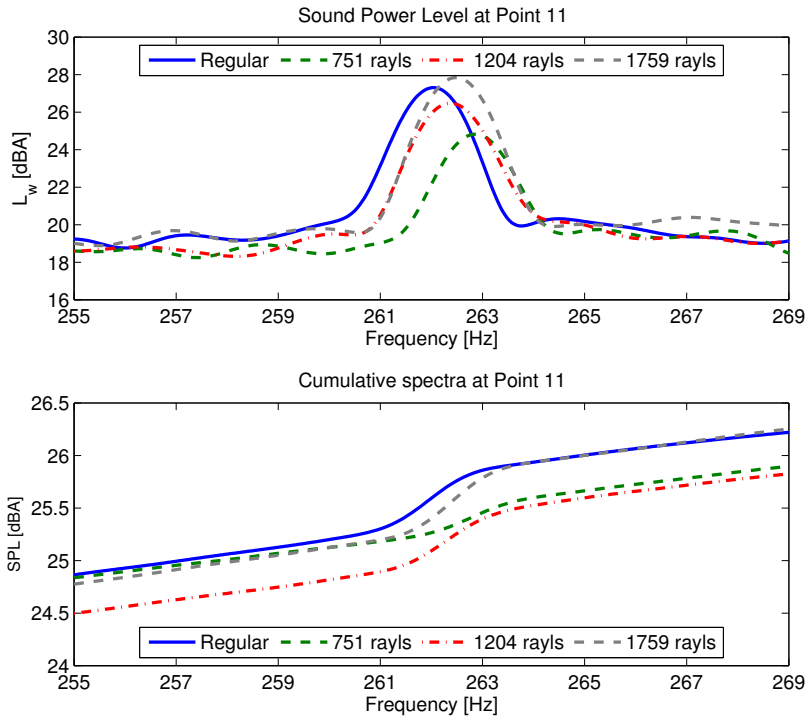

Figure 2.12. Sound power level and cumulative spectra at P=8.68Pa, Q=0.88m^3/min.

that the housing made with MPP of 751 Rayls flow resistance also reduced the blade passage frequency tone level the most. On the other hand, the overall sound power level results from the cumulative spectra shows that MPP 1204 Rayls has the lowest overall value, due to the broadband noise differences. But by looking at the amount of "jump" that was made in the cumulative spectra, the MPP 751 Rayls is more effective in reducing the blade passage tone.

Figure 2.13 shows the acoustical measurements of the fans with different housing materials at operating condition 14. This condition represents low pressure (5.91 Pa) and very high flow rate (1.39 m^3/min) region. From the sound power level spectra, it can also be seen that MPP 751 Rayls shows the best performance in blade passage tone level reduction. Moreover, the cumulative spectra also indicate that the MPP

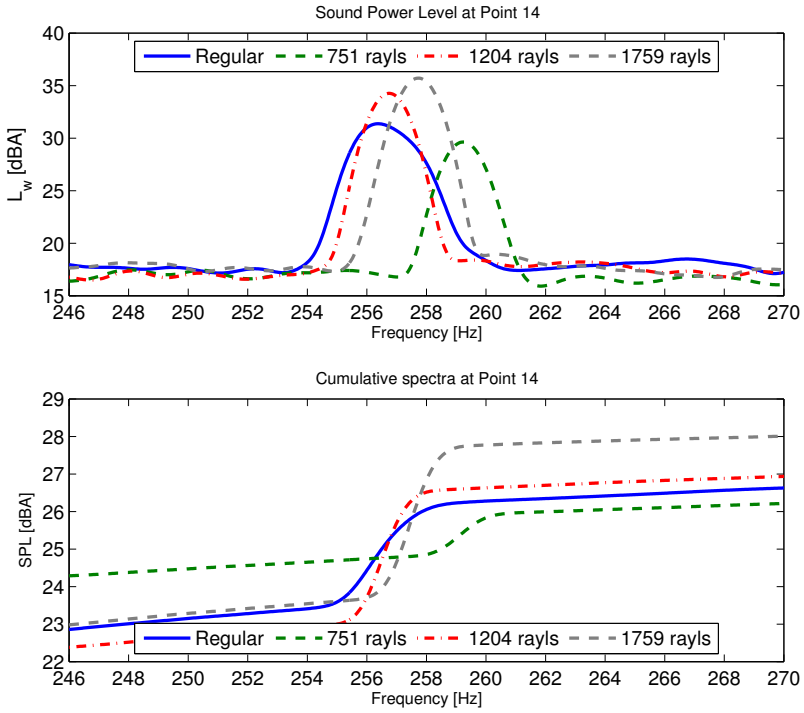

Figure 2.13. Sound power level and cumulative spectra at P=5.91Pa, Q=1.39m^3/min.

751 Rayls treatment reduces the blade passage tone the most even though the MPP 751 Rayls treatment results in higher broad band noise than other housing materials.

The blade passage frequency tone levels for all operating conditions are tabulated in Table 2.4. The MPP casing with 1759 Rayls flow resistance shows the best performance in reducing the blade passage frequency tone at operating condition 1 through operating condition 3. This region represents the very low flow rate region, which can be found in the line of 2 x 2 cm^2 opening area of the plenum in the P-Q curve. The operating conditions 4 through 6, which are located on the line of 3 x 3 cm^2 in the performance curve show that the MPP casing with 1204 Rayls flow resistance reduced the blade passage tone level the most. The MPP casing with 751 Rayls of flow resistance shows the best performance in reducing the blade passage frequency tone over the rest of the regions in the performance curve. These operating condition

Table 2.4. Blade Passage Tone levels for all cases.

	Blade Passage Tone [dBA]					Blade Passage Tone [dBA]					Blade Passage Tone [dBA]			
OP#	**Reg**	**751**	**1204**	**1759**	**OP#**	**Reg**	**751**	**1204**	**1759**	**OP#**	**Reg**	**751**	**1204**	**1759**
1	17.5	17.1	17.8	15.8	6	27.1	26.2	23.4	24.6	11	27.3	24.8	26.5	27.8
2	20.6	20.5	21.1	19.0	7	27.6	23.0	27.5	26.1	12	29.2	27.1	27.2	29.4
3	22.8	23.5	23.8	21.1	8	29.6	26.2	30.5	27.9	13	30.3	24.9	30.4	34.8
4	21.0	19.1	17.3	18.9	9	31.3	28.1	32.4	29.7	14	31.4	29.6	34.2	35.7
5	24.0	23.3	21.2	21.5	10	24.5	22.1	23.3	25.2	15	34.5	31.3	34.8	37.7

OP# - Operating Condition Points

Table 2.5. Overall sound power levels for all cases.

	Overall sound pressure [dBA]					Overall sound pressure [dBA]					Overall sound pressure [dBA]			
OP#	**Reg**	**751**	**1204**	**1759**	**OP#**	**Reg**	**751**	**1204**	**1759**	**OP#**	**Reg**	**751**	**1204**	**1759**
1	43.4	43.4	43.7	43.7	6	47.3	47.2	47.5	47.5	11	48.7	48.5	48.6	48.6
2	45.5	45.6	45.9	45.9	7	53.0	51.2	50.7	51.2	12	50.9	50.8	50.8	50.9
3	47.0	47.0	47.4	47.4	8	46.5	46.5	46.8	46.6	13	47.1	46.2	47.1	47.1
4	43.8	43.5	44.1	44.1	9	48.6	48.6	48.8	48.5	14	48.2	47.7	48.4	48.5
5	45.5	45.5	45.3	45.7	10	46.6	46.3	46.6	46.5	15	50.2	49.6	50.2	50.5

OP# - Operating Condition Points

points are located on larger opening areas such as 5 x 5 cm^2, 7 x 7 cm^2 and 10 x 10 cm^2.

Table 2.5 shows the overall sound pressure level of the fans with different fan casings at all the operating conditions. Even though the primary blade passage tones of the impermeable housing were reduced by the application of the MPP housings, the overall pressure levels remained similar. Therefore in get to achieve attenuation benefits from using the MPP duct in the overall sound power level point-of-view, extension of fan casing to the upstream and downstream regions of an axial fan were considered. The results on the modified casing research will be provided in next section.

The effectiveness of the microperforated housings in reducing the blade passage tone during different operating conditions is clearly visible in Figure 2.14(a), (b)

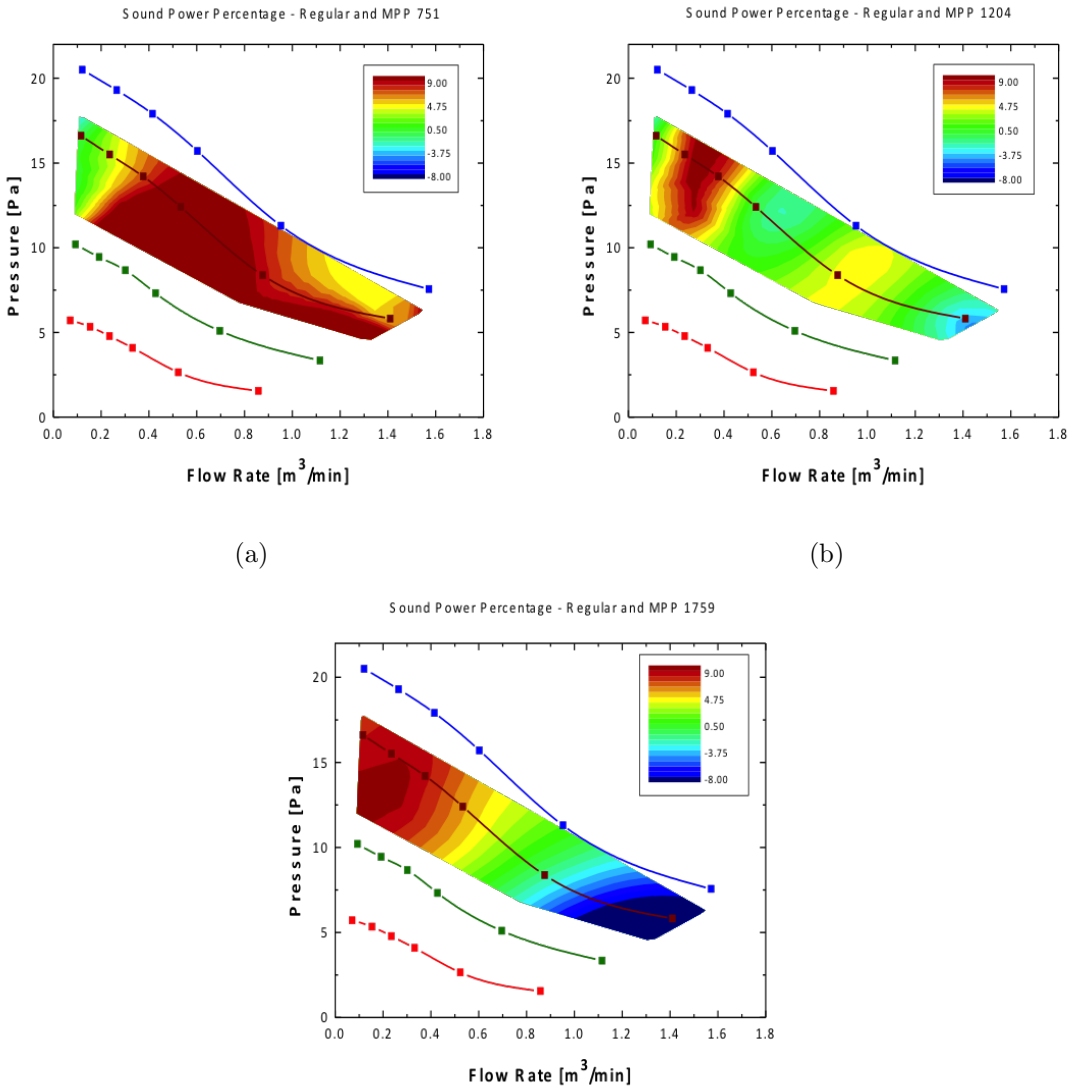

Figure 2.14. Contour plots of the Blade Passage Tone level reduction of (a) MPP751 housing, (b) MPP1204 housing and (c) MPP1759 housing compared to impermeable housing in percentage. Color bars are in % values.

and (c). These plots are the contour plots representing the percent reduction of the blade passage frequency tone sound power of each MPP casing from the unperforated regular casing over the performance curve region. The red region in the contour means the microperforated panel housing treatment reduced the blade passage tone of the

fan compared with the regular fan housing. The blue region in the contour plots indicates that the microperforated casing increases the blade passage tone of the fan compared with the regular fan housing. Figure 2.14 (c) shows that the highest flow resistance material, which is 1759 Rayls, reduced the blade passage tone level when the fan operates in the region in the very low flow rate region in the performance curve. The MPP 1204 Rayls microperforated material was also effective in the low flow rate region but less effective than MPP 1759 Rayls in the very low flow rate region.

As shown in Figure 2.14 (a), however, the MPP with 751 Rayls of flow resistance reduced the blade passage tone level of the regular cased fan in the largest area of the P-Q curve region. MPP 751 Rayls also slightly reduced the blade passage tone level in the very low flow rate region where the MPP 1759 Rayls showed the best reduction performance. Therefore it could be noticed from the figure that the blade passage tone of the fan can be reduced when the MPP with the proper flow resistance is used as the housing of the fan. Moreover, if the fan casing is made with high flow resistance materials, one can expect the best blade passage tone reduction in the low flow rate regions in the P-Q curve of the axial cooling fan.

2.4 An Axial Fan with the Microperforated Duct

2.4.1 Motivation for the Microperforated Duct for an Axial Fan

The fan is one of the most widely used devices for cooling and delivering flow in ventilation systems, fans are often the largest noise sources. Two types of the fans are normally used: (i) axial, and (ii) centrifugal. Centrifugal fans are capable of generating high static pressures compared to axial fans. However, axial fans can deal with higher air volume flow rates than a centrifugal fan and they produce relatively low noise compared to centrifugal fans. Therefore in this section, a noise control technique for an axial fan located inside a circular duct using the microperforated materials will be described.

Moreover, this is continuous research from an axial fan noise control in the previous section that replaced the impermeable housing with the MPP housing which resulted improvement in the attenuation blade passage tone levels of impremeable housing. However, the MPP housing application did not show beneficial effects in the overall sound power level point-of-view. Therefore the overall sound power level changes due to different duct materials and lengths of the ducts will also be considered in this section.

Figure 2.15 shows the configuration of that fan with inlet and outlet extended microperforated duct. By extending the inlet and outlet, the microperforated panel is expected to control the dipole-like source of the axial fan and control the inlet and outlet flow as well. Moreover, by adopting MPP elements as the duct materials, it is expected to have more beneficial effects in noise reduction due to the energy dissipation by the perforation holes on the MPP.

The experimental study of the sound power measurement of ducted fan was also made following the procedure described in the previous section using ISO 10302. The sound power radiated from the fan was obtained by changing the length of the ducts and both the MPP duct treatment and the impermeable duct treatment were measured and compared. The lengths of ducts used in this section are tabulated in

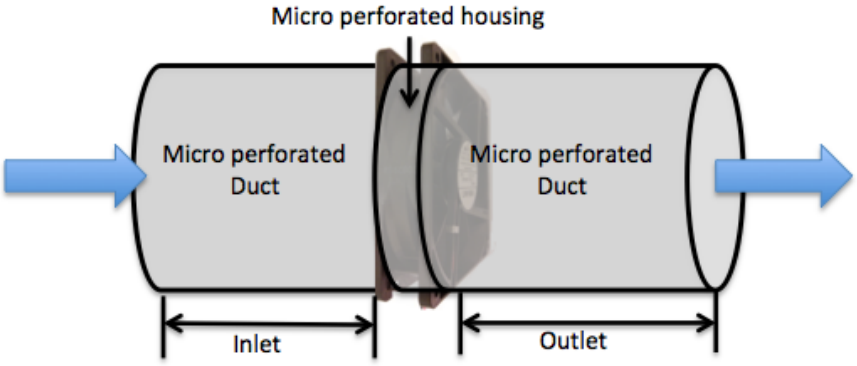

Figure 2.15. Configuration of the fan with inlet and outlet extended microperforated duct.

table 2.6. Figure 2.16 shows how the duct casing was attached to the axial fan for the sound power level measurement test set-up. The MPP used for the microperforated duct has the flow resistance of 751 Rayls, which had shown good blade passage tone attenuation performance in previous sections at most of the operating conditions. Figure 2.17 shows the actual photo of the fan located inside the MPP duct and regular duct.

Table 2.6. The lengths inlet-end and outlet-end of the ducts.

	Inlet Length [cm]	**Outlet Length [cm]**	**Total Length [cm]**
Short Duct	6	6	12
Mid Duct	13.6	13.6	27.8
Long Duct	27.8	27.8	55.6

Figure 2.16. The actual photo of microperforated duct application to the axial fan noise testing.

Figure 2.18 shows the pressure-flow rate curves of fans with both the microperforated and the unperforated ducts. The performance curves of the fans were obtained

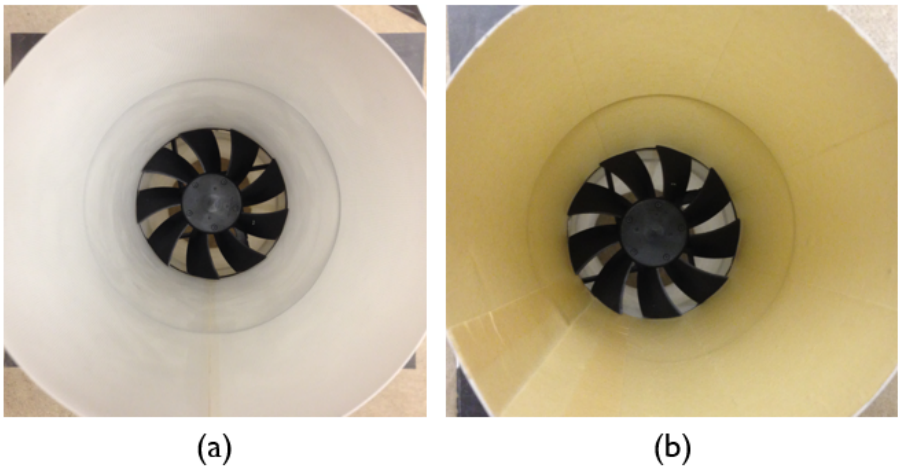

Figure 2.17. The actual photo of the fan located inside (a) the microperforated duct and (b) the impermeable (regular) duct.

by using the plenum described in the previous section. The static pressure generated inside the plenum and the flow rate at the outlet of the plenum were measured while running the fan under different voltages as well as changing the outlet opening area of the plenum. It can be seen from the figure that the performance of the fan made using the microperforated duct was essentially the same as the performance of the fan with the unperforated duct. Each different duct length was run under the same operating conditions for a fair comparison of the sound power radiated from the fans with different ducts. The operating conditions were determined from the performance curve of the fan as suggested in previous section.

Figure 2.19 shows the performance comparison between the short microperforated ducted fan and the axial fan with the microperforated panel treatment only around the housing region of the fan: i.e., there were no inlet and outlet extensions of the microperforated housing. It can be seen from the figure that the microperforated duct has a beneficial effect in the flow delivery and the pressure generation compared to the typical axial fan, especially, in the region highlighted in the figure.

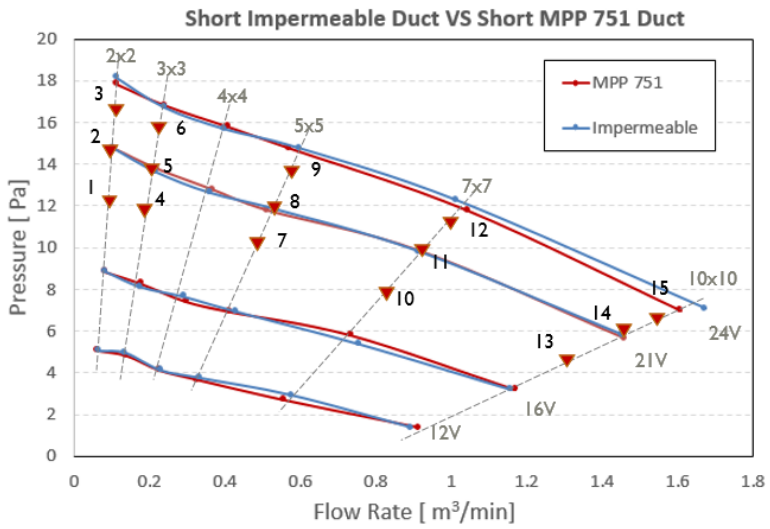

Figure 2.18. P-Q curve comparison between the regular ducted fan and the MPP ducted fan.

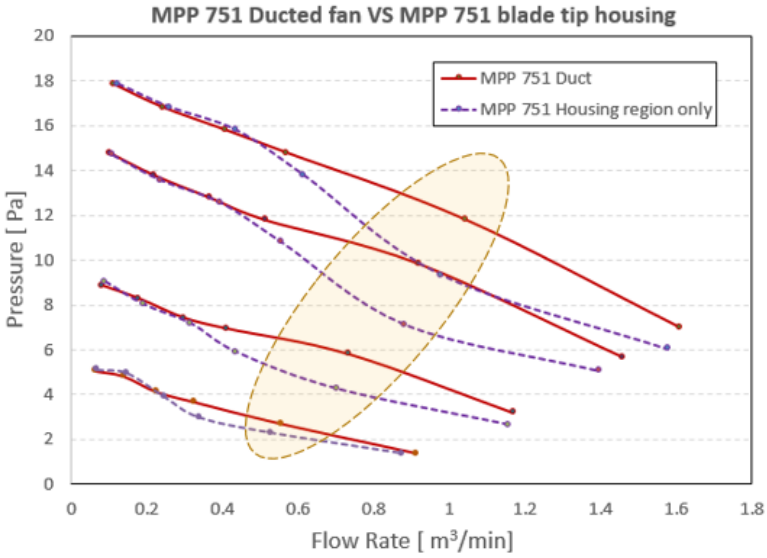

Figure 2.19. P-Q curve comparison between the regular MPP casing and the MPP duct.

2.4.2 Experimental Results for Short Duct (Total Length of 12 cm)

In the following subsections, the sound power radiated by the fan with different lengths of the ducts will be discussed. Three different lengths of the unperforated

ducts and the microperforated ducts were used for the experimental comparison. The lengths of the ducts that were used in this tests are tabulated in Table 2.6. The experimental results for the comparison studies between different duct types were obtained while operating the fan under the operating conditions that were given earlier this chapter in Figure 2.8. First the fans with short ducts, with dimension given

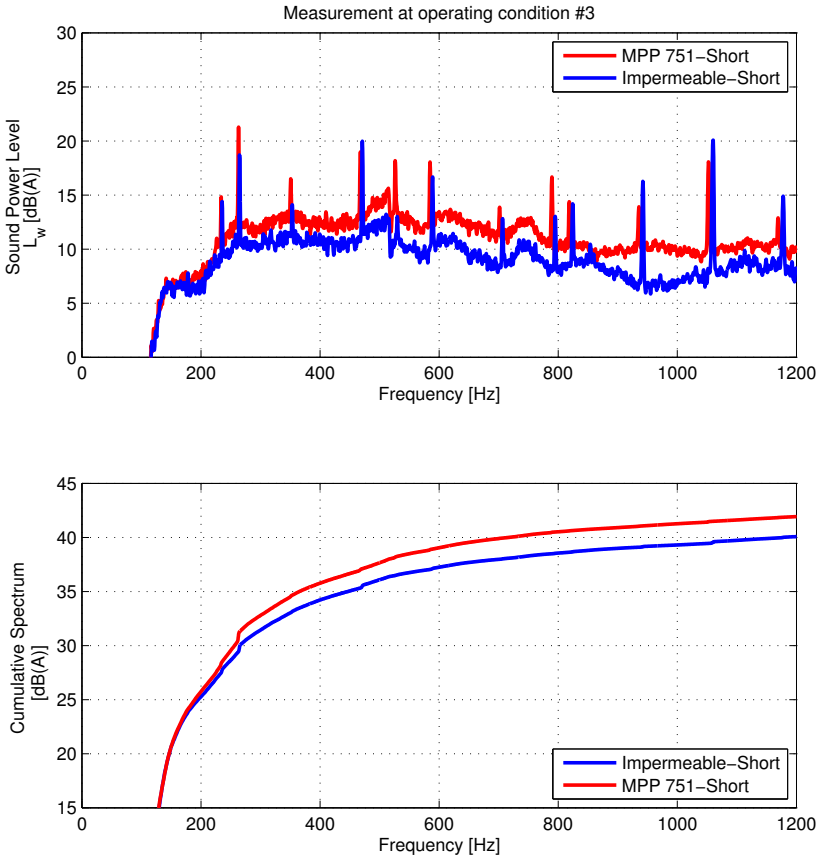

Figure 2.20. Sound power level comparison between the MPP 751 and impermeable short ducted fan at operating condition #3.

in Table 2.6, having different duct materials (the impermeable and the MPP ducts) will be considered. Figure 2.20 shows the sound power level spectra measurement and cumulative spectra results of the fan with different duct materials at operating condition 3 from Figure 2.18. Operating condition 3 is when the fan was operated at

the relatively high static pressure and low flow rate condition. It can be seen from the figure that when the length of the duct is short, the microperforated duct does not have a beneficial effect on the attenuation of the blade passage tone level compared to the unperforated duct.

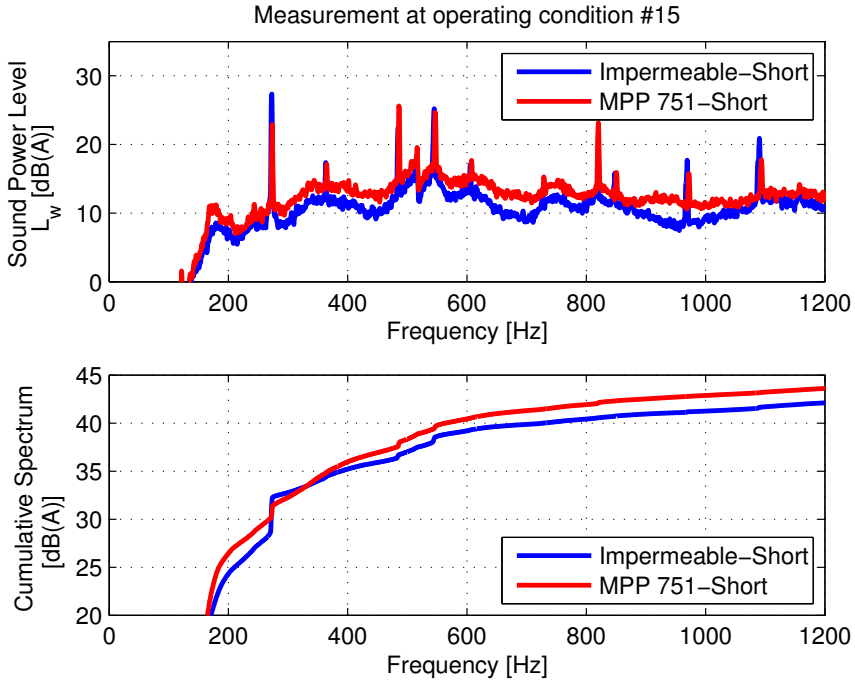

Figure 2.21. Sound power level comparison between the MPP 751 and impermeable short ducted fan at operating condition #15.

Figure 2.21 shows the measurement comparison of both ducted fans operated at condition 15 in Figure 2.18, which is the conditions at a relatively low static pressure and high flow rate. In this operating condition, the short length microperforated duct reduced the blade passage tone of the fan compared with the unperforated duct. However, an increase in the overall sound power level resulted from the use of the microperforated duct, as can be seen from the cumulative spectra, due to the increased broadband noise at this operating condition.

All of the blade passage tone levels and the overall sound power levels are tabulated in Tables 2.7 and 2.8, respectively. There are some operating conditions where

a beneficial effect in reducing the blade passage tones was obtained by using the microperforated duct and they are when the fans were operated at the relatively low static pressure and high flow delivery conditions. However, the microperforated duct was not effective in reducing the overall sound power levels of the fan compared with an impermeable duct at most of the operating conditions.

Table 2.7. Blade passage tone level comparison between the fans with MPP and the regular short ducts (12cm total) at all operating conditions.

	Blade Passage Tone [dBA]			Blade Passage Tone [dBA]			Blade Passage Tone [dBA]	
OP#	**REG**	**MPP751**	**OP#**	**REG**	**MPP751**	**OP#**	**REG**	**MPP751**
1	12.5	17.2	6	17.3	24.7	11	24.0	27.2
2	16.5	19.6	7	15.9	24.6	12	25.2	28.7
3	18.7	21.3	8	18.3	27.2	13	22.2	19.6
4	10.8	17.3	9	20.7	29.4	14	25.2	22.1
5	13.7	21.5	10	20.8	22.4	15	27.3	22.9

OP# - Operating Condition Points, REG - Unperforated Duct, MPP751 - Duct housing using MPP751

Table 2.8. Overall sound power level comparison between the fans with MPP and the regular short ducts (12cm total) at all operating conditions.

	Overall Sound Power Level [dBA]			Overall Sound Power Level [dBA]			Overall Sound Power Level [dBA]	
OP#	**REG**	**MPP751**	**OP#**	**REG**	**MPP751**	**OP#**	**REG**	**MPP751**
1	39.5	40.9	6	42.4	44.0	11	42.6	43.6
2	40.9	42.5	7	39.2	41.0	12	44.6	45.5
3	42.3	43.9	8	40.8	42.2	13	47.5	43.2
4	41.6	43.9	9	42.9	44.2	14	43.1	43.6
5	40.7	42.4	10	40.9	41.9	15	44.7	45.4

OP# - Operating Condition Points, REG - Unperforated Duct, MPP751 - Duct housing using MPP751

One more thing we can be seen from the table is that the overall sound power level at operating condition 4 is hither than the operating condition 5 where the input voltage (21 V) is higher than the operating condition 4 (19 V), which would directly affect to the rotation speed of the fan. Figure 2.22 shows the sound power level spectra

results at the operating condition 4. It can be seen from the figure that the couple of tonal noises at 517 Hz that are very similar to ball bearing noise characteristics are shown in the figure. This noise components appears when the blade passage frequency of the fan is rotating at 1560 RPM and these ball bearing components led to the higher overall sound power level and since this noise is appearing from the shaft of the fan which is located far enough from the housing area of the fan, the MPP treatment is not effective in the attenuation of this noise. These phenomena will be kept showing at different ducted fan cases having longer ducts when the fan is rotating at 1560 RPM in further studies.

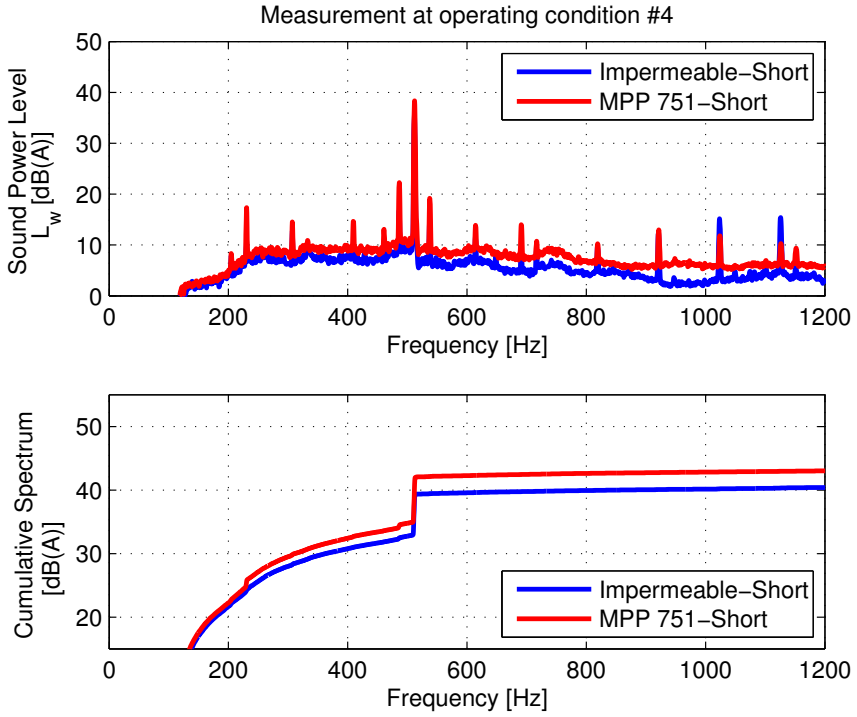

Figure 2.22. Sound power level comparison between the MPP 751 and impermeable short ducted fan at operating condition #15.

2.4.3 Experimental Results for Mid Duct (Total Length of 27.8 cm)

The total length of the MPP duct was changed to the values shown as 'Mid Duct' in Table 2.6. The inlet and outlet extended duct lengths are longer than the previous 12 cm long duct while the flow resistance of the MPP is still 751 Rayls.

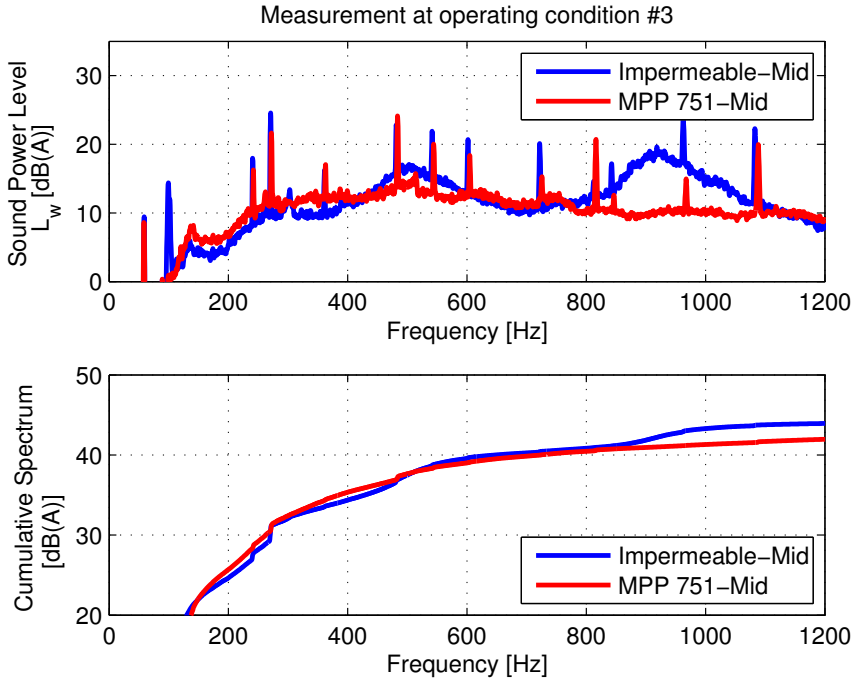

Figure 2.23. Sound power level comparison between the MPP 751 and impermeable 27.8cm duct fan at operating condition #3.

Figure 2.23 shows the comparison results of the duct casings when the fans were opearated under the condition 3 in Figure 2.18. It can be seen from the figure that the microperforated material reduces the blade passage tone of the impermeable ducted fan. Moreover, as the length of the duct gets longer, the duct mode frequency components appeared in the impermeable ducted fan case at 520 Hz and 910 Hz. However, it can also be seen from the figure that those duct modes were suppressed by the MPP duct. Figure 2.24 shows a different result in blade passage tone reduction. The comparison results for this figure were obtained by operating the fans at the relatively lower static pressure and higher flow rate region compare to the condition 3 in the

P-Q curve, which means the flow load applied to the fan was lowered due to larger flow exit area of the plenum. As a result the first duct mode appeared in the impermeable ducted fan at operating condition 3 was lowered and therefore the broadband noise around the blade passage frequency of the impermeable ducted fan was lowered and the MPP ducted fan resulted in slightly higher blade passage tone compare to the tone of impermeable ducted fan.

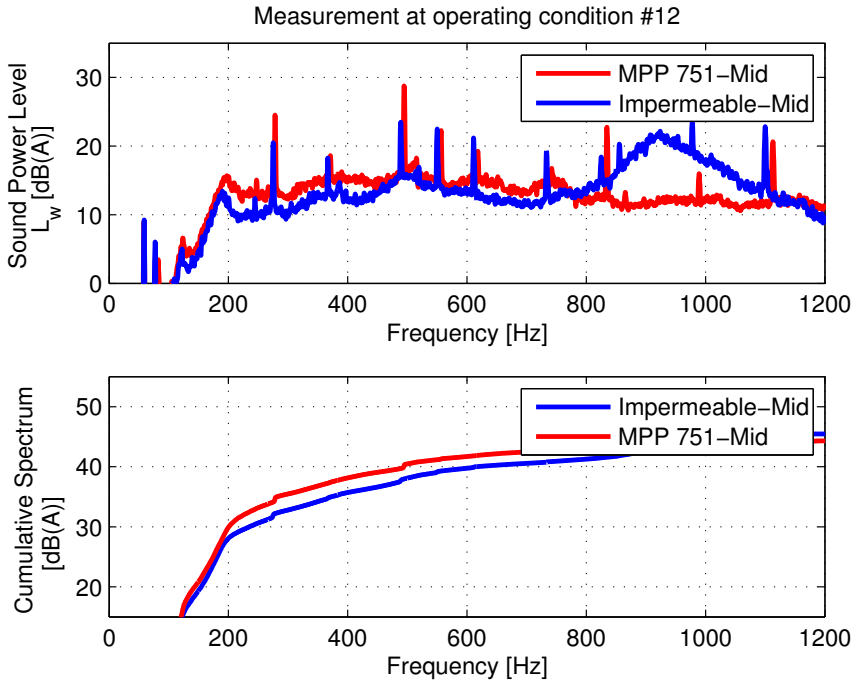

Figure 2.24. Sound power level comparison between the MPP 751 and impermeable 27.8cm duct fan at operating condition #12.

The blade passage tone reduction comparison between the MPP and unperforated ducts with the total length of 27.8 cm over the rest of the operating conditions are tabulated in Table 2.9. It can be seen that the MPP ducted fan reduced the blade passage tones at more number of operating conditions than the short ducted fan case. As it can be seen from the table taht the blade passage tone levels from the operating conditions 1 to the conditions 9 were reduced by the MPP ducted fan. It can be considered that as the length of the duct gets longer, there are more chances that

the sound wave can be dissipated as the wave travels through the duct. Moreover, the blade passage tones can be efficiently attenuated by using the MPP when the fan with medium length of the duct is operated under the conditions of relatively high static pressure and low flow rate delivery region.

Table 2.10 shows the overall sound power levels of the both types of duct fans at all operating conditions. Unlike the blade passage tones, the MPP duct reduced overall sound power levels at all operating conditions and it is because the MPP duct efficiently suppressed the duct modes that were generated in the impermeable duct.

Table 2.9. Blade Passage Tone level comparison between the fans with MPP and the regular Mid ducts (27.8 cm) at all operating conditions.

	Blade Passage Tone [dBA]			Blade Passage Tone [dBA]			Blade Passage Tone [dBA]	
OP#	**REG**	**MPP751**	**OP#**	**REG**	**MPP751**	**OP#**	**REG**	**MPP751**
1	19.8	12.7	6	25.2	20.6	11	21.0	22.3
2	22.4	17.4	7	20.7	16.2	12	20.5	24.5
3	24.6	21.6	8	22.8	18.1	13	19.6	21.8
4	21.4	12.1	9	23.0	20.4	14	23.2	21.7
5	24.2	16.7	10	19.1	19.1	15	25.5	25.2

OP# - Operating Condition Points, REG - Unperforated Duct, MPP751 - Duct housing using MPP751

Table 2.10. Overall sound power level comparison between the fans with MPP and the regular Mid ducts (12cm total) at all operating conditions.

	Overall Sound Power Level [dBA]			Overall Sound Power Level [dBA]			Overall Sound Power Level [dBA]	
OP#	**REG**	**MPP751**	**OP#**	**REG**	**MPP751**	**OP#**	**REG**	**MPP751**
1	45.6	45.0	6	44.8	43.7	11	44.5	43.7
2	43.3	42.1	7	41.4	40.9	12	46.4	45.6
3	44.9	43.8	8	43.0	42.2	13	45.5	42.9
4	41.8	41.3	9	44.9	44.0	14	44.8	43.9
5	42.9	41.9	10	42.8	42.1	15	46.7	45.7

OP# - Operating Condition Points, REG - Unperforated Duct, MPP751 - Duct housing using MPP751

2.4.4 Experimental Results for Long Duct (Total Length of 55.6 cm)

In this section, the fans with long ducts attached will be considered. Figure 2.25 shows the sound power spectra as well as cumulative spectra of both fans with the microperforated and the impermeable duct at operating condition 3. As shown in the figure, the microperforated duct reduced the blade passage frequency tone at 255 Hz as well as the broadband noise of the fan, compared with the impermeable duct. Moreover, duct modes started to appear in the spectrum of the impermeable ducted fan (e.g., the regions near 350 Hz and 500 Hz when the duct was approximately one-half, and a full wavelength in length), whereas the modes were suppressed by using the microperforated duct. It can also be seen from the cumulative spectrum that the reduction of blade passage tone and broadband noise resulted in about a 3 dB(A) reduction in the overall sound power level.

Figure 2.26 shows the comparison of both ducted fans at operating condition 14 from Figure 2.18. The blade passage tones of both ducted fans at this operating condition were similar to each other. However, duct modes exist in the impermeable ducted fan resulted the increase in the overall sound power level.

The blade passage tone levels and the overall sound power levels of the fans with both types of ducts are tabulated in Tables 2.11 and 2.12, respectively. The fan with a long duct showed a gradual improvement in the blade passage tone reduction compared to the fan with an impermeable duct at most of the operating conditions except for operating conditions 13 and 14, where the blade passage tone levels of the MPP ducted fan are a little bit higher. They are due to the reduction of duct modes sine the flow load applied to the fan was lowered by opening the flow area in the plenum larger.

2.4.5 Pressure Generated by the Ducted Fans

It was also found that the duct made of microperforated panel (MPP) improved the flow performance of the axial fan compare to the the fan with unperforated duct

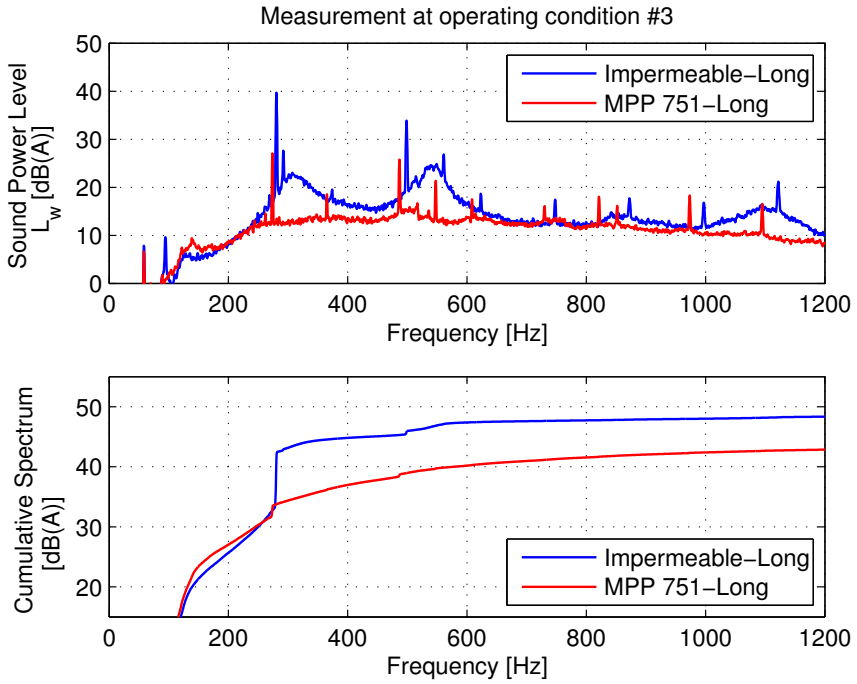

Figure 2.25. Sound power level comparison between the MPP 751 and impermeable 56.8cm duct fan at operating condition #3.

Table 2.11. Blade Passage Tone level comparison between the fans with MPP and the regular long ducts (55.6 cm) at all operating conditions.

	Blade Passage Tone [dBA]			Blade Passage Tone [dBA]			Blade Passage Tone [dBA]	
OP#	**REG**	**MPP751**	**OP#**	**REG**	**MPP751**	**OP#**	**REG**	**MPP751**
1	29.9	19.3	6	41.2	26.6	11	31.1	27.8
2	34.1	22.9	7	31.2	22.6	12	35.9	29.4
3	39.7	27.0	8	35.4	25.7	13	24.2	25.2
4	31.5	19.2	9	40.3	28.3	14	27.6	28.7
5	36.0	22.9	10	26.9	24.3	15	30.9	30.5

OP# - Operating Condition Points, REG - Unperforated Duct, MPP751 - Duct housing using MPP751

as well as the blade passage tone attenuation performance. The static pressure generated by the fan was measured by using a micro manometer (Dwyer model 1430), which has the accuracy of ± 0.06 Pa, as shown in Figure 2.27. For the pressure

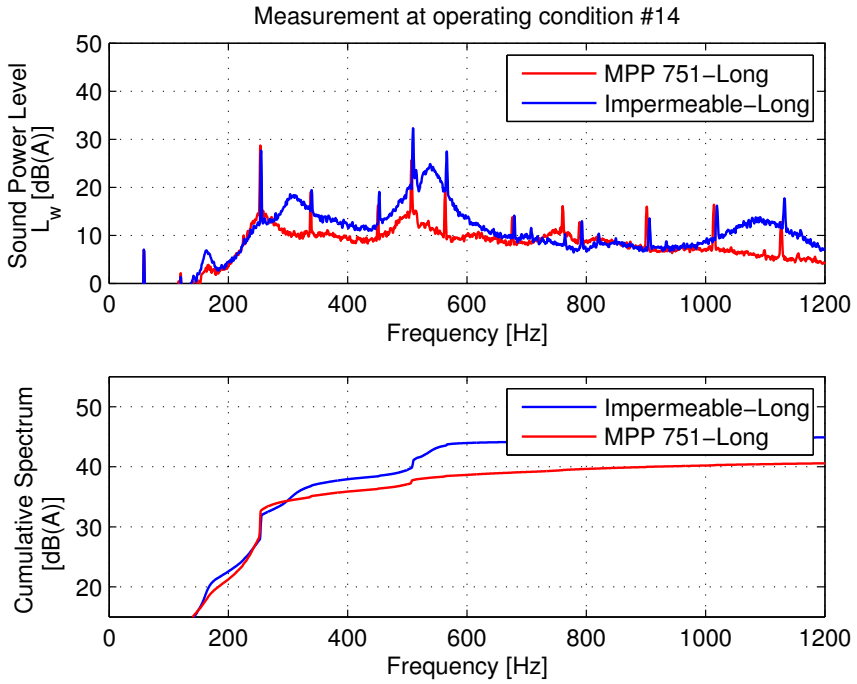

Figure 2.26. Sound power level comparison between the MPP 751 and impermeable 56.8cm duct fan at operating condition #14.

Table 2.12. Overall sound power level comparison between the fans with MPP and the regular long ducts (55.6cm total) at all operating conditions.

	Overall Sound Power Level [dBA]			Overall Sound Power Level [dBA]			Overall Sound Power Level [dBA]	
OP#	**REG**	**MPP751**	**OP#**	**REG**	**MPP751**	**OP#**	**REG**	**MPP751**
1	45.9	42.4	6	48.9	43.9	11	47.0	44.1
2	46.2	42.3	7	45.9	40.7	12	49.6	46.3
3	48.8	44.1	8	45.7	42.3	13	48.5	45.3
4	45.9	42.2	9	48.5	44.1	14	45.5	41.6
5	46.0	42.0	10	46.5	42.0	15	47.5	43.3

OP# - Operating Condition Points, REG - Unperforated Duct, MPP751 - Duct housing using MPP751

comparison between the different duct materials, the fans with different duct casings were operated at the same input voltages. In order to test the fans under various circumstances, the operating points in the P-Q curve shown in Figure 2.8 were also used for various operating conditions. To specify the voltage at each operating con-

ditions, the operating voltage of the fan for the conditions 1, 4, 7, 10, and 13 was set to 18.75V and the voltage for the conditions 2, 5, 8, 11, and 14 was set as 20.75V. The voltage for the conditions 3, 6, 9, 12 and 15 was set to 22.75V.

Table 2.13 shows the static pressure in Pa generated by the fan with each type of duct with total length of 12 cm. The MPP duct does not help much in flow point of view as well as blade passage tone attenuatoin with this duct length. Pressure values generated by 'Duct 2' type which had the total length of 27.8 cm are tabulated in Table 2.14. It can be seen from the table that as the length of the duct increased, the static pressure generated by the MPP ducted fan uses slightly increased under a number of operating conditions.

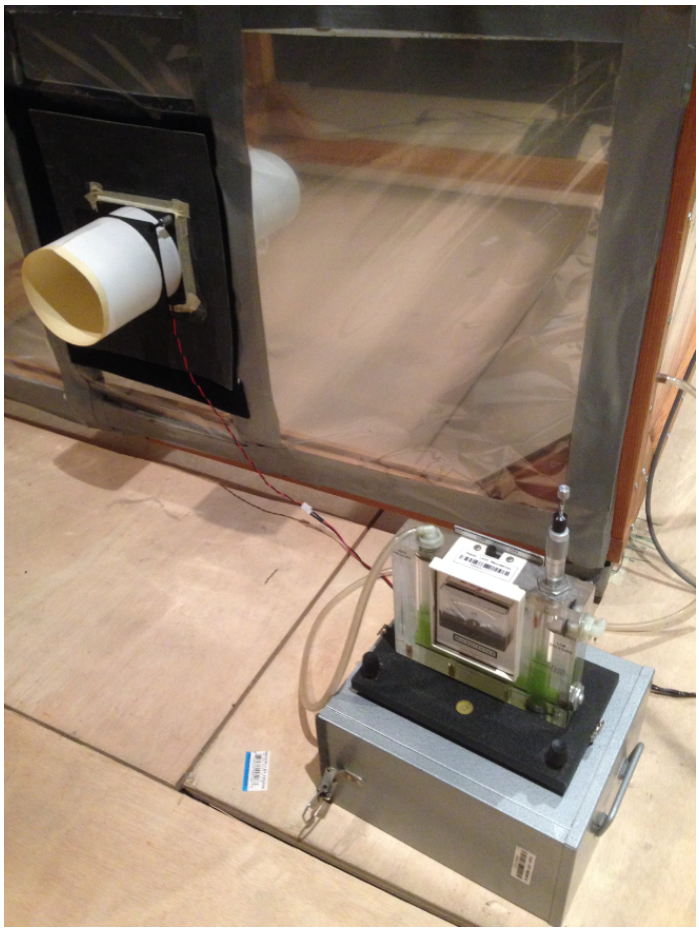

Figure 2.27. Micromanometer that attached to the plenum.

Table 2.15 shows the pressure values generated by the fans with the longest duct in this test, which is 55.6 cm. It can be noticed that the static pressure generated by the MPP duct is higher than the unperforated duct at most of the operating condtions with the long duct length. The pressure values of the MPP duct were slightly lower at some of the operating conditions such as 14 and 15. However, those points are when the flow rate is maximized by opening the flow outlet area to almost fully opened in the plenum shown in Figure 2.1.

Table 2.13. Static pressure generated by the fan with duct casing. Short-length duct (Total length: 12cm).

	Pressure [Pa]			Pressure [Pa]			Pressure [Pa]	
OP#	**REG**	**MPP751**	**OP#**	**REG**	**MPP751**	**OP#**	**REG**	**MPP751**
1	12.8	11.3	6	16.8	16.2	11	9.23	9.03
2	15.7	15.1	7	9.78	9.39	12	10.9	10.8
3	18.0	17.0	8	11.6	11.1	13	4.64	4.15
4	11.9	11.5	9	13.7	13.0	14	5.37	5.10
5	14.5	14.2	10	7.90	7.78	15	6.78	6.40

OP# - Operating Condition Points, REG - Unperforated, MPP751 - MPP751 duct

Table 2.14. Static pressure generated by the fan with duct casing. Mid-length duct (Total length: 27.8cm).

	Pressure [Pa]			Pressure [Pa]			Pressure [Pa]	
OP#	**REG**	**MPP751**	**OP#**	**REG**	**MPP751**	**OP#**	**REG**	**MPP751**
1	11.8	11.8	6	15.7	15.7	11	9.45	9.24
2	13.9	14.0	7	9.41	9.64	12	10.8	10.9
3	16.3	16.5	8	10.9	11.2	13	4.34	4.46
4	10.8	11.0	9	12.9	13.4	14	5.21	5.13
5	12.9	13.5	10	7.85	7.83	15	6.59	6.43

OP# - Operating Condition Points, REG - Unperforated, MPP751 - MPP751 duct

Table 2.15. Static pressure generated by the fan with duct casing. Long-length duct (Total length: 55.6cm).

	Pressure [Pa]			Pressure [Pa]			Pressure [Pa]	
OP#	**REG**	**MPP751**	**OP#**	**REG**	**MPP751**	**OP#**	**REG**	**MPP751**
1	10.1	10.8	6	13.5	15.2	11	7.97	8.26
2	11.9	12.9	7	8.78	9.47	12	9.83	10.7
3	13.9	15.8	8	10.9	11.1	13	4.26	4.27
4	9.80	10.8	9	12.6	13.2	14	5.06	5.07
5	11.6	12.8	10	6.69	6.93	15	6.14	6.03

OP# - Operating Condition Points, REG - Unperforated, MPP751 - MPP751 duct

According to Tables 2.13, 2.14 and 2.15, the static pressure generated by the unperforated duct becomes lower as the length of the duct increases. However, it can also be concluded from the results that substituting the unperforated duct with the MPP duct could compensate the drawback of the pressure that could be caused by extending the length of the duct.

2.4.6 Different Duct Lengths in Upstream and Downstream of the Fan

In previous sections, the same duct length combinations in the downstream and upstream sides of the fan were studied. Different lengths combinations will be considered in this section. Table 2.16 shows the two ducted fans with different length combinations. Case A is a combination of mid duct at the upstream side and long duct at the downstream side of the fan and Case B is a combination of mid duct at the upstream and long duct at the downstream side of the fan.

Figure 2.28 and Figure 2.29 show the comparison results of the impermeable duct and the MPP duct of fans with the case A lengths combination. Figure 2.28 shows the results when the ducted fan was operated at high pressure and low flow rate environment and it can be seen that the blade passage tone of the impermeable ducted fan was lower than the MPP ducted fan. However, when the fan was operated

Table 2.16. Different lengths combinations in upstream and downstream of the fan.

	Upstream Length [cm]	Downstream Length [cm]	Total Length [cm]
Case A	13.6	27.8	41.4
Case B	27.8	13.6	41.4

at relatively low pressure and high flow rate condition, the blade passage tone level of the MPP ducted fan was lower than the impermeable ducted fan as shown on Figure 2.29.

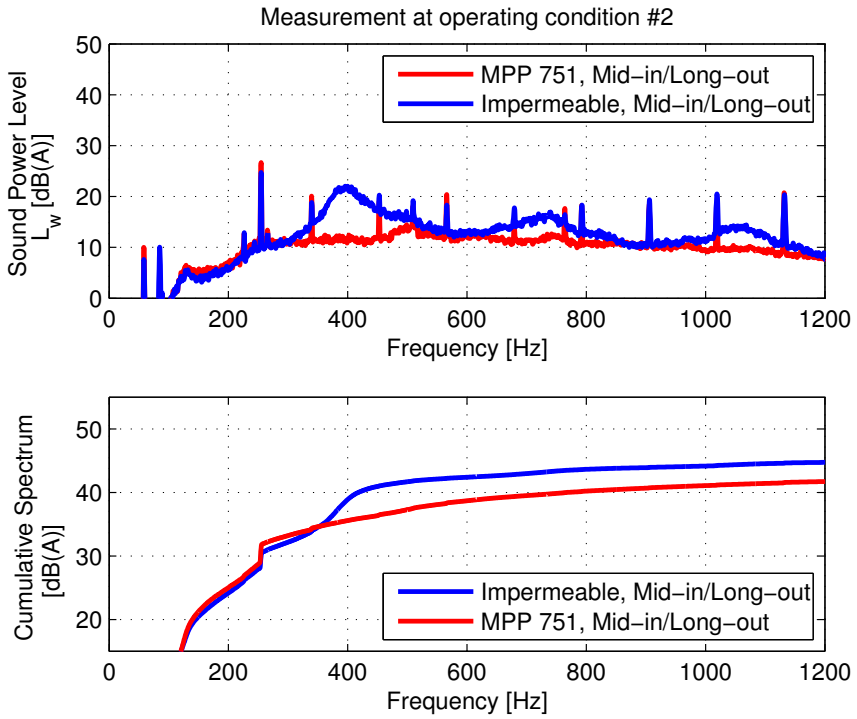

Figure 2.28. Sound power level comparison between the MPP 751 and impermeable duct having different length combinations (CASE A) at operating condition #3.

Table 2.17 and Table 2.18 shows the all the values of the blade passage tones and the overall sound power level, respectively. For the blade passage tone level results, the blade passage tones of ducted fan having longer downstream duct at high pressure

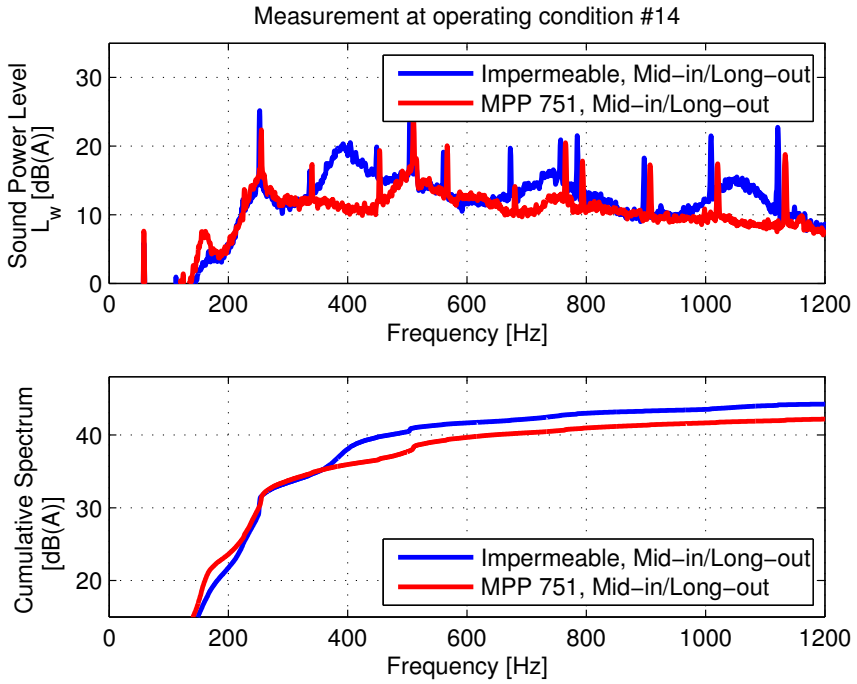

Figure 2.29. Sound power level comparison between the MPP 751 and impermeable duct having different length combinations (CASE A) at operating condition #14.

and low flow rate region do not affected by using the MPP duct whereas the MPP ducted fan reduces the blade passage tones when the fan was operated at relatively higher flow rate.

Figure 2.30 and Figure 2.31 show the acoustic measurement comparion of the MPP duct and the impermeable duct that have the case B combination of different upstream and downstream duct lengths shown in Table 2.16. Figure 2.30 shows the results when the fan was operating at condition 2 (high static pressure and low flow rate condition) and it can be seen from the figure that the MPP duct combination reduced the blade passage tone of the impermeable duct and also suppressed duct modes and resulted in a reduced overall sound power level as well.

Figure 2.31 shows the comparison results obtained by operating the fan at condition 12 (relatively low static pressure and high flow rate condition) but in this case,

Table 2.17. Blade Passage Tone level comparison between the fans with MPP and the regular ducts having different lengths combinations (Case A).

	Blade Passage Tone [dBA]			Blade Passage Tone [dBA]			Blade Passage Tone [dBA]	
OP#	**REG**	**MPP751**	**OP#**	**REG**	**MPP751**	**OP#**	**REG**	**MPP751**
1	21.6	23.3	6	28.7	29.9	11	23.8	24.7
2	24.7	26.7	7	23.5	25.0	12	26.3	25.3
3	27.7	29.0	8	26.1	27.2	13	21.2	20.0
4	23.4	24.5	9	27.8	29.2	14	25.2	22.3
5	25.8	27.4	10	21.4	21.4	15	27.1	23.6

OP# - Operating Condition Points, REG - Unperforated Duct, MPP751 - Duct housing using MPP751

Table 2.18. Overall sound power level comparison between the fans with MPP and the regular ducts having different lengths combinations (Case A).

	Overall Sound Power Level [dBA]			Overall Sound Power Level [dBA]			Overall Sound Power Level [dBA]	
OP#	**REG**	**MPP751**	**OP#**	**REG**	**MPP751**	**OP#**	**REG**	**MPP751**
1	44.5	43.1	6	46.8	44.8	11	45.2	43.3
2	45.5	43.3	7	42.6	41.2	12	47.2	45.2
3	47.2	45.1	8	44.4	42.6	13	46.0	42.9
4	43.4	41.8	9	46.1	44.4	14	45.0	43.4
5	45.0	42.9	10	43.4	41.9	15	46.9	45.2

OP# - Operating Condition Points, REG - Unperforated Duct, MPP751 - Duct housing using MPP751

the MPP duct had a higher blade passage tone than the regular duct but the MPP duct resulted in low overall sound power level. The additional results of all other operating conditions are tabulated in Table 2.19.

By looking at Table 2.19, it can be seen that MPP duct creates less blade passage tones compared to the regular duct at operating conditions from 1 to 6, of which the operating conditions having the relatively high static pressure and low flow rate region in Figure 2.18. The trends are vice versa at operating conditions from 7 to 15. Therefore it can be considered that the MPP duct reduces the blade passage tones more efficiently at relatively low flow rate region with the combination of longer upstream duct length than the upstream region. Which is opposite results from

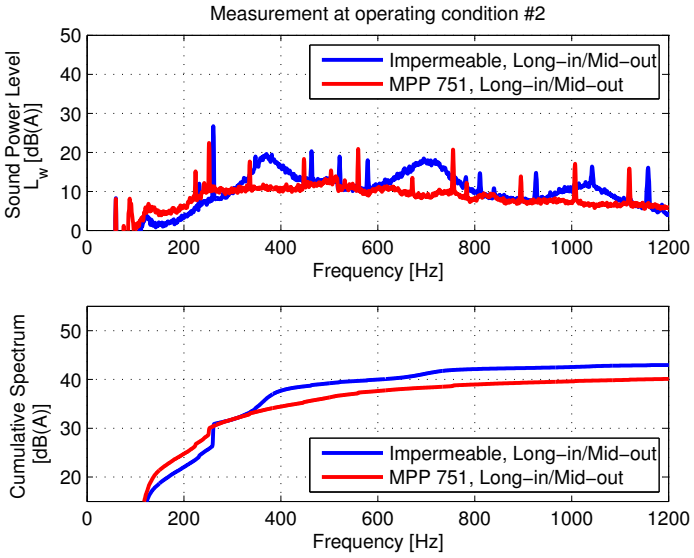

Figure 2.30. Sound power level comparison between the MPP 751 and impermeable duct having different length combinations (CASE B) at operating condition #2.

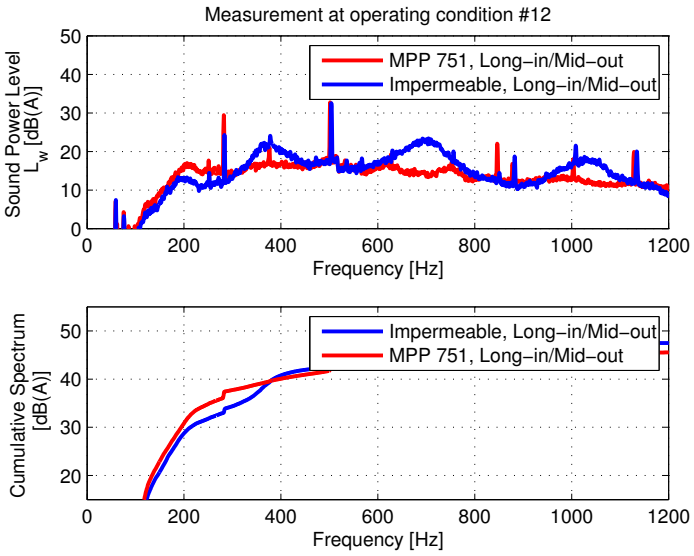

Figure 2.31. Sound power level comparison between the MPP 751 and impermeable duct having different length combinations (CASE B) at operating condition #12.

the case A combination where the MPP duct with shorter upstream duct length combination had shown better attenuation of the blade passage tone at low flow rate operating conditions.

However, the overall sound power levels at all the operating conditions are tabulated in Table 2.20. It can be seen from the table that the MPP duct shows less overall sound power level compare to regular duct except for operating condition 1, 4 and 13. These conditions were created by running the fan at 19V, which is 5V less than the fan's rated voltage, and leaving the opening areas of the plenum described in Figure 2.1 as 4 cm^2, 9 cm^2 and 100 cm^2, respectively. Therefore the rotation speed of the fan becomes lower than manufacturer's rated RPM at these conditions and generates ball bearing noise at 517 Hz. Again, this is the similar results of ball bearing noise which were able to seen from the previous subsection 2.4.2. So the overall sound power levels at these conditions are affected by the physical properties of the fan rather than the duct materials. These phenomena can be clearly visible in Figure 2.32 and Figure 2.33.

Table 2.19. Blade Passage Tone level comparison between the fans with MPP and the regular ducts having different lengths combinations (Case B).

	Blade Passage Tone [dBA]			Blade Passage Tone [dBA]			Blade Passage Tone [dBA]	
OP#	**REG**	**MPP751**	**OP#**	**REG**	**MPP751**	**OP#**	**REG**	**MPP751**
1	23.1	19.7	6	29.7	27.7	11	22.1	27.0
2	26.7	22.4	7	23.8	24.3	12	24.3	29.4
3	29.8	25.2	8	26.4	27.4	13	15.6	27.1
4	24.3	21.5	9	29.0	29.7	14	19.7	30.6
5	26.8	24.7	10	20.0	23.4	15	22.8	33.1

OP# - Operating Condition Points, REG - Unperforated Duct, MPP751 - Duct housing using MPP751

Table 2.20. Overall sound power level comparison between the fans with MPP and the regular ducts having different lengths combinations (Case B).

	Overall Sound Power Level [dBA]			Overall Sound Power Level [dBA]			Overall Sound Power Level [dBA]	
OP#	**REG**	**MPP751**	**OP#**	**REG**	**MPP751**	**OP#**	**REG**	**MPP751**
1	42.3	50.5	6	45.5	43.5	11	46.2	44.3
2	43.8	41.6	7	42.2	41.5	12	48.3	46.5
3	45.7	43.3	8	43.8	42.3	13	44.3	48.7
4	42.1	48.1	9	45.8	44.3	14	43.3	42.0
5	43.6	41.7	10	44.2	42.6	15	45.1	43.9

OP# - Operating Condition Points, REG - Unperforated Duct, MPP751 - Duct housing using MPP751

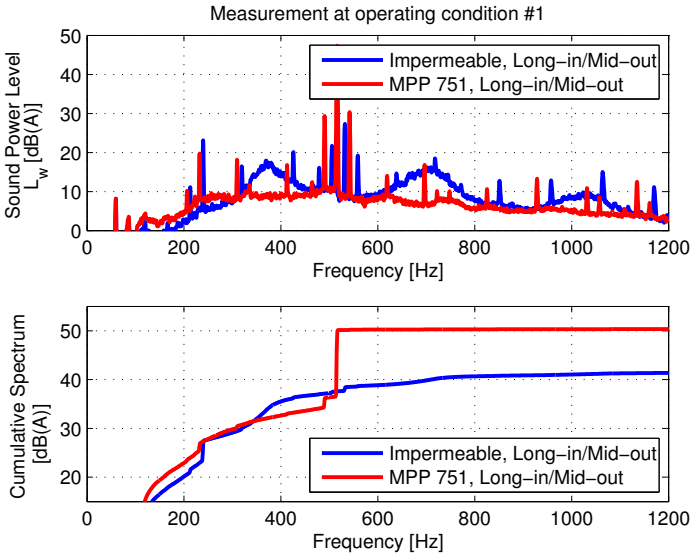

Figure 2.32. Sound power level comparison between the MPP 751 and impermeable duct having different length combinations (CASE B) at operating condition #1.

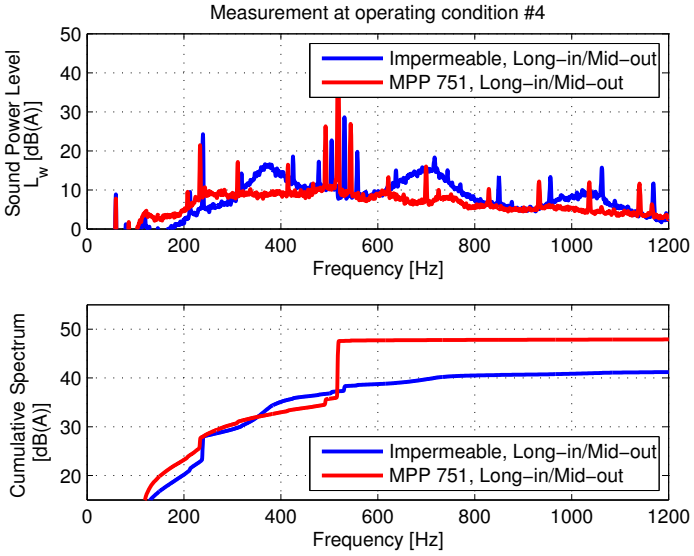

Figure 2.33. Sound power level comparison between the MPP 751 and impermeable duct having different length combinations (CASE B) at operating condition #4.

3. FAN NOISE CONTROL: NOISE FIELD RECONSTRUCTION

In the previous chapter we have seen the acoustical performance of axial fans with various MPP treatments around its housing regions and it could be seen that MPP could lower the blade passage tone of an axial fan and overall sound power level when compared with the same configuration of impermeable housing region treatments. Therefore in this chapter, the noise field of MPP treated axial fan will be studied by using Nearfield Acoustic Holography (NAH) methodology to see how the MPP treatments affect the noise field of the fan.

3.1 Multi-Reference Planar Nearfield Acoustic Holography (NAH)

The sound field of the axial fan used in study was assumed to be a source composed of a number of incoherent sources in order to use multi-reference NAH. Therefore the Singular Value Decomposition (SVD)-based partial field decomposition methodology was adopted to decompose the total sound field of the fan into uncorrelated signals. In order to perform this, the number of references must be equal or larger than incoherent sources in the total field [21].

3.1.1 Singular Value Decomposition(SVD)

To begin with, the relationship between multi-reference source signals and the hologram measurement surface can be considered as following equation:

$$\begin{bmatrix} p_1 \\ p_2 \\ \vdots \\ p_N \end{bmatrix} = \begin{bmatrix} h_{11} & h_{12} & \dots & h_{1M} \\ h_{21} & h_{22} & \dots & h_{2M} \\ \vdots & \vdots & \ddots & \vdots \\ h_{N1} & h_{N2} & \dots & h_{NM} \end{bmatrix} \begin{bmatrix} r_1 \\ r_2 \\ \vdots \\ r_M \end{bmatrix} \tag{3.1}$$

where, p_N represents the Nth signal on the hologram (array) and N is the total number of measurement points on the array surface, r_M represents the Mth reference signals that can be obtained by using reference microphones. Here M is the total number of reference microphones and this number has to be equal or larger than the number of incoherent sources in the total sound field. Equation (3.1) can be written in following form:

$$\mathbf{p} = \mathbf{H}_{pr}\mathbf{r} \tag{3.2}$$

where, $\mathbf{p}$ is an N by 1 matrix, $\mathbf{H_{pr}}$ is an M by N transfer function matrix and $\mathbf{r}$ is an N by 1 matrix. Cross-spectra between the array surface and the reference signals can be written as follow:

$$\mathbf{S_{pr}} = \mathrm{E}\{\mathbf{pr^H}\} \tag{3.3}$$

where, E denotes the expectation operator and the superscript H denotes the Hermitian transpose. Equation (3.2) and Equation (3.3) can be combined into the following equation:

$$\mathbf{S_{pr}} = \mathbf{pr^H} = \mathbf{H}_{pr}\mathbf{S}_{rr} \tag{3.4}$$

where, $\mathbf{S_{rr}}$ represents cross-spectral matrix of reference signals and the latter can be decomposed by using Singular Value Decomposition (SVD) as:

$$\mathbf{S}_{rr} = \mathbf{V}\Lambda\mathbf{V}^{\mathrm{H}} \tag{3.5}$$

where, $\mathbf{V}$ is the M by N unitary matrix and Λ is an N by N diagonal matrix where the Nth diagonal element represents the Nth singular value. By using the above equations the following relations can be obtained:

$$\mathbf{S}_{pp} = \mathbf{H}_{pr}\mathbf{S}_{rp} = \mathbf{H}_{pr}\mathbf{S}_{rr}\mathbf{H}_{pr}^{\mathrm{H}} \tag{3.6}$$

$$\mathbf{H}_{pr} = \mathbf{S}_{rp}^{\mathbf{H}}\mathbf{V}\Lambda^{-1}\mathbf{V}^{\mathrm{H}} \tag{3.7}$$

$$\mathbf{P} = \mathbf{H}_{pr}\mathbf{V}\Lambda^{1/2} = \mathbf{S}_{rp}^{\mathrm{H}}\mathbf{V}\Lambda^{-1/2} \tag{3.8}$$

where, $\mathbf{P}$ in Equation (3.8) represents the partial field vector that was obtained after applying the SVD procedure.

3.1.2 Planar NAH Theory

Once the partial pressure field at $z = z_h$ (z_h is the hologram surface location) is obtained by using SVD, planar NAH theory was applied [42]. If the hologram surface $z_h \leq z_s$ (source surface) then the pressure filed in wavenumber domain can be written as follow:

$$P(k_x, k_y, z_s) = P(k_x, k_y, z_h)e^{ik_z(z_s - z_h)} \tag{3.9}$$

where, k_x, k_y are k_z the x, y, and z wavenumber components in Cartesian coordinate systems. Here k_z can be calculated as:

$$k_z = \begin{cases} \sqrt{k^2 - k_x^2 - k_y^2} & \text{if} \quad k_x^2 + k_y^2 \leq k^2 \\ i\sqrt{k_x^2 + k_y^2 - k^2} & \text{otherwise} \end{cases} \tag{3.10}$$

Also k is the wavenumber defined as $k = \omega/c_0$ and c_0 is the speed of sound in the air. The particle velocity can be obtained as:

$$\dot{W}(k_x, k_y, z_s) = \frac{k_z}{\rho_0 c_0 k} e^{ik_z(z_s - z_h)} P(k_x, k_y, z_h) \tag{3.11}$$

Then, by applying the 2D-inverse Fourier transform, both the pressure and particle velocity field can be obtained.

3.1.3 Wavenumber Filter

In order to remove measurement noise from the results, a wavenumber filter was applied in the wavenumber domain to remove evanescent wave components in the measured signals. If $k_c \geq k$, where k_c is the cut-off wavenumber, the wavenumber filter can be represented as below:

$$W(k_x, k_y) = \begin{cases} 1 - \exp[(\sqrt{k_x^2 + k_y^2}/k_c - 1)/\alpha]/2 & \text{if} \sqrt{k_x^2 + k_y^2} \leq k_{c\leq} \\ \exp[(1 - \sqrt{k_x^2 + k_y^2}/k_c)/\alpha]/2 & \text{otherwise.} \end{cases} \tag{3.12}$$

where, α is the filter slope that is determined from the dynamic range of the measurement system, signal-to-noise ratio (SNR), hologram height, (z_h), and the wavenumber components of a source [42, 43].

3.2 Microphone Array Set-up

Figure 3.1 shows the configurations of the eight-by-six microphones array and the locations of six reference microphones. The gap between each microphone on the array is 10 cm. The fan was located at 15 cm away from the array surface. Figure 3.2 shows the photo of the micophones array and reference microphones set-up.

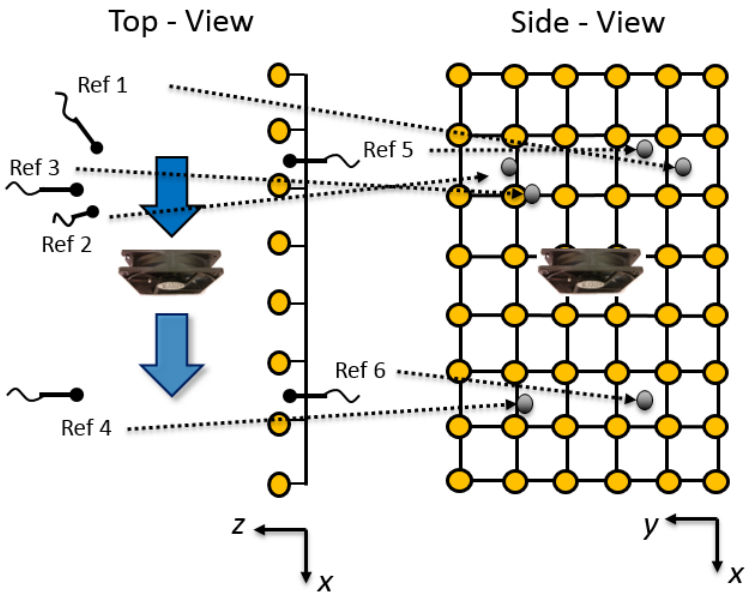

Figure 3.1. Configuration of Microphones array and the of reference microphones.

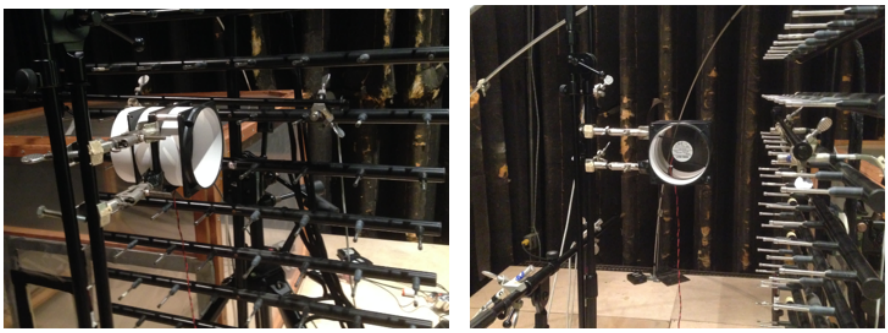

Figure 3.2. Photo of Microphones array and the of reference microphones set-up.

3.3 Acoustic Holography Results

Figure 3.3 shows the six singular value spectra obtained by applying SVD to the six-by-six reference cross-spectral matrix when the regular fan (shown on Figure 2.4) was operated at its rated voltage (24V, 1880 RPM). It can be seen from the figure that the first and second SVD spectra show the dominant first blade passage frequency tone at 282 Hz. However, the first SVD spectrum shows the more dominant harmonic blade passage frequencies, therefore the first SVD was used in obtaining the partial field in this study.

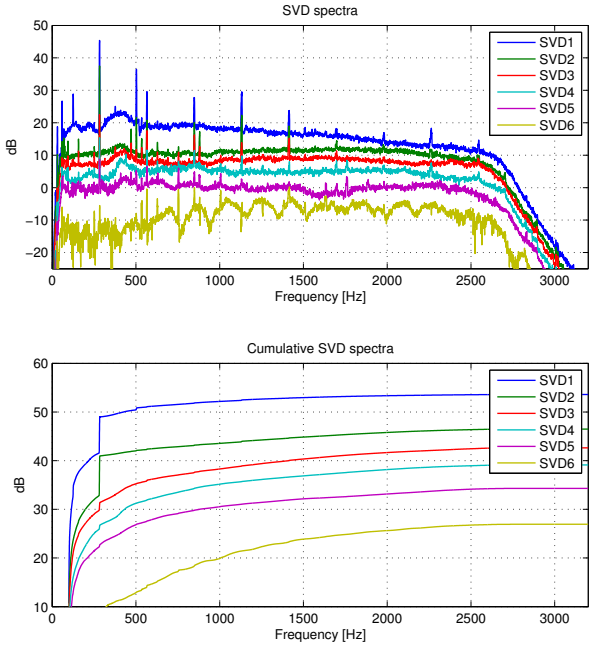

Figure 3.3. Six singular value spectra of regular fan at rated voltage (24V) and rotation speed (1880 RPM).

3.3.1 Results of Axial Fans with Regular Housings

Figure 3.4 shows the 1st SVD spectrum comparison of the fan with a regular housing and the fan with MPP housing, which were discussed in Chapter 2. The

MPP having flow resistance of 751 Rayls was used as the housing material for MPP fan. It can be seen that the 1st blade passage tones are the critical noise sources of these fans with regular housing types.

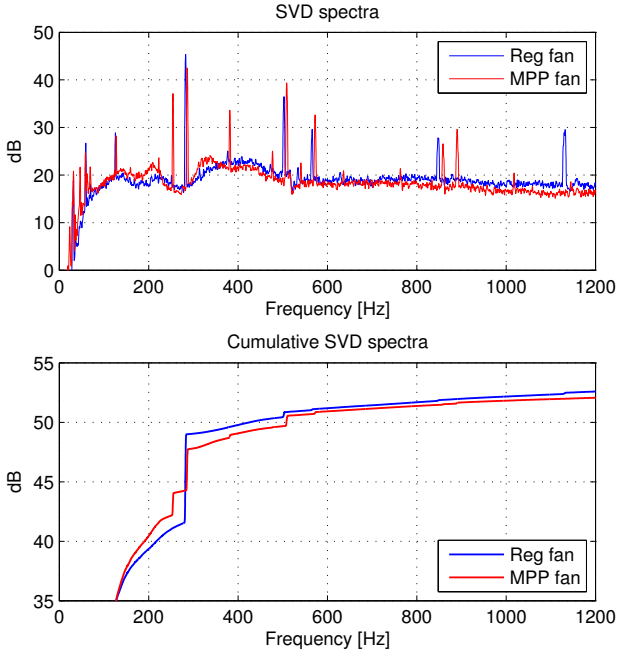

Figure 3.4. 1st singular value spectra of regular fans.

The partial sound fields of the fans with both housing materials at the 1st blade passage frequency are shown on Figure 3.5. The real part of the pressures of both fans form a dipole source around the fans and the magnitudes of the sound fields of both fans in their downstream regions are higher than their upstream regions. However, it can be seen from the figure that the MPP housing suppressed about an average of 4 dB of noise at both upstream and downstream regions.

Figure 3.6 shows the partial sound fields of the fans with regular housing materials at 2nd blade passage frequency. It can be seen from the figures that both the impermeable housing and MPP housing created almost perfect dipole sources but the fan with MPP housing has higher magnitude than the fan with impermeable housing. Although MPP has higher magnitude in the 2nd blade passage tones, this would not

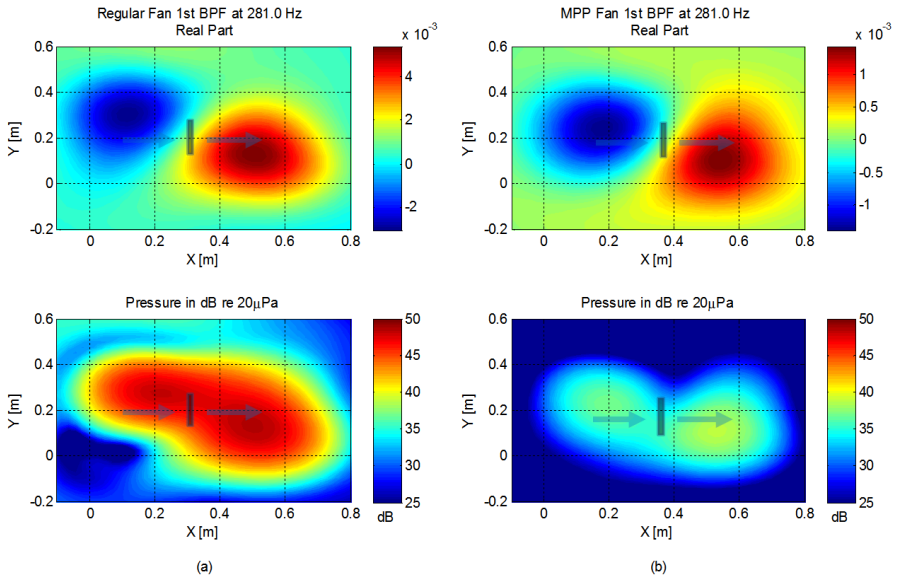

Figure 3.5. Partial fields of regular fan with (a) impermeable housing and (b) MPP housing at 1st blade passage frequency.

affect to the overall sound pressure level since most of the noise affecting the overall level was from the 1st blade passage tone and it was found that MPP housing efficiently suppressed the 1st blade passage tone.

3.3.2 Results of Fans with Short Ducts

Figure 3.7 shows the 1st singular value spectra comparison between the impermeable short duct and the MPP short duct. The lengths of short ducts were the same as the values tabulated in Table 2.6. It can be seen from the figure that the MPP short duct does not perform well in reducing the blade passage tone as we have seen from the previous chapter. However, the MPP short duct starts to suppress noise at the 3rd blade passage tone: therefore, its overall sound pressure level seems to be reduced compared with the impermeable short duct.

Figure 3.8 shows the partial fields of both short duct materials at the 1st blade passage frequency. It can be seen from the figure that in the impermeable short

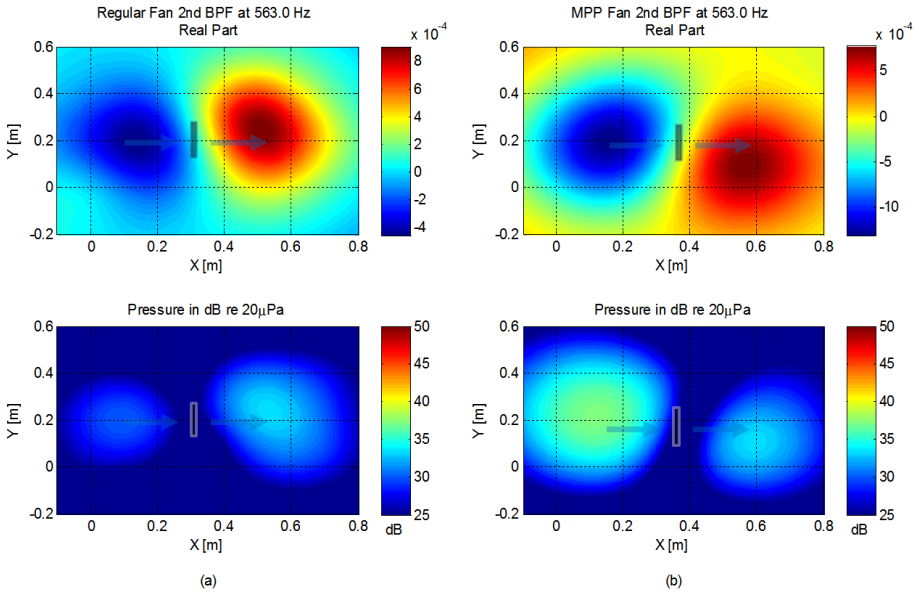

Figure 3.6. Partial fields of regular fan with (a) impermeable housing and (b) MPP housing at 2nd blade passage frequency.

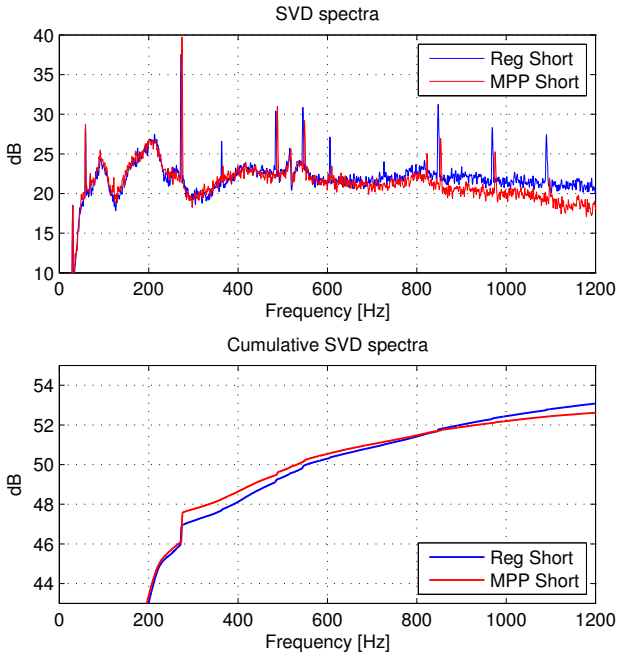

Figure 3.7. 1st singular value spectra of fans with short ducts.

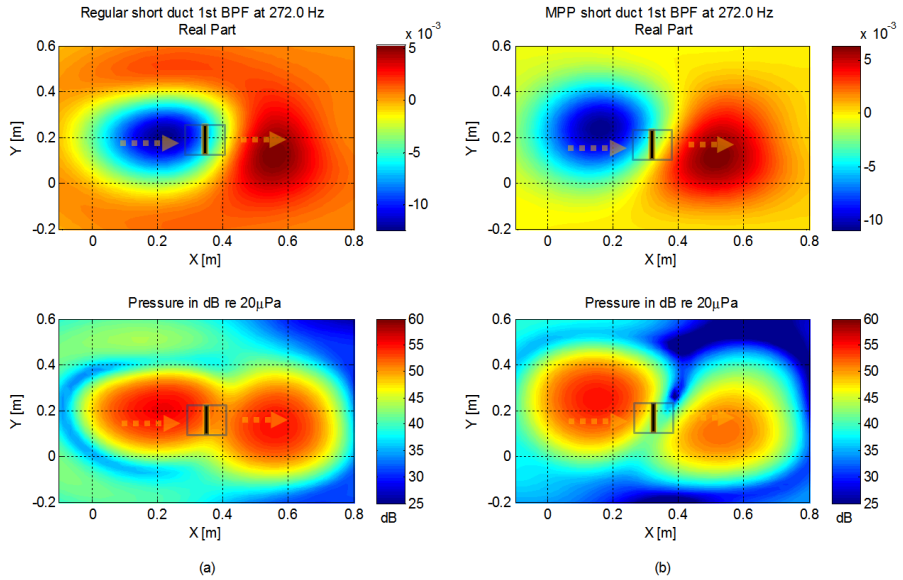

Figure 3.8. Partial fields of fans with short ducts made with (a) impermeable housing and (b) MPP housing at 1st blade passage frequency.

duct case it looks like the noise sources at the upstream and downstream regions are controlled by the duct and concentrated at the flow path created by the duct. On the other hand, the partial field of MPP short duct shows an almost perfect dipole-like source. This can be due to the noise control mechanism of MPP, which is to dissipate the sound energy as the sound wave pass through the perforations.

Figure 3.9 shows the partial fields of the short ducted fans at the 2nd blade passage frequency and they are also showing perfect dipole-like sound sources. However, the MPP duct does not perform well in reducing 2nd blade passage tone here.

Figure 3.10 shows the partial fields of the short ducts at the 3rd blade passage frequency. As shown in Figure 3.7, the MPP short duct starts to perform well in reducing the sound. The noise at the downstream region of MPP duct was reduced whereas the upstream region is where the 3rd blade passage frequency tone was generated.

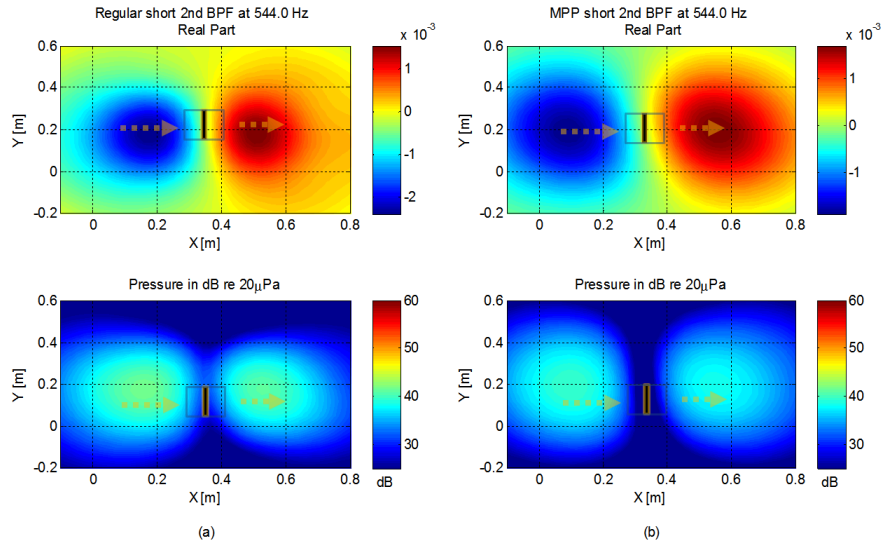

Figure 3.9. Partial fields of fans with short ducts made with (a) impermeable housing and (b) MPP housing at 2nd blade passage frequency.

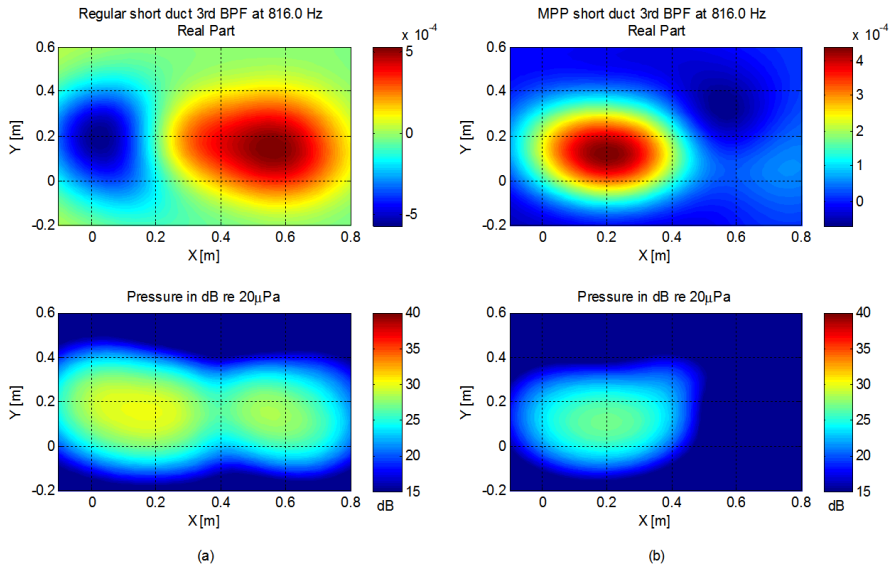

Figure 3.10. Partial fields of fans with short ducts made with (a) impermeable housing and (b) MPP housing at 3rd blade passage frequency.

3.3.3 Results of Fans with Mid Ducts

Figure 3.11 shows the 1st singular value spectra of fans with impermeable mid duct and MPP mid duct. It can be observed from the figure that as the length of the duct become longer, duct modes occurred in impermeable mid duct case whereas those phenomena were suppressed by MPP mid duct as we already discussed in the previous chapter. Moreover, it can be seen that the second and the third humps in the singular value spectra of the impermeable mid duct play critical roles in increasing the overall sound pressure level.

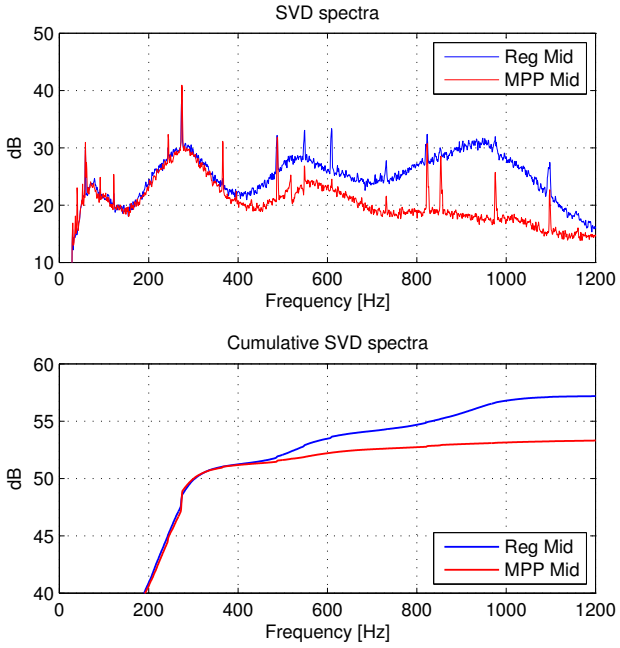

Figure 3.11. 1st singular value spectra of fans with mid ducts.

Figure 3.12 shows the partial fields of fans with mid ducts at the 1st blade passage frequency. Again, it can be seen from the figure that upstream and downstream noise sources of the impermeable mid duct seem to be concentrated in the flow path due to the duct whereas the noise source of the MPP duct is uniformly dissipated around the ducted fan. Figure 3.13 shows the partial fields of the 2nd blade passage frequency

regions for both ducted fans. The noise source of the impermeable mid duct was acted like monopole. It can be considered as if the particle velocity vector fields of the fan and duct mode at this frequency became in phase to each other therefore the sound radiation was maximized at this frequency. However, the MPP duct shows a weak dipole source around the fan since it suppressed the duct mode from Figure 3.11.

Figure 3.14 shows the partial fields of both ducted fans at the broadband frequency region of 947 Hz. This region is where the third hump occured in Figure 3.7. It can be seen from the figure that the impermeable mid duct regained relatively strong dipole compared with MPP duct at this frequency region.

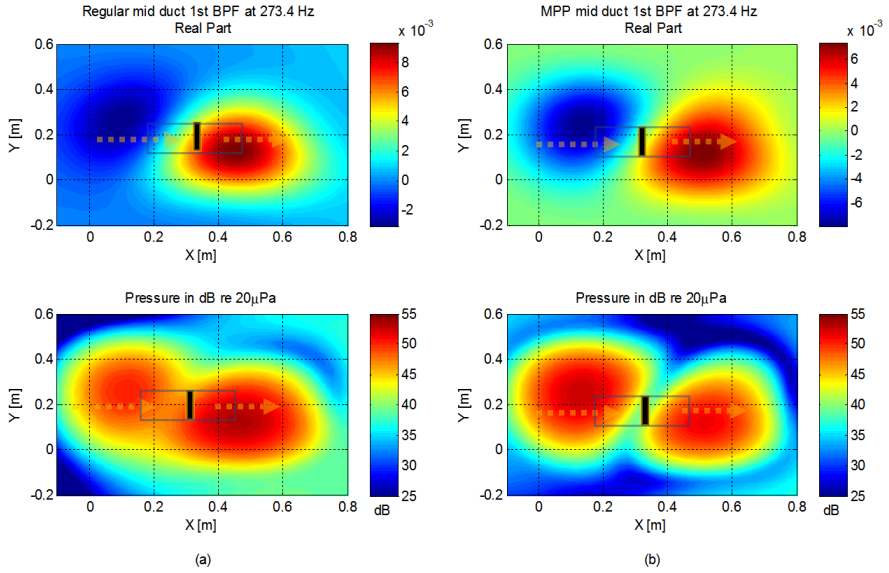

Figure 3.12. Partial fields of fans with mid ducts made with (a) impermeable housing and (b) MPP housing at 1st blade passage frequency.

3.3.4 Results of Fans with Long Ducts

As shown in Figure 3.15, which is the 1st singular value spectra comparison between the fans with impermeable long duct and MPP long duct, the MPP long duct

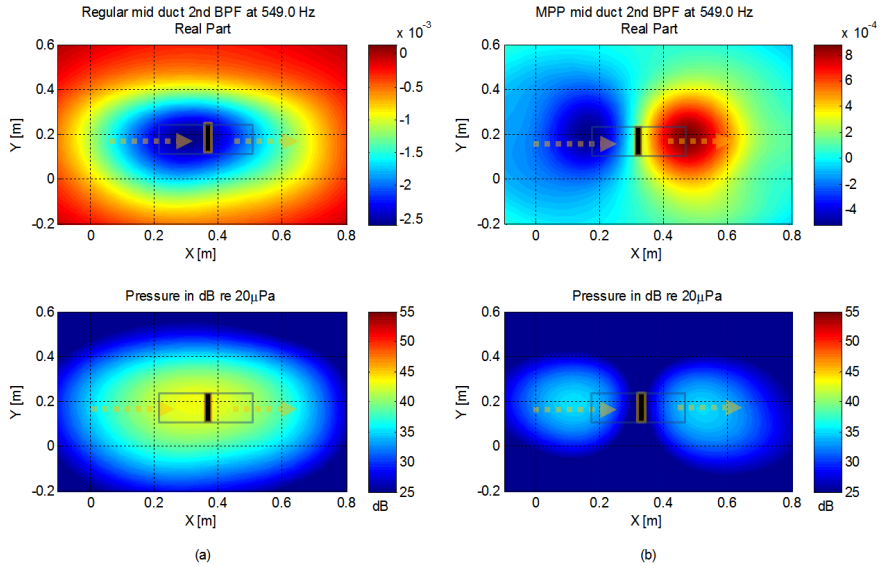

Figure 3.13. Partial fields of fans with mid ducts made with (a) impermeable housing and (b) MPP housing at 2nd blade passage frequency.

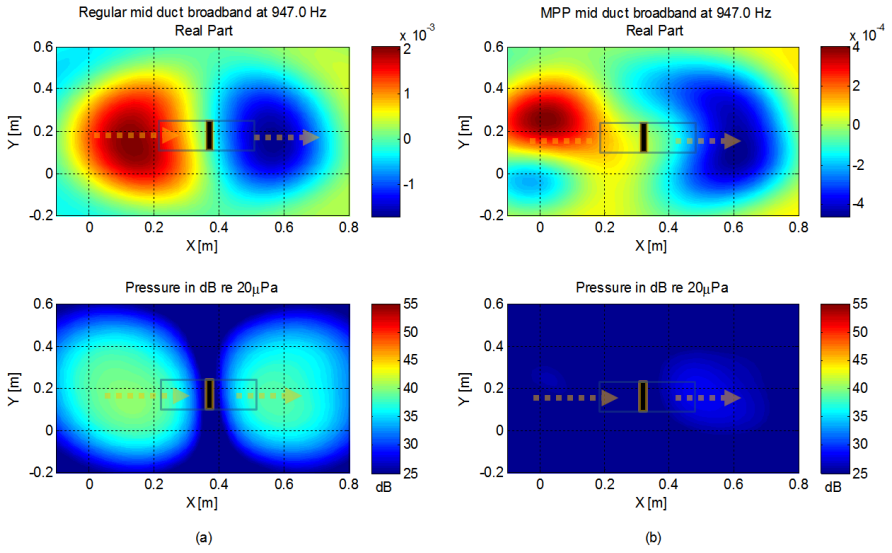

Figure 3.14. Partial fields of fans with mid ducts made with (a) impermeable housing and (b) MPP housing at broadband region at 947Hz.

performs well in both the reduction of blade passage tone and the overall sound pressure level. The duct mode components are also shown in impermeable duct whereas those components are completely removed by using MPP duct.

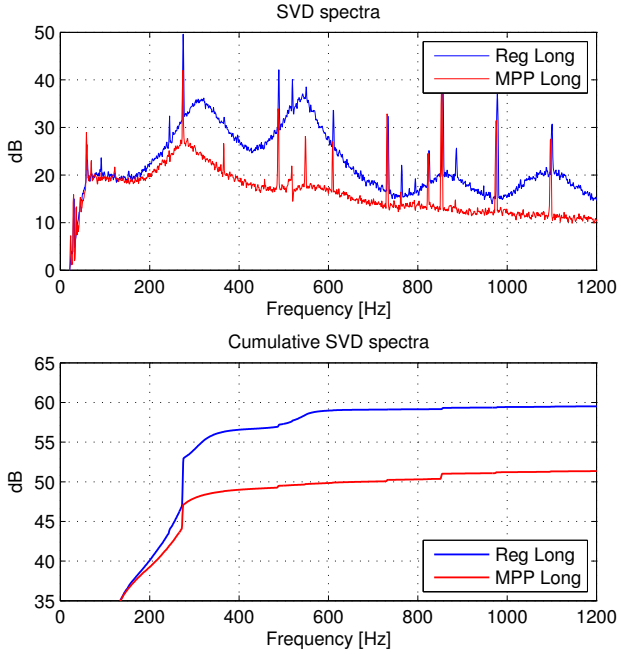

Figure 3.15. 1st singular value spectra of fans with long ducts.

Figure 3.16 shows the partial fields of the fans with long ducts at the 1st blade passage frequency. It can be seen that the noise source of the impermeable duct was again strongly concentrated in the flow path created by the duct. Moreover, it looks like the monopole-like source that were seen in the 2nd blade passage frequency of impermeable mid duct case (Figure 3.13 was shifted to lower frequency in the long duct case). On the other hand, the MPP long ducted fan is still showing weak dipole noise source around the fan, which seems like the long MPP duct is dissipating sound better than the other shorter duct cases since it allows the sound wave to travel longer so that the sound energy has more chance to be dissipated.

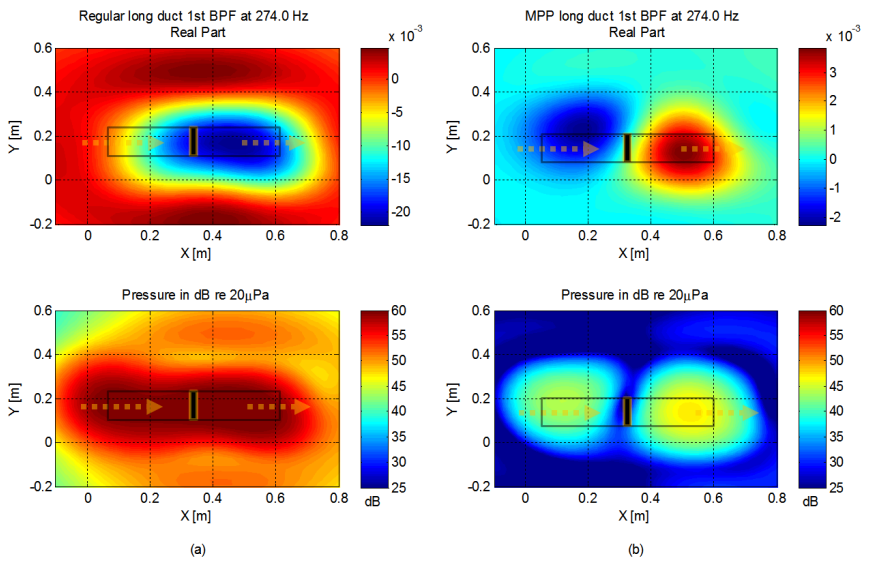

Figure 3.16. Partial fields of fans with long ducts made with (a) impermeable housing and (b) MPP housing at 1st blade passage frequency.

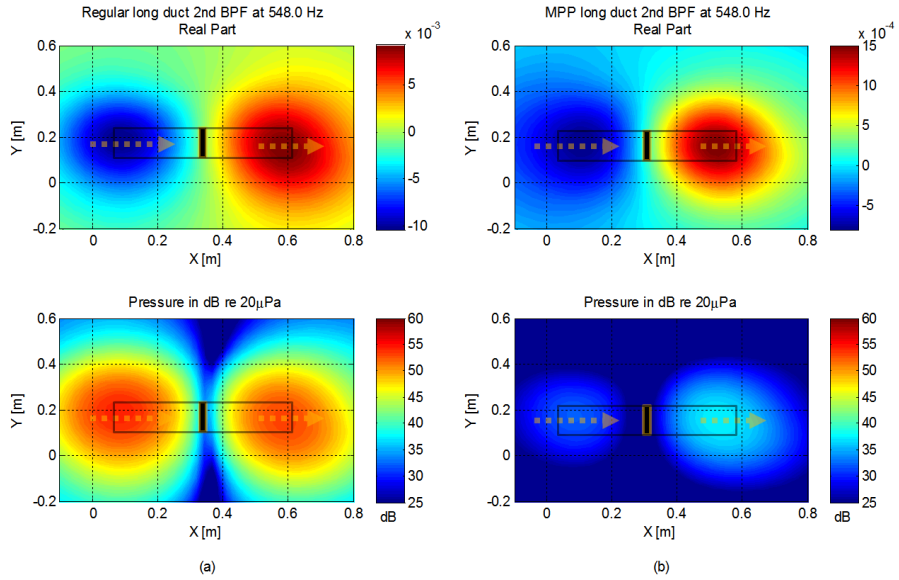

Figure 3.17. Partial fields of fans with long ducts made with (a) impermeable housing and (b) MPP housing at 3rd blade passage frequency.

Figure 3.17 shows the partial fields of long ducted fans at 2nd blade passage frequency. The impermeable long duct has relatively strong dipole source compared to the MPP long duct, which has weaker dipole source around the fan.

4. ACOUSTIC SILENCER DESIGN USING THE MICROPERFORATED PANEL (MPP)

In this chapter, the application of microperforated panels (MPP) into acoustic silencer design will be provided. The MPP will be used as a cylindrical tube lining in the acoustic muffler to connect the inlet-end and the outlet-end of the muffler. Figure 4.1 shows the actual photos of the muffler that was used in this study.

4.1 Description of Muffler

Figure 4.2 shows the designs of the single chamber and the double chamber mufflers that were used in this study. The dual-chamber configuration was created by adding a divider with thickness of 2.0 cm in the location shown in Figure 4.2 (b). The overall length of the silencer was 9.6 cm, and the inner and outer diameters were 2.9 cm and 15.2 cm, respectively. The thickness of the divider used to separate the chambers of the double chamber muffler was 2 cm.

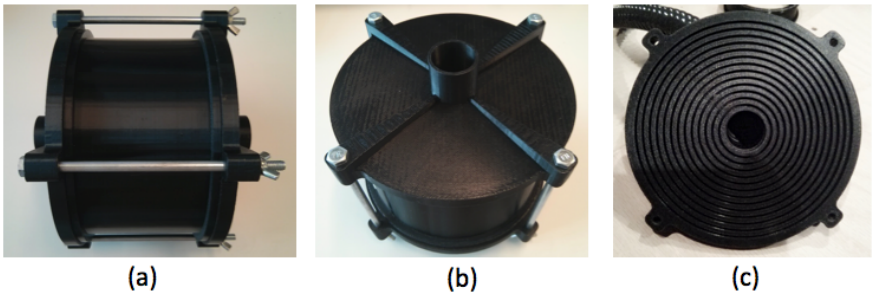

Figure 4.1. (a) Side-view and (b) Top-view of the muffler used in this study. (c) Inside of the muffler. The grooves exist for attaching the cylindrical MPP tube.

Figure 4.3 shows how the MPP lining was placed inside the silencer. The MPP lining had a diameter, d_i, of 2.9 cm, and was directly connected to the inlet and outlet of the silencer as a tube. Figure 4.4 (a) shows a photo of the single-chamber muffler with the MPP lining inserted (and with one end removed), and Figure 4.4 (b) shows the dual-chamber muffler without the MPP lining. The microperforated film used to create the tube lining is shown in Figure 4.5. The properties of the MPP are tabulated in Table 4.1.

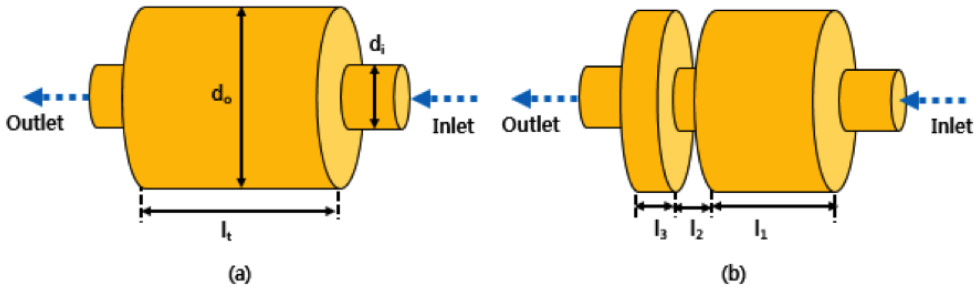

Figure 4.2. Configuration of (a) single-chamber silencer, $d_i = 2.9$cm $d_o = 15.2$cm, and (b) double-chamber silencer, $l_1 = 5.6$cm, $l_2 = 2.0$cm, $l_3 = 2.0$cm, l_1+l_2+l_3=l_t.

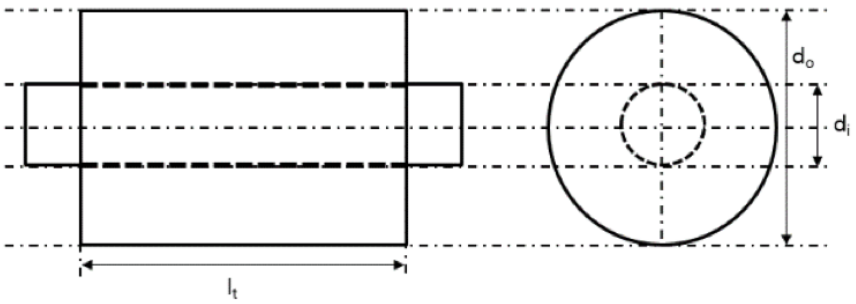

Figure 4.3. MPP tube liner attachment inside the acoustic silencer.

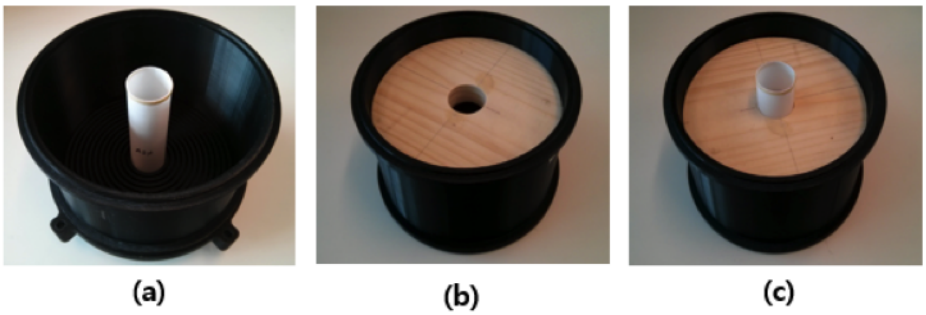

Figure 4.4. (a) Single-chamber with MPP lining tube (b) dual-chamber without MPP lining and (c) with MPP lining .

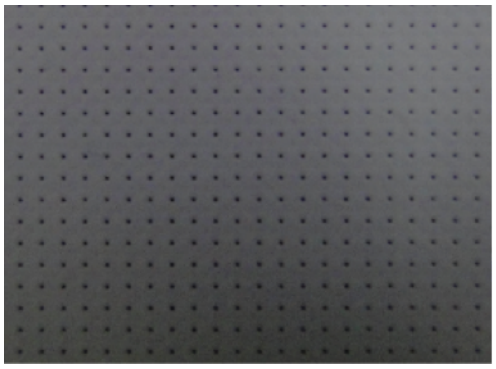

Figure 4.5. The microperforated panel (MPP) with a flow resistance of 454 Rayls.

Table 4.1. Properties of microperforated panel used for lining.

	Hole Diameter [μm]	**Thickness [mm]**	**Flow Resistance [Rayls]**
MPP 454	103.6	0.3	454

4.2 Prediction Model using Finite Element Model (FEM)

4.2.1 Theoretical Modeling of the Microperforated Panel Linings

In this work, the microperforated panel (MPP) was modeled as an equivalent fluid having acoustical properties calculated using the Johnson-Champoux-Allard (JCA) model [5, 6]. The acoustical parameters for the MPP lining, such as perforation

rate, flow resistivity and perforation hole size, were estimated by using the empirical equation that was suggested by Jauoen and Bécot [8]. However, in the present case, the radius of the perforation holes and the flow resistance of the MPPs that were used for the experiment were known values; therefore the porosity was estimated by using the Equation (4.4), below. The diameter of the perforations and the flow resistance of the material are tabulated in the Table 4.1.

The general complex density expression used for the MPP modeling, as given by Johnson and Koplik [5] was

$$\tilde{\rho}_{cs}(\omega) = \frac{\alpha_\infty \rho_0}{\phi}\left[1 - j\frac{\sigma\phi}{\omega\rho_0\alpha_\infty}\sqrt{1 + j\frac{4\alpha_\infty^2\eta\rho_0\omega}{\sigma^2\Lambda^2\phi^2}}\right] \tag{4.1}$$

where, ϕ is perforation rate (i.e., porosity), α_∞ is dynamic tortuosity, σ denotes the flow resistivity (i.e., the flow resistance per unit thickness), η denotes the dynamic viscosity of air, and Λ denotes the viscous characteristic length. If the shape of the perforations is circular, then $\Lambda = r$, the radius of perforation. The dynamic tortuosity, α_∞ in Equation (4.1), was initially suggested by Ingard [44], after which, Atalla and Sgard followed that approach to account for the flow distortion typical of screen perforations [7]. The dynamic tortuosity can be calculated as:

$$\alpha_\infty = 1 + 2\frac{\varepsilon}{h} \tag{4.2}$$

where,

$$\varepsilon = (1 - 1.13\zeta - 0.09\zeta^2 + 0.27\zeta^3)\frac{8r}{3\pi} \text{ and } \zeta = 2\sqrt{\frac{\phi}{\pi}} \tag{4.3}$$

The expression for the static air flow resistivity, σ , is:

$$\sigma = \frac{8\eta}{(\phi r^2)} \tag{4.4}$$

And, as noted above, the latter expression was inverted to yield an estimate for the porosity of the MPP film. Finally, the dynamic bulk modulus of the MPP was calculated as:

$$\tilde{K}(\omega) = \frac{\gamma P_0/\phi}{\gamma - (\gamma-1)\left[1 - j\frac{8\kappa}{\Lambda'^2 C_p \rho_0 \omega}\sqrt{1 + j\frac{\Lambda'^2 C_p \rho_0 \omega}{16\kappa}}\right]^{-1}} \tag{4.5}$$

In Equation (4.5), C_p is the specific heat at a constant pressure, κ is the thermal conductivity of the air, and Λ' denotes the thermal characteristic length of the screen perforations. In this case, it is equal to radius of the perforations, r.

4.2.2 Silencer Modeling using FEM

In this study, the Finite Element Method (FEM) was adopted to model the mufflers. Plane wave methods can be used to calculate the sound attenuation of simple circular expansion mufflers in the frequency range within which only plane waves can propagate within the muffler's expanded section. In that case the power transmission coefficient and the transmission loss, respectively, can be calculated as:

$$T_{\Pi} = \frac{4}{4\cos^2 kL + (s_{ex}/s + s/s_{ex})^2 \sin^2 kL} \tag{4.6}$$

$$\mathrm{TL} = 10\log_{10}\left(\frac{1}{T_{\Pi}}\right) \tag{4.7}$$

where, T_{Π} represents the power transmission coefficient, k represents the wavenumber, L is the length of the expanded section of the muffler, s is the tube cross-sectional area upstream and downstream of the muffler, and s_{ex} is the cross-sectional area of the expanded section.

However, at higher frequencies, higher order modes can propagate in the expanded section, which generally results in a reduction of sound attenuation [26]. This phenomenon can be clearly seen in Figure 4.6, which shows the transmission loss of the

simple expansion muffler illustrated in Figure 4.2. At 2751 Hz, the cut-on frequency of the first radial mode in the expanded section, the transmission loss is reduced in both the measurement and FEM results: the analytical, plane wave solution cannot capture this phenomena. Thus, the finite element method was used to calculate all the results shown in following sections.

The two acoustical parameters defining the equivalent fluid model of the MPP, i.e., the density and bulk modulus of the microperforated panel were calculated by using the equations that were described in the previous section. Those properties were then used in the commercial software ABAQUS^{TM} to model the microperforated panel lining in the FEM simulation model. Figure 4.7 (a) shows the CAD model of the expansion muffler used in this study. Figure 4.7 (b) is the finite element model of the air-filled interior of the chamber. Figure 4.7 (d) is the finite element model of the MPP tube lining and the obtained density and bulk modulus properties were implemented in this MPP model. The acoustic field in the FEM model satisfies the following Helmholtz equation [45]:

$$\nabla \cdot \left(-\frac{\nabla p}{\rho_0} \right) - \frac{\omega^2 p}{c^2 \rho_0} = 0 \tag{4.8}$$

where, p is the steady-state sound pressure in the duct and within the muffler, and c is the speed of sound in air.

Figure 4.8 shows the FE modeling of the muffler with the MPP tube lining. The muffler in the figure is a portion of the full model described in Figure 4.7 (b). The portion is about a 3.6 degree slice in the circumferential direction. Figure 4.8 (a) is the side view of the muffler with the MPP and (b) is a close-view of the MPP modeling. Air backing area exists to describe the air gap, which is created when the real MPP is attached to the groove of the muffler described in Figure 4.1 (c). These parts were connected using "surface tie connection controller" embedded in ABAQUS^{TM}.

In the FEM model, the mesh controller that is embedded in ABAQUS^{TM} was used. The combination of acoustical wedge-shaped elements and acoustical tetrahedral-

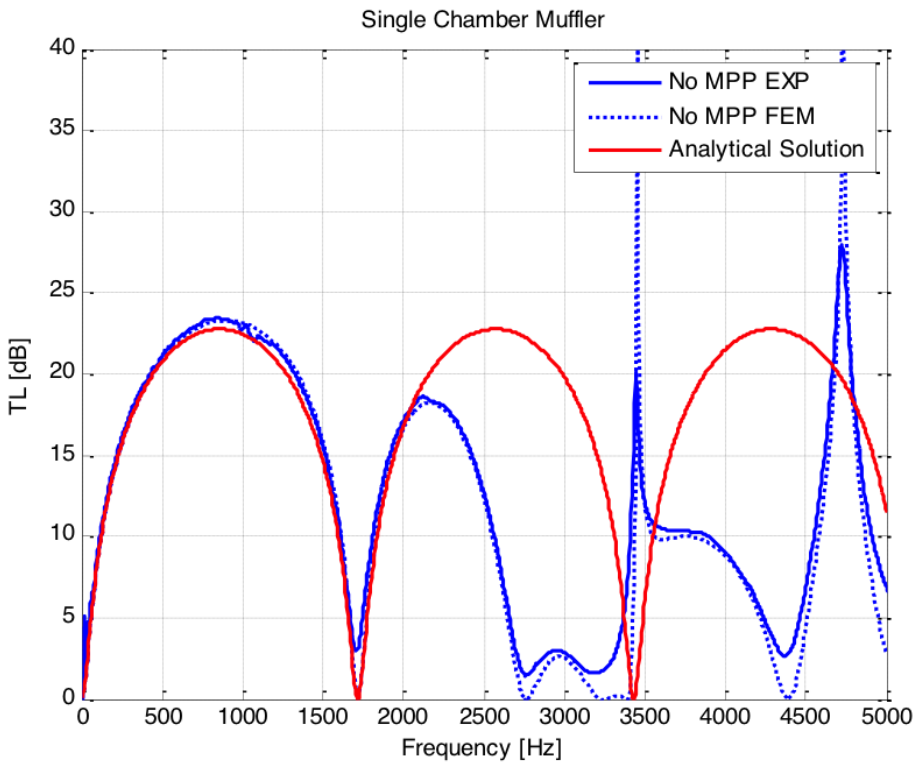

Figure 4.6. The transmission loss results comparisons among the measurement, the FEM simulation, and the analytical, plane wave solution.

shaped elements were used in the muffler modeling. In the MPP FEM model, periodic rigid boundary conditions were implemented within the cross-section of the MPP layer to prevent transmission through the equivalent fluid layer in the axial direction: i.e., to make the MPP lining locally reacting. Figure 4.9 shows how the rigid boundaries were added to the model to create the local reaction characteristics of the MPP in the FE model. Figure 4.9 (a) shows the rigid cut created in the circumferential direction of the MPP tube lining. This rigid section is created in the middle of every 3.6 degree slice of the MPP tube. Figure 4.9 (b) shows the rigid sections created in the axial (wave propagation) direction. These rigid cuts were made in every 0.012 m to create eight sections in the MPP cylindrical tube. At these rigid boundaries, and

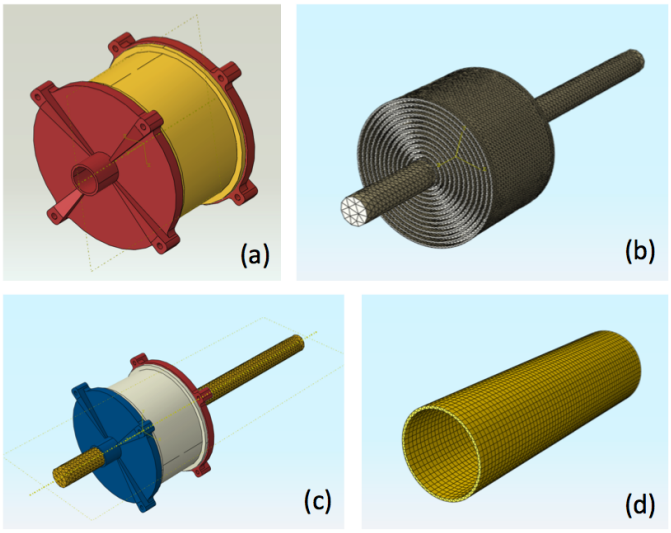

Figure 4.7. The FEM model of (a) the silencer, (b) air inside the chamber, (c) full muffler model and (d) MPP tube modeling.

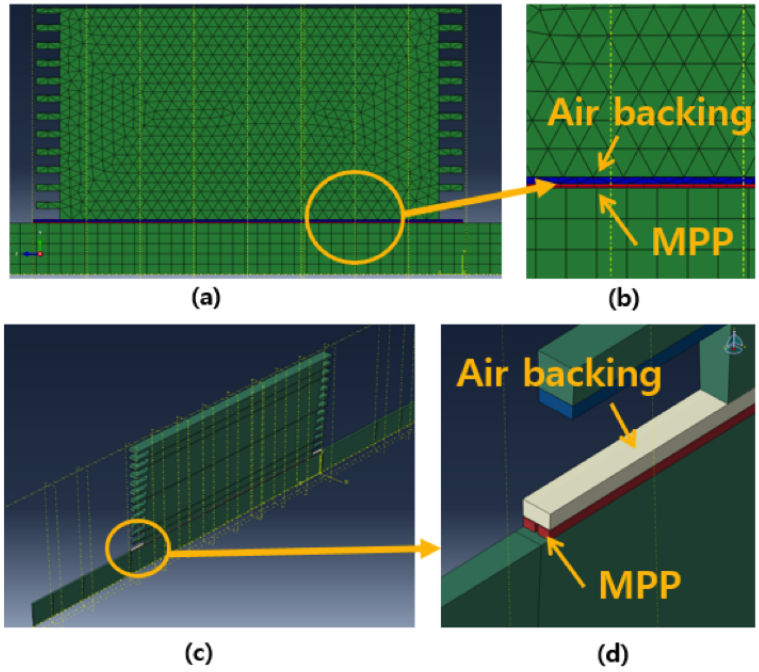

Figure 4.8. Cross-sectional view of FEM modeling of both the muffler and the MPP.

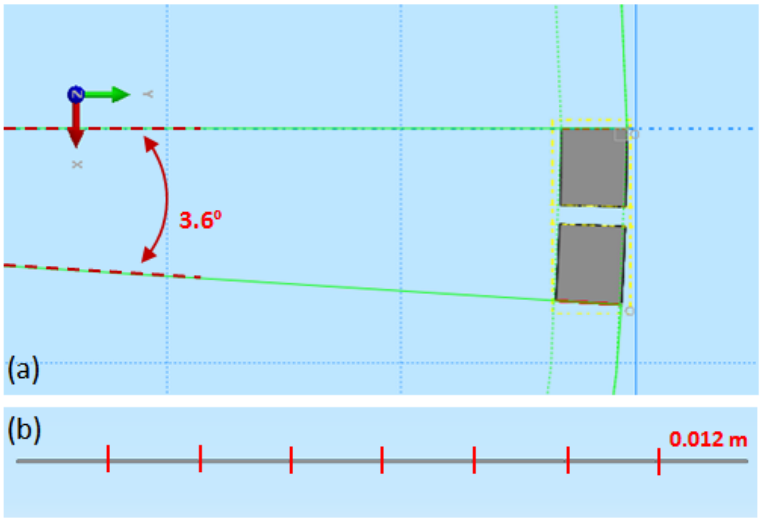

Figure 4.9. Cross-sectional view of FEM modeling of both the muffler and the MPP.

at all other surfaces within the muffler, the hardwall boundary condition was applied:

$$\left(-\frac{\nabla p}{\rho_0}\right) \cdot \mathbf{n} = 0 \tag{4.9}$$

where, $\mathbf{n}$ is the normal direction vector.

At the downstream end of the FEM model, the tube section was anechoically terminated by applying the following condition [45]:

$$\nabla \cdot \left(-\frac{\nabla p}{\rho}\right) = -p\frac{i\omega}{\rho_0 c} \tag{4.10}$$

Because of the anechoic termination, the transmission loss of the simulation model could be calculated by using a three-point method as shown in Figure 4.10, which is the schematic configuration of the transmission loss calculation. In that approach,

$$p_1 = p_i e^{ikx_1} + p_r e^{-ikx_1} \tag{4.11}$$

$$p_2 = p_i e^{ikx_2} + p_r e^{-ikx_2} \tag{4.12}$$

where, p_1 and p_2 are the pressures at two points in the inlet pipe of the muffler, x_1 is the distance of the first measurement point from the inlet-end and x_2 is the distance of the second measurement point from the inlet-end. By solving Equation (4.11) and Equation (4.12), one obtains:

$$p_i = -\frac{1}{2i \sin k(x_2 - x_1)} [p_1 e^{-ikx_2} - p_2 e^{-ikx_1}] \tag{4.13}$$

Then, the transmission loss of the muffler can be calculated as:

$$\mathrm{TL} = 20\log_{10}\left\{\frac{|p_i|}{|p_3|}\right\} + 10\log_{10}\left(\frac{S_i}{S_o}\right) \tag{4.14}$$

where, S_i and S_o are the inlet and outlet tube areas (identical in this case), respectively, and p_3 is the pressure evaluated in the downstream, anechoically terminated duct section.

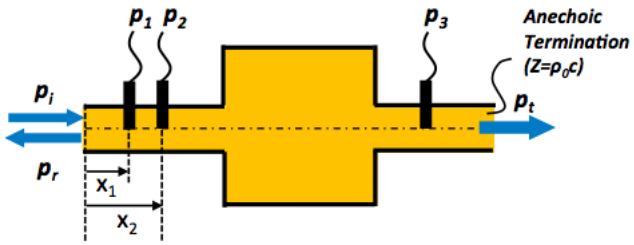

Figure 4.10. The configuration describing the transmission loss calculation using three-point measurement.

Figure 4.11 describes each steps in the modification of the MPP FEM model. Figure 4.11 (a) shows the regular MPP model, (b) shows the rigid boundary conditions were applied only in the axial direction of the MPP tube lining and (c) shows that the rigid boundary conditions were applied in both the axial and circumferential direction of the MPP tube lining.

Figure 4.12 shows the transmission loss results of the different MPP FE models and measurements. The experimental results were obtained by following the measurement procedure which will be described in the next section. 'MPP 454 FE regular model' in the results referred to the simple FE model without any local reaction modification shown in Figure 4.11 (a).

'LR model 1' and 'LR model2' in the figure indicate the simulation model shown in Figure 4.11 (b) and (c), respectively. 'LR model 1' did not make any difference from the 'Regular model' in the transmission loss results.The rigid boundary section that were added in the wave propagation direction helped the FE model to be closely matched with the measured result. The conspicuous improvement in the 'LR model 2' from the 'LR model 1' and the regular model is at the 2nd lobe of the transmission loss, where the 'LR model1' and the regular model made about a 4 dB difference at the highest peak. 'LR model 2' also caused the prediction model to show good agreement in the 1st lobe region of the transmission loss. 'LR model 1' and 'regular model' were 2 dB higher from the measurement result but 'LR model 2' shows reasonable agreement with the measured transmission loss results.

Figure 4.13 shows the transmission loss comparison results between the proposed locally reacting MPP model and the rigid porous MPP model without dividers. The blue line in the figure is the measured transmission loss of the prototype muffler with the MPP having 454 Rayls flow resistance. The solid green line is the rigid porous MPP model without the internal rigid boundaries, which was modeled using ABAQUS^{TM}, and the light green dotted line shows the result of the same MPP system, but modeled using COMSOL^{TM}. The two codes gave essentially identical results. It can be seen that the MPP model without internal boundaries predicts a

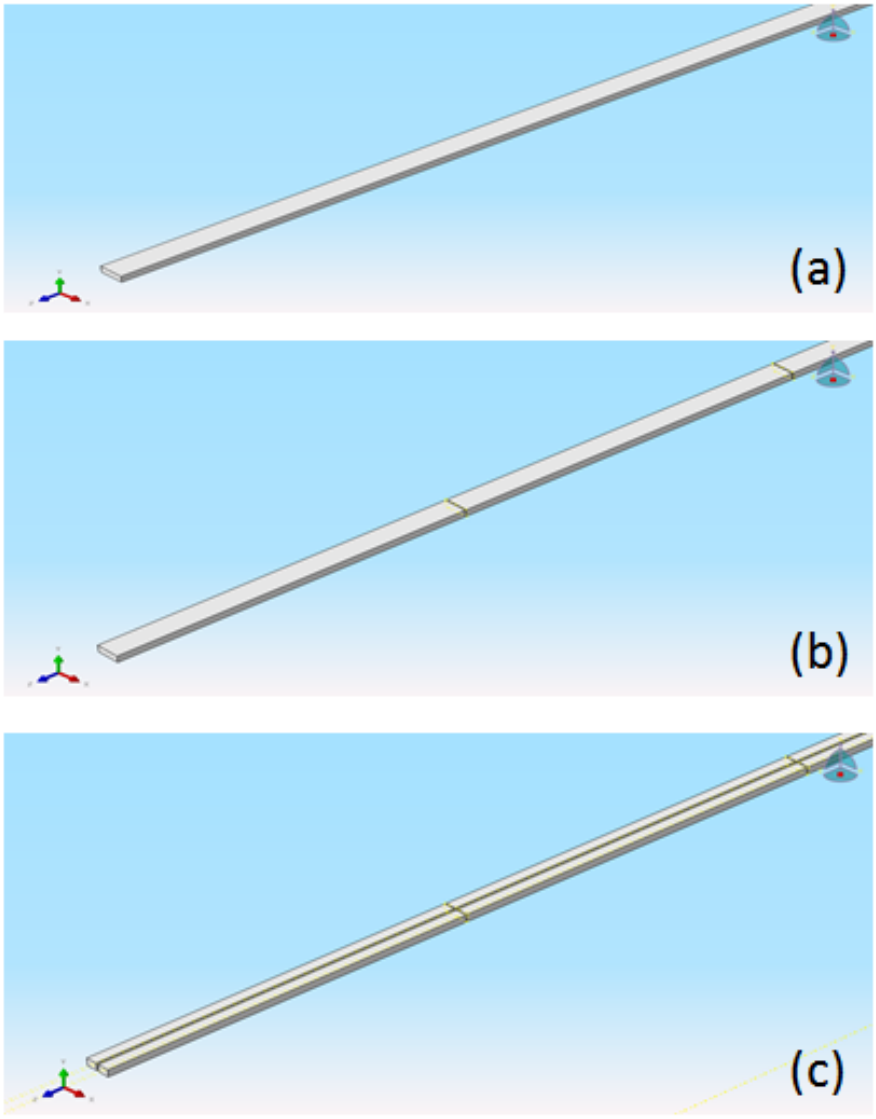

Figure 4.11. (a) Regular MPP model, (b) Local reaction model 1: MPP model modified using rigid boundary conditions in axial direction and (c) Local reaction model 2: boundary conditions in both the axial and circumferential directions.

lower transmission loss peak at the second lobe than was measured. On the other hand, the results of the model with internal boundaries, plotted in red, show good agreement at the peak level. It can be concluded that the use of the internal bound-

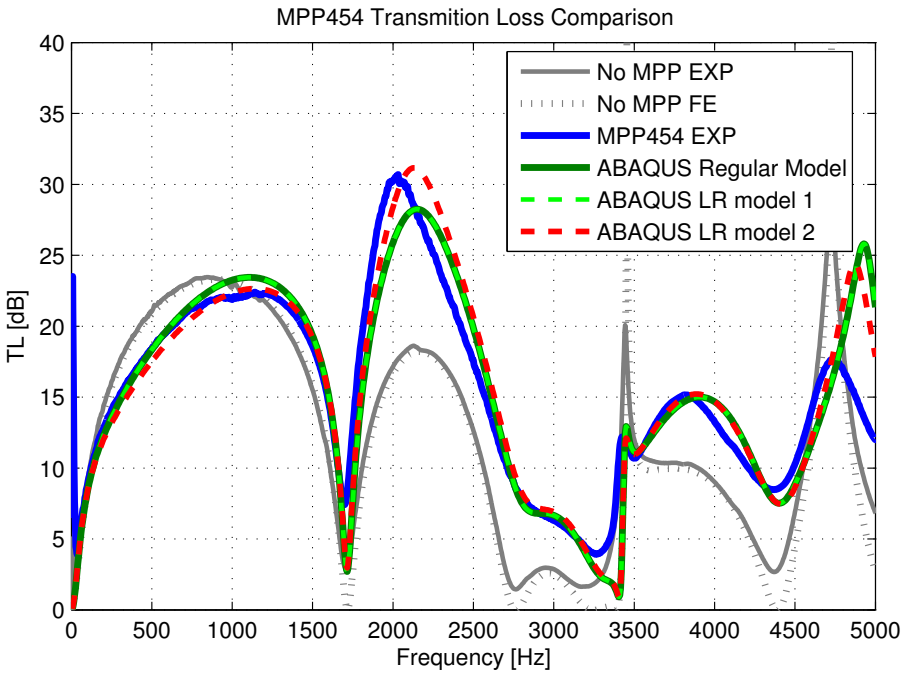

Figure 4.12. Cross-sectional view of FEM modeling of both the muffler and the MPP.

aries to create an effectively locally reacting MPP results in more precise predictions than the model without internal boundaries, although the differences are not large.

In order to validate the suggested FE model technique for the MPP, a different MPP with a lower flow resistance was used as the tube lining in the muffler. Figure 4.14 shows another example transmission loss comparison results of the muffler using MPP tube liner with 273 Rayls of flow resistance. Again, the prediction was made using proposed methodology with rigid boundary sections to create a locally reacting MPP. It can be seen from the figure that the predicted transmission loss shows good agreement with the measured transmission loss.

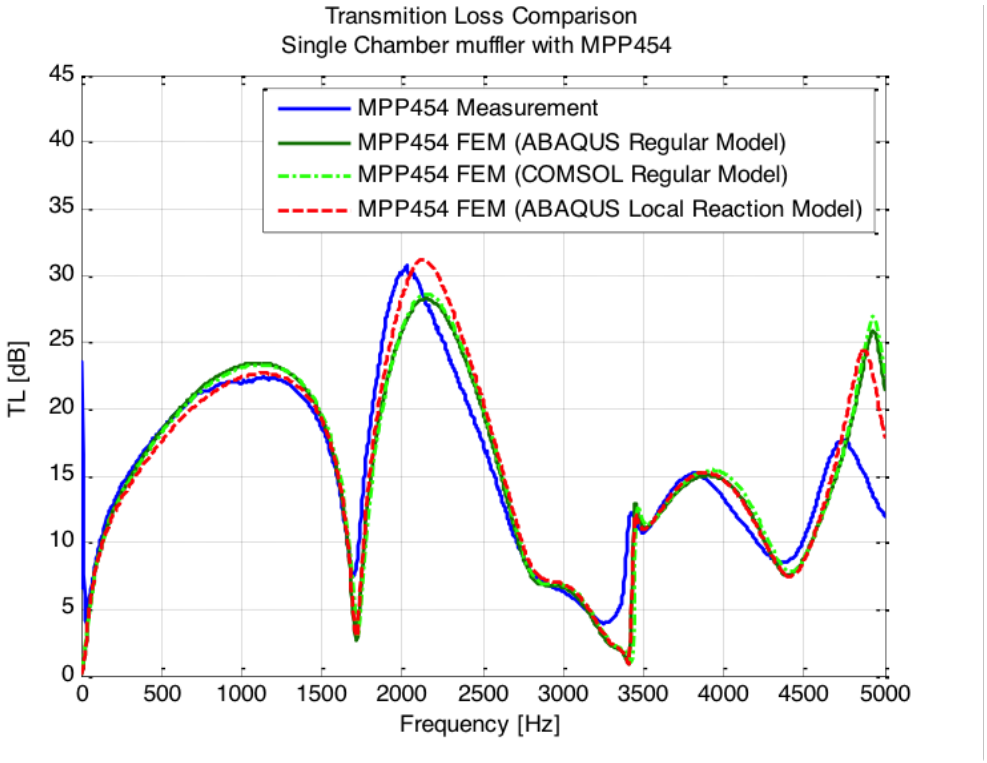

Figure 4.13. The transmission loss comparison between the MPP model without internal rigid boundaries and the proposed MPP model with internal rigid boundaries.

4.3 Experimental Validation Procedure

4.3.1 Standing Wave Tube Set-up

The acoustic attenuation of the silencers that were used in this study was measured using a standing wave tube. The transmission loss of the silencer was calculated using a four-microphone measurement following the procedure described in ASTM E 2611-09.17 When using the four-microphone measurement to determine the transmission loss, the two-load method was used: i.e., measurements were made with two different tube terminations. Figure 4.15 shows a picture of the silencer mounted between the upstream and downstream sections of the standing wave tube.

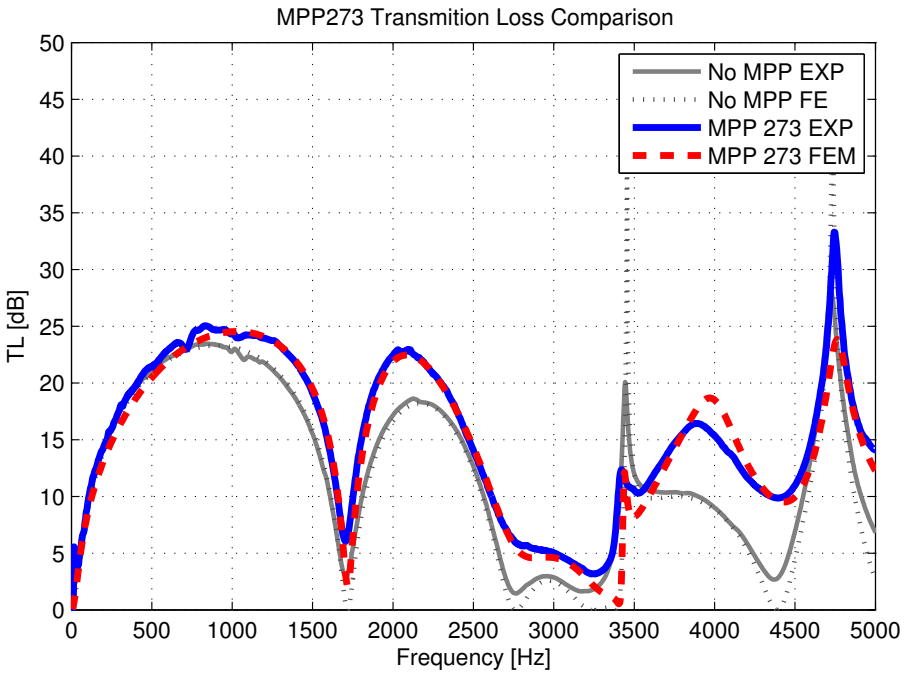

Figure 4.14. Cross-sectional view of FEM modeling of both the muffler and the MPP.

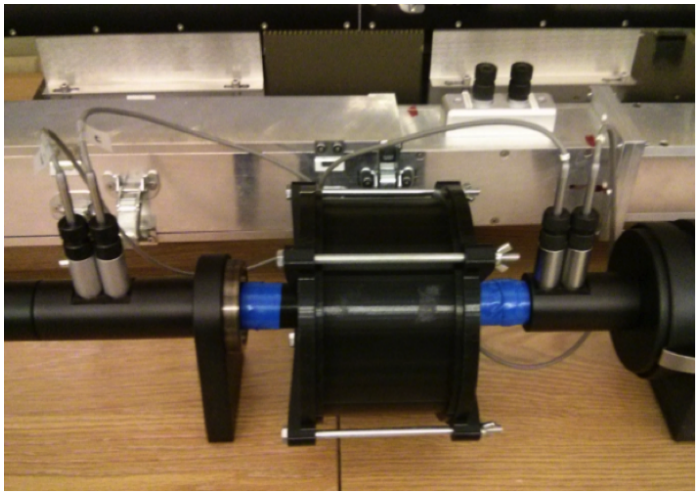

Figure 4.15. The silencer mounted in the middle of the standing wave tube when measuring the transmission loss using the 4-microphone measurement technique.

4.3.2 Transmission Loss Calculation using Four-Microphone Measurement

Figure 4.16 shows the configuration of the standing wave tube for the four-microphone measurement using the two-load method. In the two-load method, a nearly anechoic termination was used as one of two loads by adding sound absorbing material at the termination end, and a rigid termination was used as the other load case.

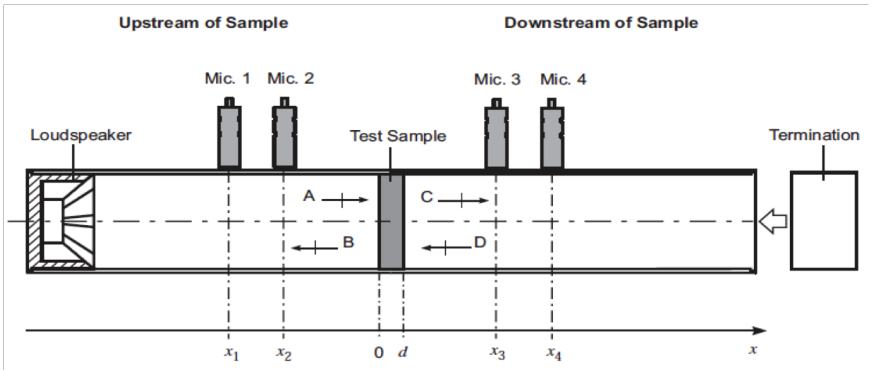

Figure 4.16. Standing wave tube configuration using 4-microphone and 2-load method.

The transmission loss of the muffler can be calculated from the transfer matrix calculation.

$$\begin{bmatrix} P \\ V \end{bmatrix}_{x=0} = \begin{bmatrix} T_{11} & T_{12} \\ T_{21} & T_{22} \end{bmatrix} \begin{bmatrix} P \\ V \end{bmatrix}_{x=d} \tag{4.15}$$

The components in the transfer matrix can be obtained from the standing wave tube measurement shown in the figure, where, P is the complex acoustic pressure and V is the complex particle velocity. Then the complex pressures and the particle velocities at the front and back of the sample is as follow:

$$P|_{x=0} = A + B \tag{4.16}$$

$$P|_{x=d} = Ce^{-jkd} + Be^{jkd} \tag{4.17}$$

$$V|_{x=0} = \frac{A - B}{\rho_0 c} \tag{4.18}$$

$$V|_{x=d} = \frac{Ce^{-jkd} + Be^{jkd}}{\rho_0 c} \tag{4.19}$$

where, ρc is the characteristic impedance of air. Here A, B, C and D are plane wave component amplitude and these plane wave components can be calculated from the following relations:

$$P_1 = Ae^{-jkx_1} + Be^{jkx_1} \tag{4.20}$$

$$P_2 = Ae^{-jkx_2} + Be^{jkx_2} \tag{4.21}$$

$$P_3 = Ce^{-jkx_3} + De^{jkx_3} \tag{4.22}$$

$$P_4 = Ce^{-jkx_4} + De^{jkx_4} \tag{4.23}$$

Since the two-load method is adopted in the transmission loss calculation in this study, it is required to measure P_1, P_2, P_3 and P_4 at each load case. Then, we can calculate the transfer matrix components T_{11},T_{12},T_{21} and T_{22} in Equation (4.15) by using the following equations:

$$T_{11} = \frac{P^{(a)}|_{x=0} V^{(b)}|_{x=d} - P^{(b)}|_{x=0} V^{(a)}|_{x=d}}{P^{(a)}|_{x=d} V^{(b)}|_{x=d} - P^{(b)}|_{x=d} V^{(a)}|_{x=d}} \tag{4.24}$$

$$T_{12} = \frac{-P^{(a)}|_{x=0} P^{(b)}|_{x=d} - P^{(b)}|_{x=0} P^{(a)}|_{x=d}}{P^{(a)}|_{x=d} V^{(b)}|_{x=d} - P^{(b)}|_{x=d} V^{(a)}|_{x=d}} \tag{4.25}$$

$$T_{21} = \frac{V^{(a)}|_{x=0} V^{(b)}|_{x=d} - V^{(b)}|_{x=0} V^{(a)}|_{x=d}}{P^{(a)}|_{x=d} V^{(b)}|_{x=d} - P^{(b)}|_{x=d} V^{(a)}|_{x=d}} \tag{4.26}$$

$$T_{22} = \frac{-P^{(b)}|_{x=d} V^{(a)}|_{x=0} + P^{(a)}|_{x=d} V^{(b)}|_{x=0}}{P^{(a)}|_{x=d} V^{(b)}|_{x=d} - P^{(b)}|_{x=d} V^{(a)}|_{x=d}} \tag{4.27}$$

where, a and b denotes each termination used for two-load measurement method. Then, the pressure transmission coefficient and reflection coefficients for the case of an anechoic termination, T_a and R_a, respectively, can be calculated as following:

$$T_a = \frac{2e^{jkd}}{T_{11} + \frac{T_{12}}{\rho_0 c} + \rho_0 c T_{21} + T_{22}} \tag{4.28}$$

$$R_a = \frac{T_{11} + \frac{T_{12}}{\rho_0 c} - \rho_0 c T_{21} - T_{22}}{T_{11} + \frac{T_{12}}{\rho_0 c} + \rho_0 c T_{21} + T_{22}} \tag{4.29}$$

The normal incidence transmission loss of a sample can be calculated as:

$$TL = 10\log\frac{1}{|T_a|^2} \tag{4.30}$$

4.4 Comparison of Results

4.4.1 Single Chamber Muffler with MPP Lining

Figure 4.17 shows the transmission loss results for the single-chamber silencer with and without the MPP lining. The solid line in each case represents the FEM prediction result and the dotted line shows the corresponding measurement result. It can be seen from the figure that the FEM results match well with the measurement results in both cases. The addition of the MPP lining tube increased the acoustic attenuation performance significantly in the region between 1700 Hz and 3400 Hz. In addition, in the frequency range from 3700 Hz to 4500 Hz, the attenuation was increased by about 5 dB by using the MPP lining.

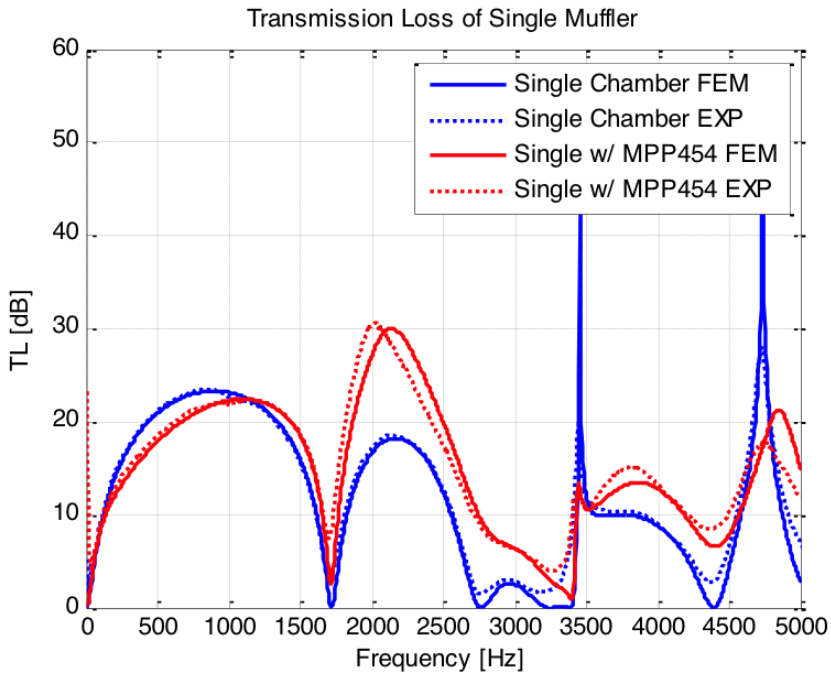

Figure 4.17. The transmission loss comparison between the single-chamber silencer with and without the MPP lining.

4.4.2 Dual Chamber Muffler with MPP Lining

Figure 4.18 shows the comparison of the single-chamber and the double-chamber silencer cases. The FEM prediction for the double-expansion chamber case also shows reasonable agreement the measurements. The first 'lobe' that appeared in the single-expansion chamber case became smaller and moved to the low frequency region in the double-chamber case, and the second 'lobe' became broader. The transmission loss in the frequency region between 500 Hz and 2600 Hz was also significantly improved in the double-expansion chamber case.

Figure 4.19 shows the sound attenuation performance of the double-chamber silencer when the MPP lining tube was fitted. It can be seen from that figure that the transmission loss at 480 Hz was improved by using the MPP lining, although the transmission loss in the frequency region from 500 Hz to 2800 Hz was reduced to 30 dB at most. Note especially that the transmission loss near 4600 Hz for the

double-expansion chamber without the MPP lining was almost 0, whereas the sound attenuation result in that region was improved by almost 10 dB by the addition of the MPP lining.

4.4.3 Single Chamber Muffler with Double Layered MPP Linings

Since the benefit of using a MPP lining could be clearly seen in the previous results, the addition of one more MPP lining was also studied. Figure 4.21 shows the modified configuration in which two MPP layers were used. The same MPP that was used for a single layer silencer was used for the additional MPP lining. Figure 4.22 shows a photo of the double-layer MPP lining mounted in the single-chamber and dual-chamber silencers.

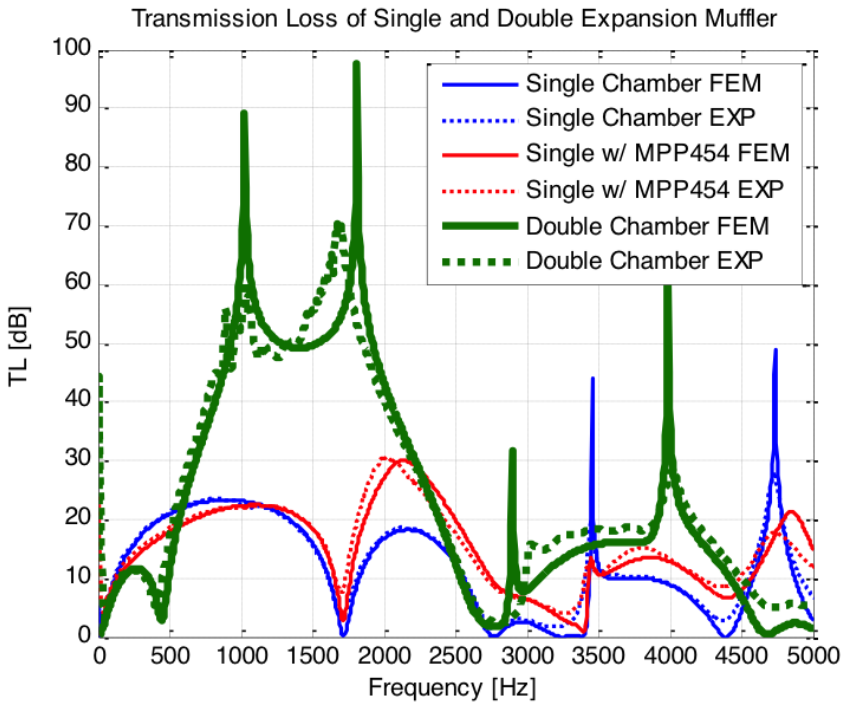

Figure 4.18. The comparison between the single-chamber silencer and the double-chamber silencer.

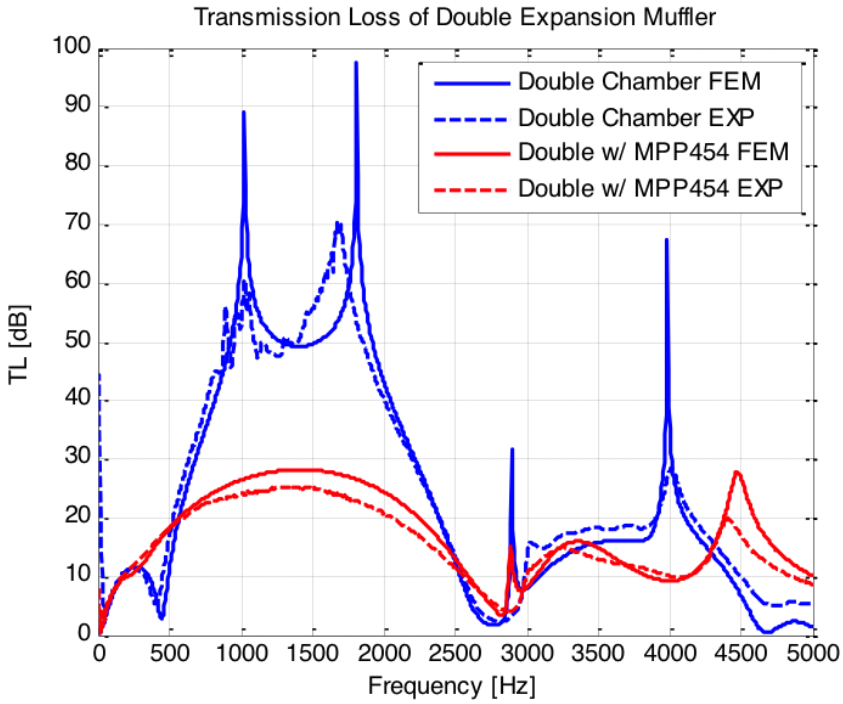

Figure 4.19. The transmission loss comparison between the double-chamber silencer with and without the MPP lining.

The predicted and measured sound attenuation results for the double-layered MPP linings installed in the single-chamber muffler are shown on Figure 4.23. It can be seen from the figure that within each lobe of the transmission loss, the measurements seems to have lower peak values than the prediction results. However, the transmission loss minima near 1700 Hz, 3400 Hz and 5000 Hz occur exactly as predicted, and the measurement results in those regions seem to be "better" than the predicted result (i.e., the measured transmission loss is higher than the predicted value). Note also that the addition of the second MPP layer generally increases the TL at high frequencies.

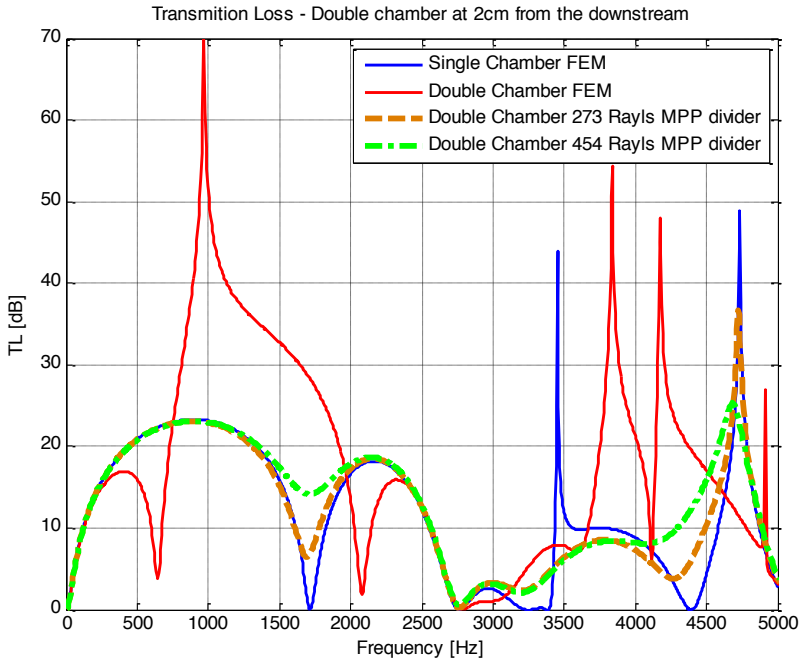

Figure 4.20. The transmission loss comparison between the dual chamber muffler using the rigid divider and MPP dividers.

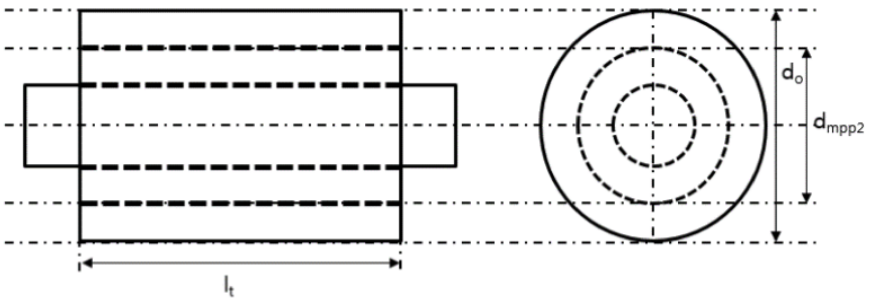

Figure 4.21. The configuration of double-layer MPP lining in the silencer, $d_{mpp2} = 8.5$cm.

4.4.4 Dual Chamber Muffler with Double Layered MPP Linings

The sound attenuation results for the double-layered MPP linings implemented in the dual-chamber silencer are shown in Figure 4.24. Unlike the single-chamber case,

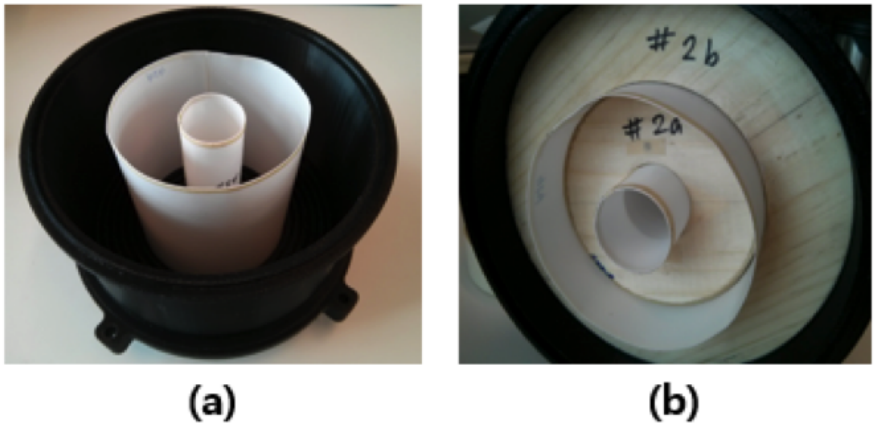

Figure 4.22. The silencer mounted in the middle of the standing wave tube when measuring the transmission loss using the 4-microphone measurement technique.

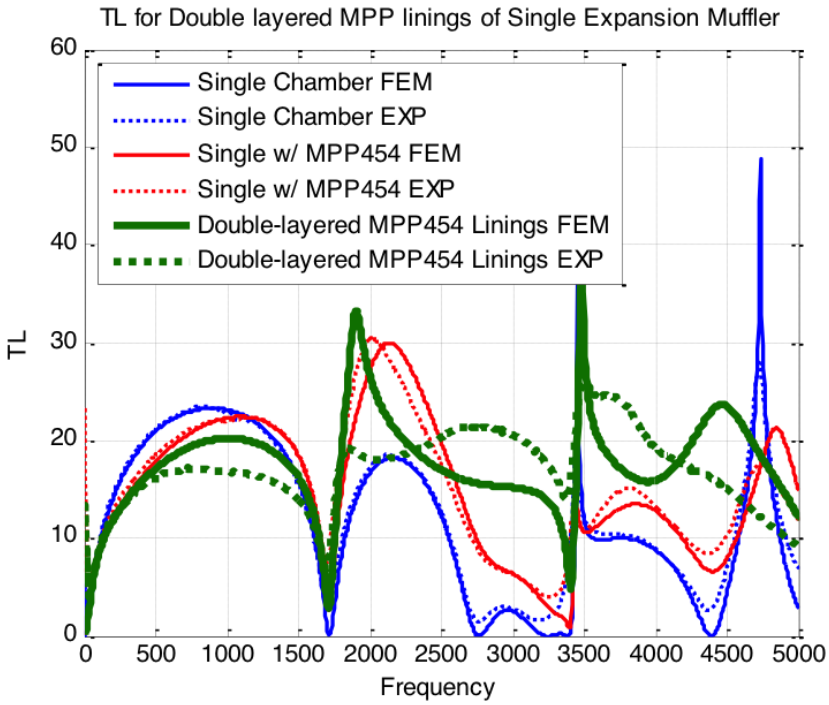

Figure 4.23. The sound attenuation results of double-layer MPP lining of the single-chamber silencer.

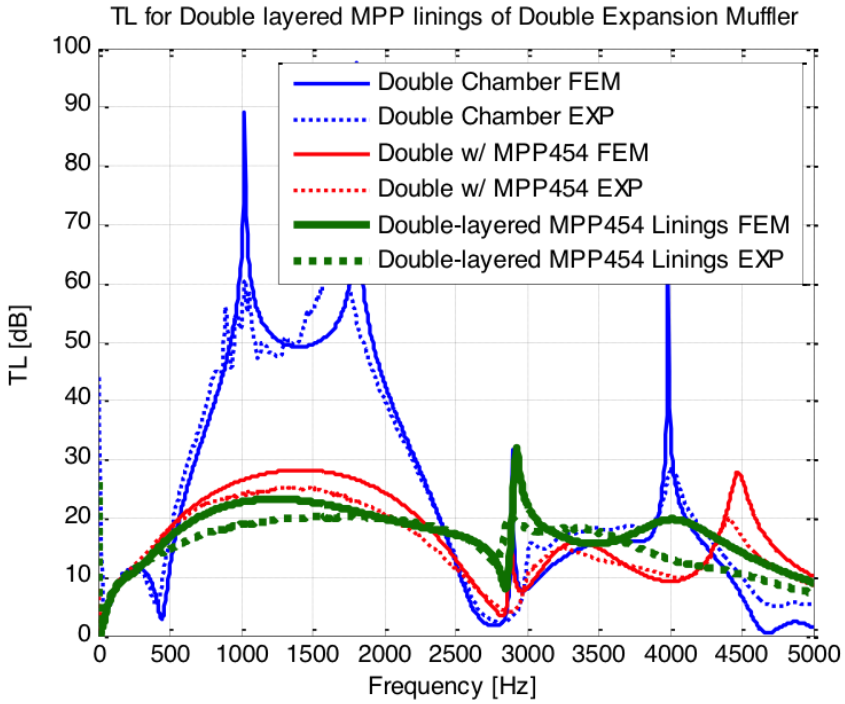

Figure 4.24. The sound attenuation results of the double-layer MPP linings implemented to the dual-chamber silencer.

the predicted results follow the measurement results reasonably well. Even though the peak transmission loss in the frequency region between 500 Hz and 2500 Hz was significantly lowered, by 50 dB from the double-expansion silencer-only case and 5 dB from the silencer with a single MPP lining case, it can be seen that the double-layered MPP lining substantially improved the 2800 Hz region of the transmission loss results: i.e., the sharp minimum in the transmission loss has been effectively eliminated.

4.4.5 Flow Measurement of the Silencer with MPP Linings

The previous results have shown that microperforated linings improved the acoustic attenuation performance of the silencer by effectively eliminating the sharp minima in the transmission loss. However, the microperforated linings were also found

to reduce the pressure-drop caused by the expansion muffler. Figure 4.25 shows the pressure drop versus flow rate for the MPP-lined single-expansion silencer with MPP's having different flow resistances. The flow rate was measured in standard liters per minute, and Inlet-End only in the figure means that the pressure drop was measured using only the inlet flange of the expansion muffler. It can be seen from the figure that the addition of the microperforated panel linings to the expansion muffler reduced the pressure drop significantly compared to the unlined expansion muffler. Moreover, it was found that a MPP having higher flow resistance reduces the pressure drop produced by the silencer. However, the use of a high flow resistance MPP tube reduces the acoustic attenuation performance; therefore, an optimized selection of flow resistance of the MPP is required to obtain the best trade-off between flow performance and acoustic performance.

Figure 4.26 shows the pressure drop measurement results for several different configurations. It can be seen from the figure that the double-chamber silencer does not increase the pressure drop compared to the single-chamber silencer. Moreover, with the addition of a second MPP lining, the pressure drop of the double chamber muffler is approximately the same as that of single-layered MPP lining case.

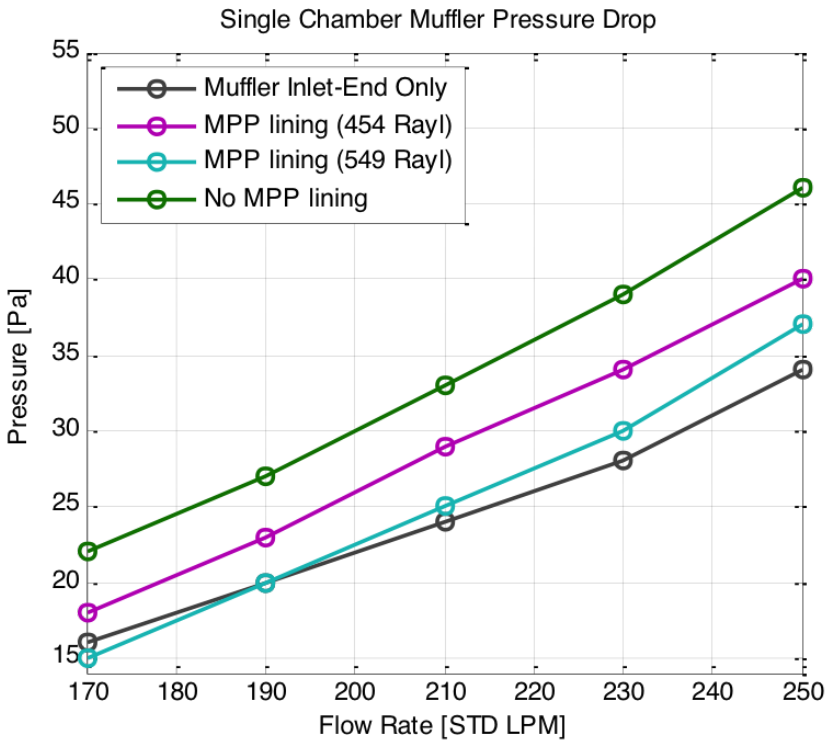

Figure 4.25. The silencer mounted in the middle of the standing wave tube when measuring the transmission loss using the 4-microphone measurement technique.

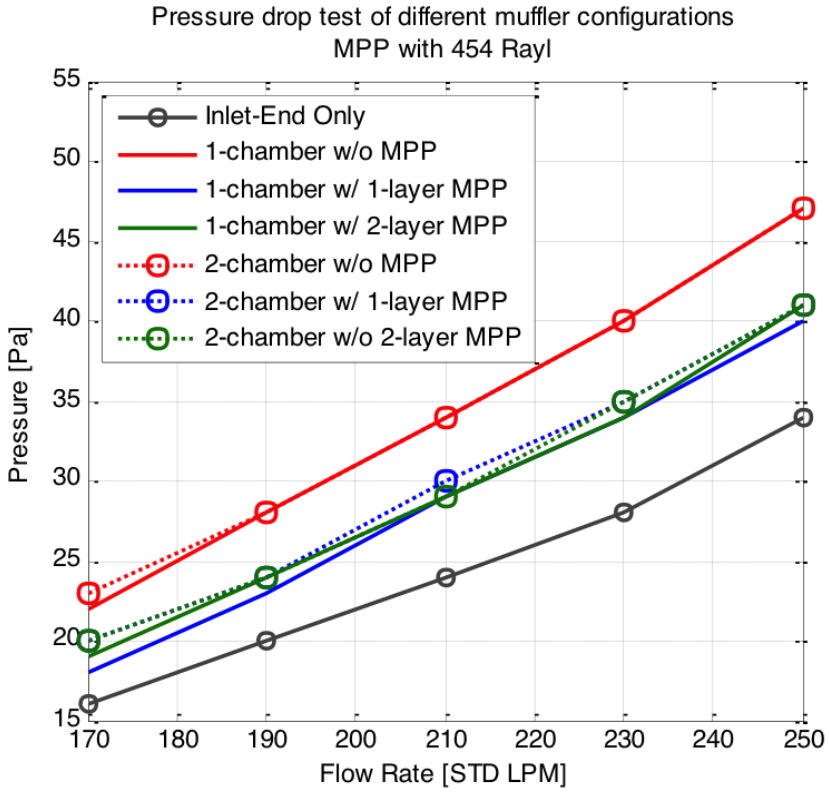

Figure 4.26. The silencer mounted in the middle of the standing wave tube when measuring the transmission loss using the 4-microphone measurement technique.

5. ACOUSTIC SILENCER WITH MEAN FLOW EFFECT

Acoustical silencers are often used in systems which contain flow, such as HVAC ventilation systems. Therefore in this chapter, a silencer with an MPP lining that conveys a low speed mean flow will be considered. In addition to the mean flow effect inside the muffler, different internal structural designs of the muffler, such as inlet and outlet extensions, will be considered to enhance the acoustical performance over the speech interference range.

FEM techniques that were suggested in the previous chapter were also used to predict the acoustic performance of silencers with an MPP lining with mean flow effect as well as different internal structural designs. In order to develop an appropriate FE model considering flow effect: 1) The transmission loss of of a MPP liner with mean flow effect was measured using the standing wave tube measurement, 2) a FE model of MPP considering mean flow effect was developed based on the measurement, and 3) a MPP lining model was implemented in the FE prediction model of actual muffler model and the results were validated with the measurement.

5.1 Transmission Loss Measurement of MPP Liner with Mean Flow Effect

A four-microphone standing wave tube was used in combination with the two-load method [46] to measure the transmission loss of microperforated panel duct linings exposed to a grazing mean flow. A square standing wave tube was used in the measurements, as shown in Figure 5.1. Figure 5.2 shows the schematic configuration of the transmission loss measurement of the MPP lining using the two-load method. The outlet of the standing wave tube was left open to create the first load. For the second load, the outlet of the standing wave tube was connected with a square duct

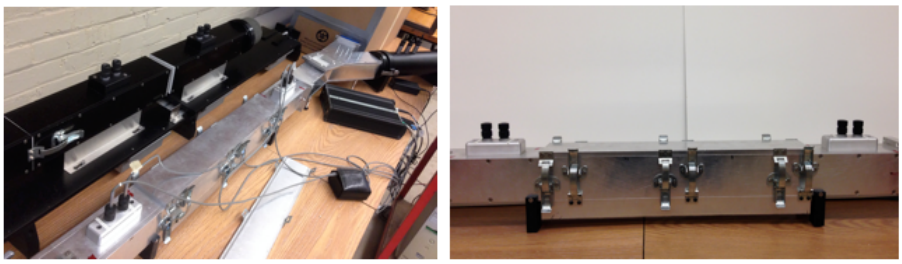

Figure 5.1. The square standing wave tube that was used for the measurements.

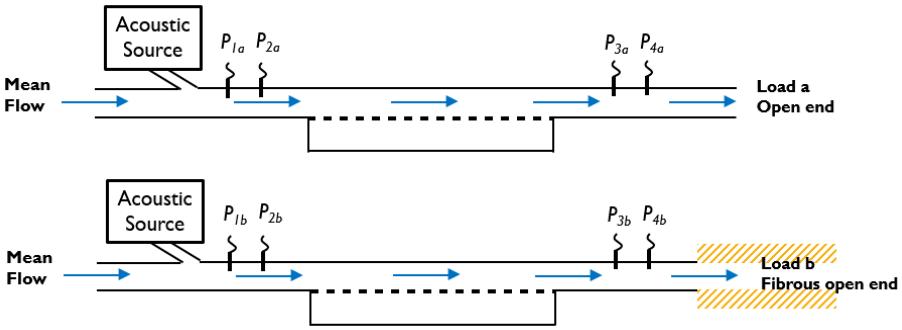

Figure 5.2. Configurations of the four-microphone standing wave tube measurement using the two-load method and considering the mean flow effect. (Dashed line represents the MPP liner).

that was lined with fibrous material and which had the same cross-sectional open area as the main square duct.

In order to find the acoustic attenuation performance of a MPP lining, the MPP was placed in the bottom of the standing wave tube as shown in Figure 5.3 with an air backing space behind the MPP as shown in Figure 5.2. The properties of the MPP used in this work are tabulated in Table 5.1.

Table 5.1. Material properties of the microperforated panel.

	Hole diameter [μm]	**Thickness [mm]**	**Flow resistance [Rayls]**
MPP 549	126.6	0.35	549

Figure 5.3. A picture of the MPP lining installation inside the square type standing wave tube.

5.2 Acoustic Pressure inside the Duct with Mean Flow Effect

The transfer matrix calculation for the two-load method standing wave tube measurement are described in reference [47]. The acoustic pressure within the uniform tube with a mean flow can be written as follow:

$$p(z) = Ae^{-jk^+z} + Be^{jk^-z} \tag{5.1}$$

$$v(z) = \frac{1}{Y}\{Ae^{-jk^+z} - Be^{+jk^-}\} \tag{5.2}$$

where, v is the particle velocity and Y is the corresponding characteristic impedance: i.e.,

$$Y = Y_0\left\{1 - \frac{\alpha(M)}{k_0} + j\frac{\alpha(M)}{k_0}\right\} \tag{5.3}$$

The wavenumbers for the forward and backward going waves inside the tube are, respectively,

$$k^+ = \frac{k_0 - j\alpha(M)}{1+M} = \frac{k_0 - j\alpha(M)}{1-M^2}(1-M) = k_c(1-M) \tag{5.4}$$

$$k^{-} = \frac{k_0 - j\alpha(M)}{1 - M} = \frac{k_0 - j\alpha(M)}{1 - M^2}(1 + M) = k_c(1 + M) \tag{5.5}$$

$$k_c = \frac{k_0 - j\alpha(M)}{1 - M^2} \tag{5.6}$$

where, M is the Mach number, k_0 is ω/c and $\alpha(M)$ is the total aeroacoustic attenuation in a moving medium resulting from viscothermal effects and turbulent flow friction:

$$\alpha(M) = \alpha + FM/2D \tag{5.7}$$

In Equation (5.7), F is Froude's friction factor, D is the hydraulic diameter, which in this case is the length of one side of the square duct, and α is the attenuation constant, which can be rewritten as:

$$\alpha = \frac{1}{rc}\left(\frac{\omega\mu}{2\rho}\right)^{1/2} \tag{5.8}$$

where, r is half of the hydraulic diameter D, c is the ambient sound speed and μ is the dynamic viscosity of the air. Then, Equations (5.1) and (5.2) can be rewritten as:

$$p(z) = e^{jMk_cz}(Ae^{-jk_cz} + Be^{jk_cz}) \tag{5.9}$$

$$v(z) = \frac{e^{jMk_cz}}{Y}(Ae^{-jk_cz} - Be^{jk_cz}) \tag{5.10}$$

Equations (5.9) and (5.10) can then be described in the following transfer matrix form for a uniform cross-section duct system having length l:

$$\begin{bmatrix} p \\ v \end{bmatrix}_{z=0} = e^{-jMk_cl} \begin{bmatrix} \cos k_cl & jY \sin k_cl \\ (j/Y)\sin k_cl & \cos k_cl \end{bmatrix} \begin{bmatrix} p \\ v \end{bmatrix}_{z=l} \tag{5.11}$$

The transfer matrix calculation for the system having a load as shown in Figure 5.2 can be expressed as:

$$\begin{bmatrix} p_{1a} \\ v_{1a} \end{bmatrix} = \begin{bmatrix} A_{12} & B_{12} \\ C_{12} & D_{12} \end{bmatrix} \begin{bmatrix} T_{11} & T_{12} \\ T_{21} & T_{22} \end{bmatrix} \begin{bmatrix} A_{34} & B_{34} \\ C_{34} & D_{34} \end{bmatrix} \begin{bmatrix} p_{4a} \\ p_{4a}/Z_a \end{bmatrix} \tag{5.12}$$

where, Z_a is the impedance at the load in Figure 5.2 and the transfer function, H_{ij}, can be defined as:

$$H_{ij,a} = p_{ia}/p_{ja} \tag{5.13}$$

$$H_{ij,b} = p_{ib}/p_{jb} \tag{5.14}$$

where, subscripts a and b in the subscript denote the different load conditions. Then, transfer matrix components, T_{11}, T_{12}, T_{21}, and T_{22} can be calculated by using the following relations:

$$(H_{34,a})T_{11} + \{C_{34} + (D_{34}/B_{34})(H_{34,a} - A_{34})\}T_{12} = H_{24,a} \tag{5.15}$$

$$(H_{34,a})T_{21} + \{C_{34} + (D_{34}/B_{34})(H_{34,a} - A_{34})\}T_{22} = (H_{14,a} - A_{12}H_{24,a})/B_{12} \tag{5.16}$$

$$(H_{34,b})T_{11} + \{C_{34} + (D_{34}/B_{34})(H_{34,b} - A_{34})\}T_{12} = H_{24,b} \tag{5.17}$$

$$(H_{34,b})T_{21} + \{C_{34} + (D_{34}/B_{34})(H_{34,b} - A_{34})\}T_{22} = (H_{14,b} - A_{12}H_{24,b})/B_{12} \tag{5.18}$$

Equation (5.11) can then be used to obtain the transfer matrix components, A_{12}, B_{12}, C_{12}, D_{12}, A_{34}, B_{34}, C_{34}, and D_{34}:

$$\begin{bmatrix} A_{12} & B_{12} \\ C_{12} & D_{12} \end{bmatrix} = e^{-jMk_cl_{12}} \begin{bmatrix} \cos k_cl_{12} & jY \sin k_cl_{12} \\ (j/Y)\sin k_cl_{12} & \cos k_cl_{12} \end{bmatrix} \tag{5.19}$$

$$\begin{bmatrix} A_{34} & B_{34} \\ C_{34} & D_{34} \end{bmatrix} = e^{-jMk_cl_{34}} \begin{bmatrix} \cos k_cl_{34} & jY \sin k_cl_{34} \\ (j/Y)\sin k_cl_{34} & \cos k_cl_{34} \end{bmatrix} \tag{5.20}$$

Finally, the transmission loss can be calculated by using the equations

$$T_a = \frac{2e^{jkd}}{T_{11} + T_{12}/\rho_0 c + \rho_0 c T_{21} + T_{22}} \tag{5.21}$$

$$TL = 20\log_{10}\left|\frac{1}{T_a}\right| \tag{5.22}$$

where, T_a is the normal incidence pressure transmission coefficient.

5.3 Prediction Model

In this work, the transmission loss measurement of an MPP lining exposed to grazing mean flow was modeled using the Finite Element Method (FEM). The MPP used for the measurement was modeled as an equivalent fluid having acoustical properties calculated using the well-known Johnson-Champoux-Allard (JCA) model [5,6] as suggested in Chapter 4.The calculated complex density and complex bulk modulus by using JCA model were then substituted into the FEM model of the MPP. The commercial software ABAQUS^{TM} was used to run the FEM model.

5.3.1 MPP Modeling

In modeling the MPP, the technique suggested in Chapter 4 were used. In order to make the FEM model of MPP locally reacting, periodic rigid boundary conditions were implemented within the cross-section of the MPP lining to prevent transmission through the equivalent fluid layer in the axial direction, as shown in Figure 5.4.

Figure 5.5 shows the FEM model of the standing wave tube measurement that was described in the previous section. In ABAQUS^{TM}, the acoustic field in a duct with mean flow is defined using the following variational form, which can be derived from the Helmholtz equation: [48]

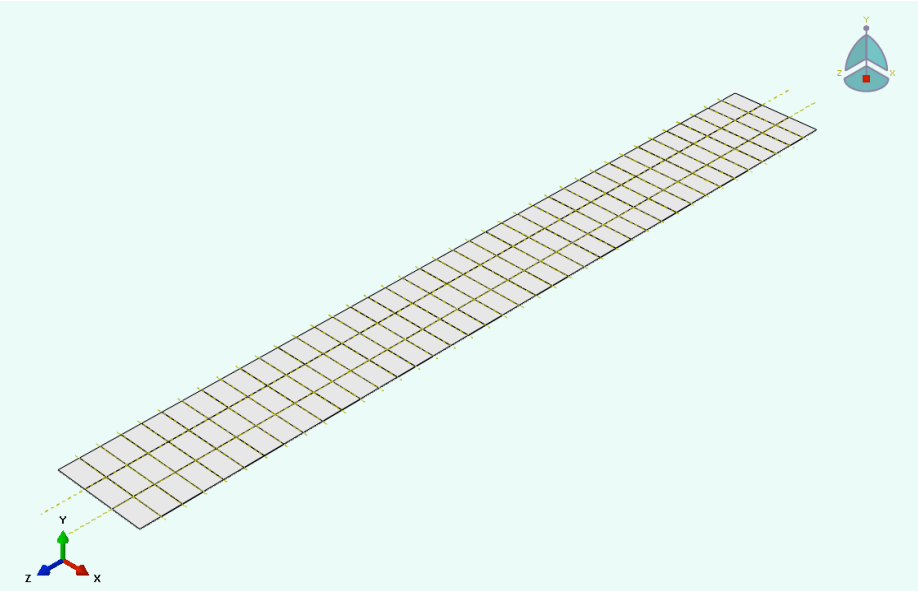

Figure 5.4. The MPP FE model that rigid inclusions to make the MPP locally reacting.

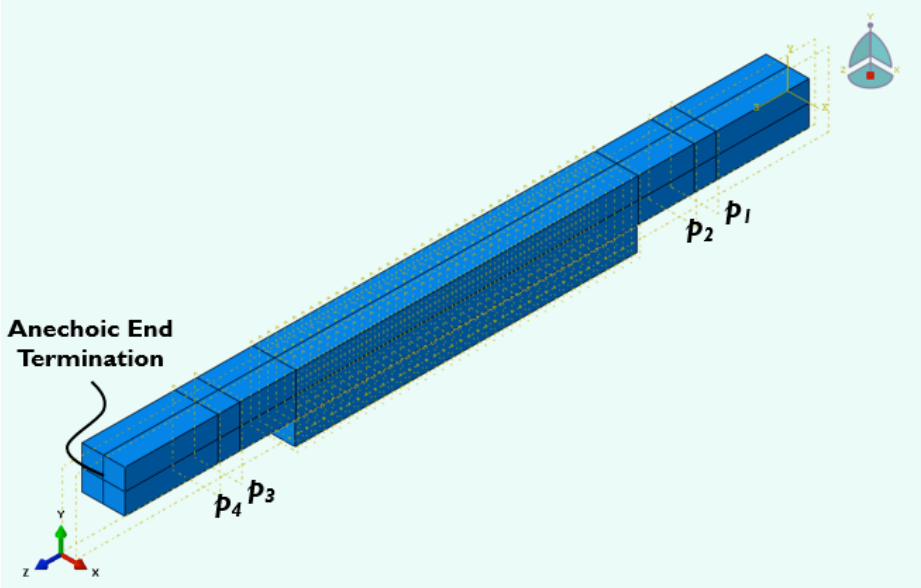

Figure 5.5. The FE model of the square duct type standing wave tube.

$$\int_V \left[\frac{1}{\omega^2\rho_0}\nabla\delta\tilde{p}\cdot(I-\tilde{\mathbf{v}}\tilde{\mathbf{v}})\cdot\nabla\tilde{p}-\frac{j}{\omega\rho_0 c}(\nabla\delta\tilde{p}\cdot\tilde{\mathbf{v}}\tilde{p}-\delta\tilde{p}\tilde{\mathbf{v}}\cdot\nabla\tilde{p})-\frac{1}{K}\delta\tilde{p}\tilde{p}\right]dV$$
$$+\int_S \frac{1}{\omega^2\rho_0}\delta\tilde{p}\left[\mathbf{n}^-\cdot(I-\tilde{\mathbf{v}}\tilde{\mathbf{v}})\cdot\nabla\tilde{p}-\frac{j\omega}{c}\mathbf{n}^-\cdot\tilde{\mathbf{v}}\tilde{p}\right]dS=0 \tag{5.23}$$

where, $\delta\tilde{p}$ is the arbitrary variational field, $\tilde{\mathbf{v}}$ denotes the velocity field vector, $\mathbf{n}$ is the normal direction vector and $\tilde{p}$ is the steady-state sound pressure along the duct, which, if it is one-dimensional, can be described as:

$$\tilde{p} = Ae^{-\frac{jkx}{1+M}} + Be^{\frac{jkx}{1-M}} \tag{5.24}$$

where, $k = \omega/c$, and A and B are determined by the boundary conditions. The pressure at the inlet end of the square duct was set to $\tilde{p} = 1$. The surrounding area of the model, except for the inlet and the outlet, was modeled as a hardwall boundary, as expressed by the equation:

$$\left((1 - M^2)\nabla\tilde{p} - \frac{j\omega}{c}M\tilde{p}\right) \cdot \mathbf{n} = 0 \tag{5.25}$$

An anechoic termination was applied at the outlet end of the duct by using following equation:

$$\left((1 - M^2)\nabla\tilde{p} - \frac{j\omega}{c}M\tilde{p}\right) \cdot \mathbf{n} = p\frac{i\omega}{Z_{anechoic}} \tag{5.26}$$

5.4 MPP Lining inside the Square Duct with Flow Effect

Figure 5.6 shows the transmission loss comparison between the measurements and the predictions of the empty standing wave tube without an MPP lining attached: i.e., the MPP lining was removed from Figure 5.2. It can be seen from both the measurement and the prediction results that the mean flow of 8.5 m/s (M = 0.025) did not create a noticeable change in the transmission loss of the empty standing wave tube.

Figure 5.7 shows the transmission loss comparison between the measurements and the FEM predictions when the MPP lining was attached. When the MPP lining was

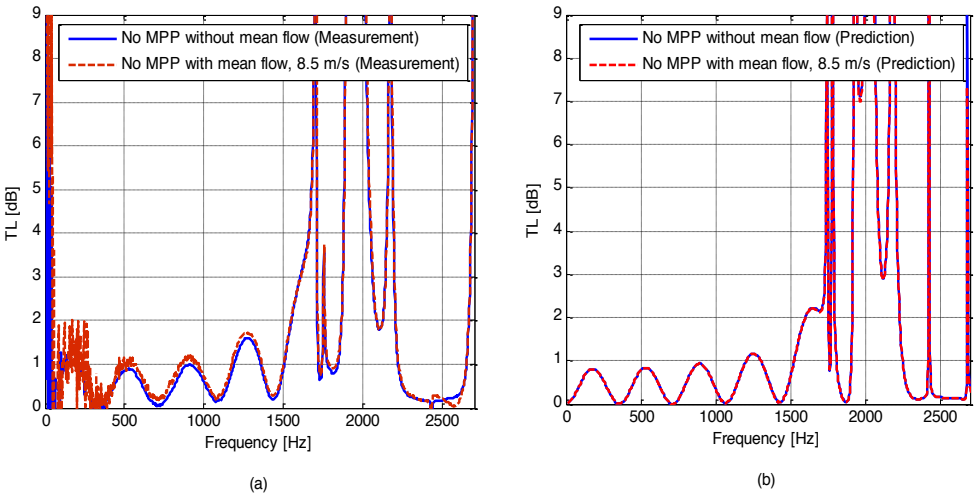

Figure 5.6. Transmission loss of standing wave tube without MPP lining. (a) Measurement results and (b) prediction results.

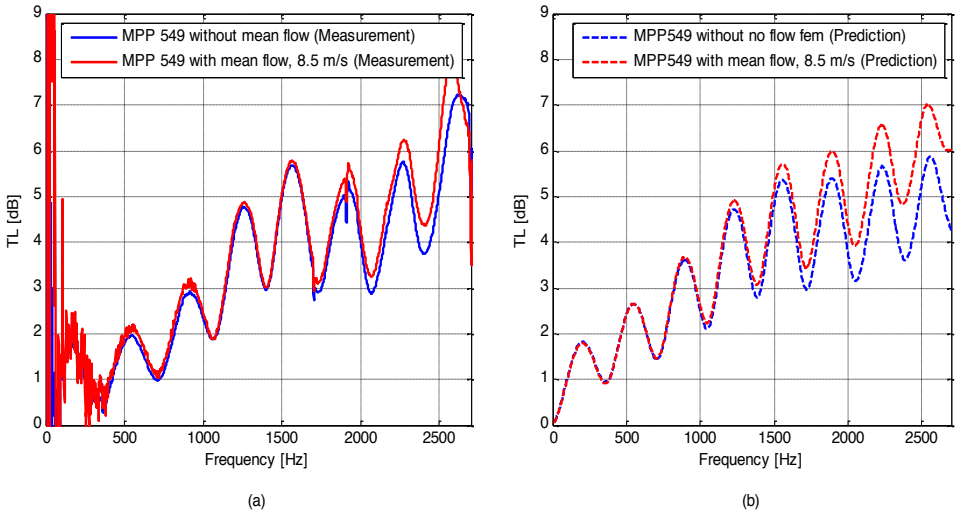

Figure 5.7. Transmission loss of standing wave tube with MPP lining. (a) Measurement results and (b) prediction results.

attached, the local maxima of the transmission loss above the 1500 Hz frequency range were increased due to the mean flow velocity, and it can be seen from the figure that the FEM prediction results represented this trend accurately.

It is known that the grazing flow on regular perforated panel has considerable effect [37]. However, it can be concluded from the results shown in this section that the effect of grazing flow on the MPP is very small. Therefore the MPP can be modeled without considering flow effect at the relatively low flow velocity but the grazing flow effect on the MPP treatment inside a silencer will still be considered through this chapter.

5.5 Acoustic Silencers with Flow Effect

5.5.1 Single Chamber Silencer without MPP Tube Liner

The mean flow effect will be considered in application to the prototype silencer used in Chapter 4, as shown in Figure 5.8. Figure 5.9 shows how the acoustic silencer was attached to the standing wave tube for the transmission loss measurement. The brown box shown on Figure 5.9(a) is the flow generator to provide mean flow through the standing wave tube. The flow velocity created by the generator inside the tube was about 21.6 m/s, which is Mach number of 0.06. The current silencer design is aiming for the HVAC duct applications, in which the flow velocity does not exceed 20 m/s therefore this low Mach number will be acceptable. Figure 5.9(b) and (c) are the two load conditions, respectively.

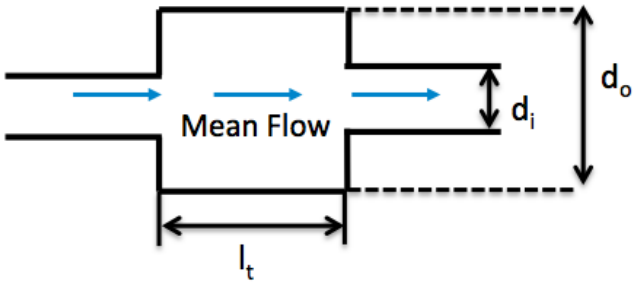

Figure 5.8. Configuration of single-chamber silencer with mean flow effect, di=2.9 cm, do=15.2 cm, lt=9.6 cm.

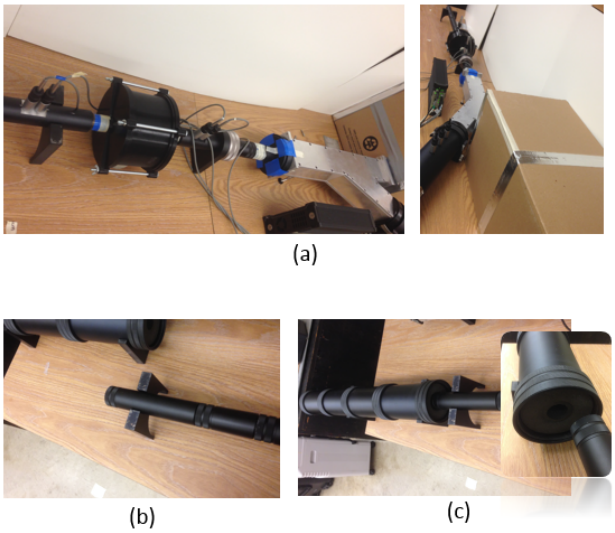

Figure 5.9. (a) The prototype muffler attached to the standing wave tube for the transmission loss measurement using four-microphone and two-load method with mean flow generated from the box. (b) 1st load: open end. (c) 2nd load: open end surrounded by the fibrous material.

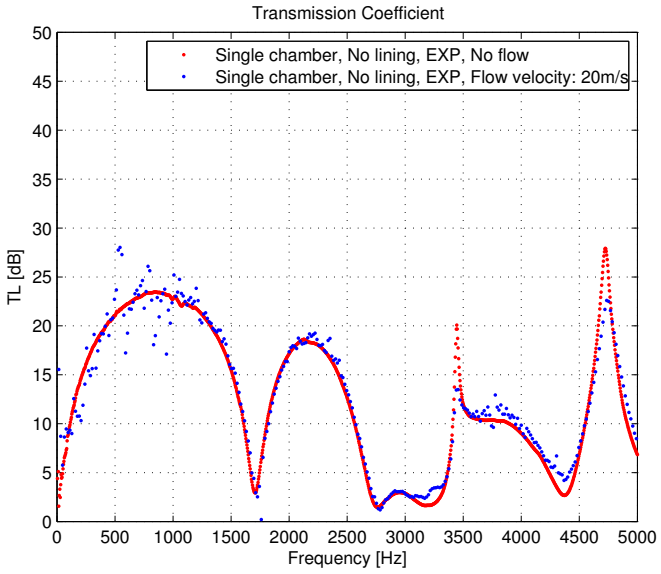

Figure 5.10. Measured transmission loss comparisons of single chamber muffler with and without mean flow effect.

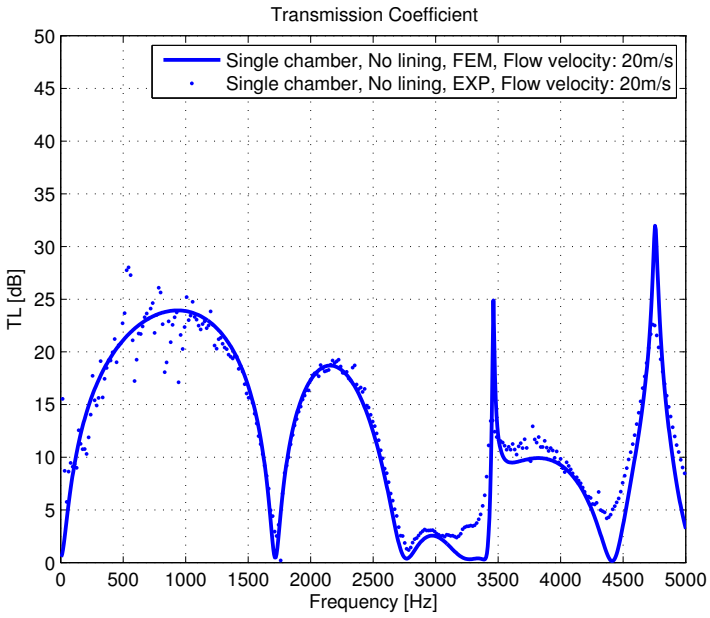

Figure 5.11. Transmission loss comparison between measured result and predicted result when mean flow applied.

Figure 5.10 shows the measured transmission loss comparison of the single chamber silencer with and without mean flow effect. It can be seen from the figure that at this relatively low Mach number, the sound attenuation performance of the silencer is not affected by the flow effect. Figure 5.11 shows the transmission loss comparison between the measurement and the predicted result using the FE model. It can be seen from the figure that the predicted TL shows trend similar to the measurements, but shows zero minima. However, this also shows that the mean flow is not critical in the sound attenuation performance of the silencer prediction model.

5.5.2 Single Chamber Silencer with MPP Tube Liner

Figure 5.12 shows the configuration of the single chamber muffler with MPP tube connecting the inlet and outlet of the silencer. This configuration was already con-

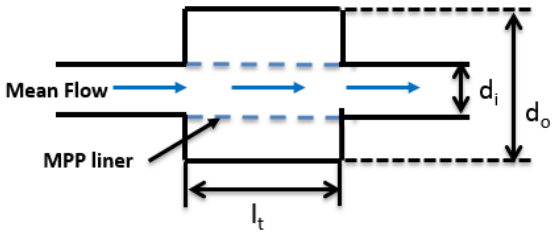

Figure 5.12. Configuration of single-chamber silencer with MPP tube liner, di=2.9 cm, do=15.2 cm, lt=9.6 cm.

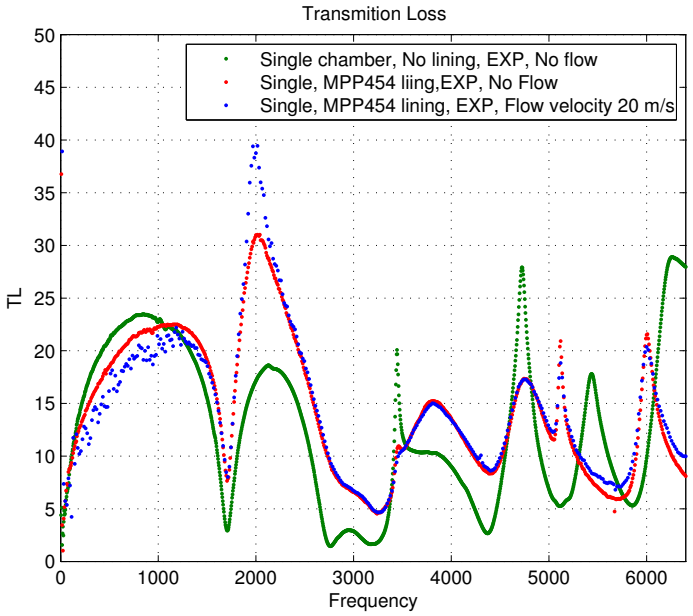

Figure 5.13. Measured transmission loss results comparison.

sidered in Chapter 4. The flow resistance of MPP used here is 454 Rayls, which had shown good attenuation performance in the previous chapter.

Figure 5.13 shows the transmission loss comparison results of the single chamber silencer with MPP tube liner. It can also be seen in the figure that the mean flow inside the silencer with MPP tube is not critical. The transmission loss comparison between the FE prediction and the measured result is shown on Figure 5.14. It can be seen that the FE prediction model captured the important characteristics of transmission

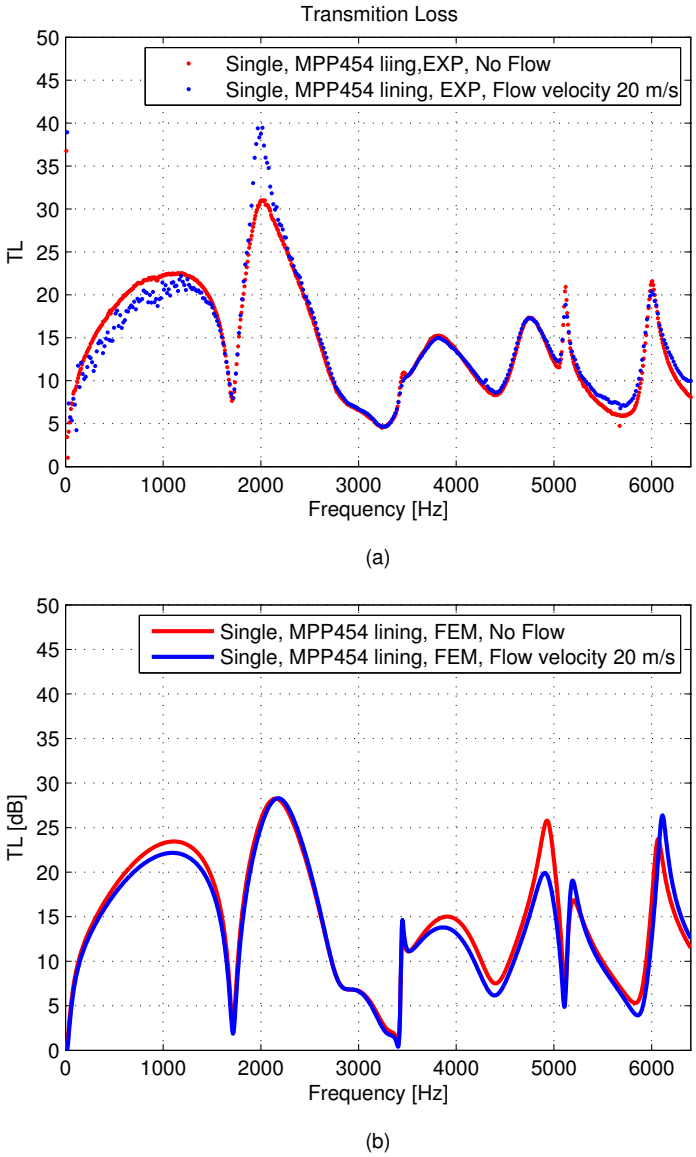

Figure 5.14. Measured transmission loss results comparison of the silencer with and without flow effect. (a) Measurement resultts and (b) Predicted results.

loss trend of the measurement. Although the prediction model underestimates the TL values at some frequency ranges such as 1800 Hz, 3200 Hz, 4200 Hz, and 5900 Hz, the overall mode characteristics of the silencer are well represented in the results.

5.6 Internal Structural Designs of an Acoustic Silencer

It was shown in the previous section that the suggested FEM model could be used to predict the acoustic attenuation performance of the MPP lining in the presence of mean flow. In this section, different internal structural designs of an acoustic silencer will be considered first using FEM prediction and the models will be validated using the standing wave tube measurements. The same prototype muffler that was used in Chapter 4 shown in Figure 4.2 will be used in this chapter and the target frequency range of the acoustic silencer will also be the speech interference range (500 - 4000 Hz).

5.6.1 Dual Chamber Acoustic Silencer using MPP Divider

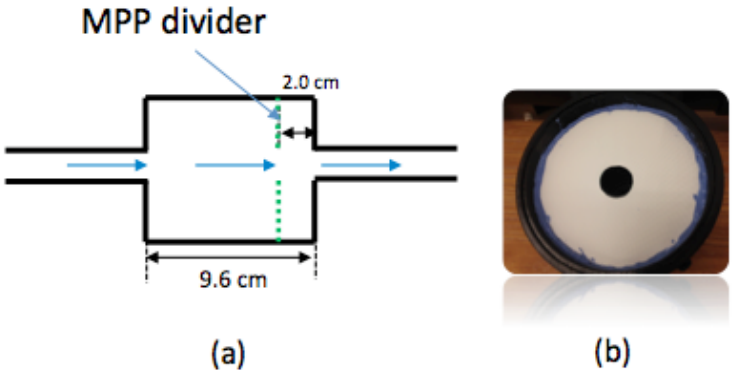

Figure 5.15. (a) The configuration of dual chamber muffler with the location of divider and (b) the actual photo of MPP divider attached to the muffler.

One of the internal structural designs that will be considered in this section is multiple expansion chambers that are divided by microperforated panels instead of rigid dividers. In chapter 4, it was found that the additional divider inside the expansion chamber of the muffler splits the chamber into two and this divider creates

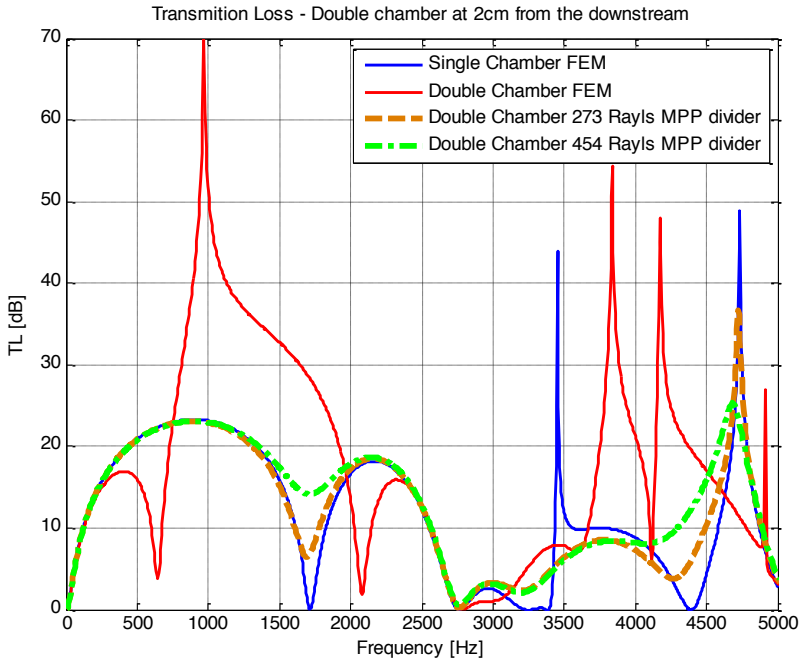

Figure 5.16. The transmission loss comparison between the dual chamber muffler using the rigid divider and MPP dividers.

different quarter wavelengths from the single chamber so it is possible to manipulate the maxima and minima in the transmission loss curve of the muffler. However, the drawback of this divider is that the divider does not remove the minima of single chamber muffler and those minima are shifted to other frequency region. In Figure 4.18, for instance, minimum value of the single chamber muffler occurred at 1700 Hz, and it was shifted to lower frequency region at 500 Hz due to added rigid divider.

In order to improve this drawback, the rigid divider was replaced with a microperforated panel. Figure 5.15 show the configuration and the actual photo of the dual chamber muffler with MPP divider. Figure 5.16 shows the transmission loss comparisons between the dual chamber mufflers with the rigid divider and with MPP dividers. In the comparison, two different MPP's with different flow resistances were considered, one has 273 Rayls and the other has 454 Rayls of flow resistance. It can be seen from the figure that the MPP divider brings up the minima at 600 Hz and

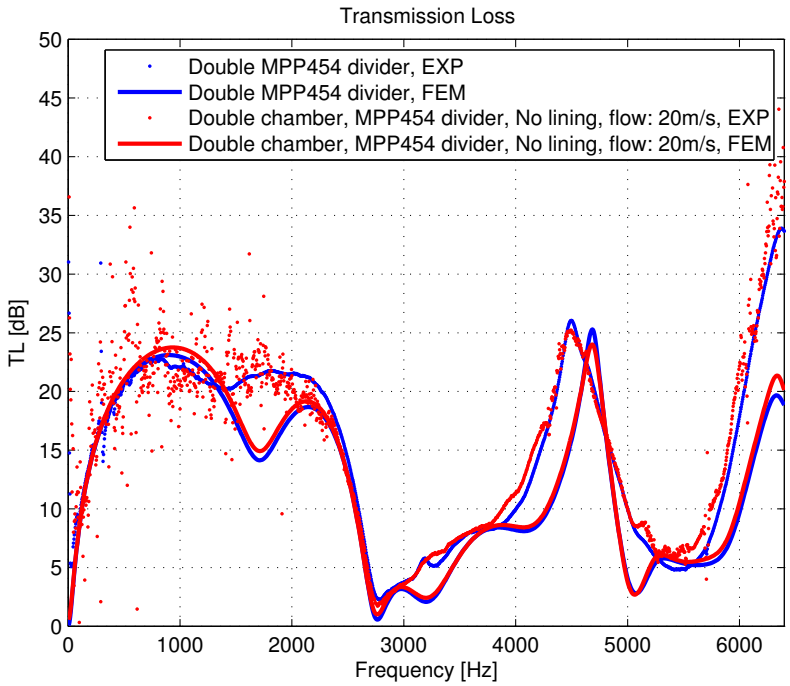

Figure 5.17. The transmission loss comparison between measurement and prediction results of dual chamber muffler using the MPP divider.

2100 Hz, which exist in the dual chamber muffler with rigid divider case. Moreover, the beneficial effect of the rigid divider, which was to remove the minimum value at 1700 Hz, is still maintained with the MPP dual chamber muffler. The MPP divider having 454 Rayls of flow resistance showed better acoustic attenuation performance than that of 273 Rayls MPP: therefore, an MPP having 454 Rayls of flow resistance was chosen for further measurements and prediction. Figure 5.17 shows the transmission loss comparison between the measurement and prediction of dual chamber silencer with MPP 454 Rayls divider shown in Figure 5.18. Two dotted lines and two solid lines represent measurement and prediction results, respectively. Even though there is some noise in the measured TL of dual chamber with flow, the mean flow does not affect to the attenuation performance of the dual chamber with MPP divider.

The dual chamber silencer with MPP tube liner was also considered. A flow resistance of 454 Rayls of MPP was used for the tube lining material as shown on

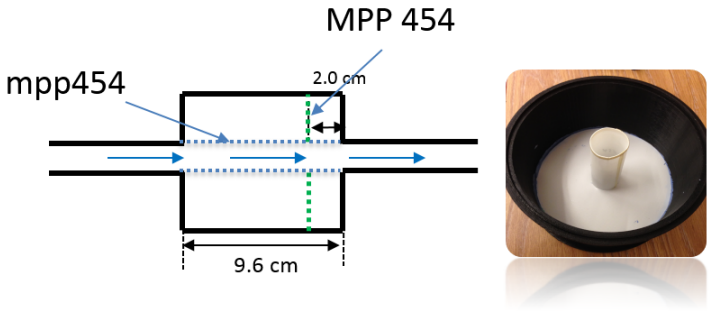

Figure 5.18. MPP dual chamber with single MPP tube linings configuration.

Figure 5.18. Figure 5.19 shows the measured and predicted transmission loss results comparison of the MPP dual chamber silencers with and without mean flow effect. Figure 5.19(a) shows the measured transmission loss results and (b) shows the predicted transmission loss results. Both measurement and prediction results show good agreement to each other especially in the low frequency region between 0 Hz and 1800 Hz; a small reduction of acoustic attenuation performance can be seen when there is flow effect inside the silencer. However, the prediction results showed an overestimation of performance in region between 1800 Hz and 2500 Hz.

Since the prediction model shows reasonable agreement to the measurement results. A MPP dual chamber silencer with double layers of MPP 454 tube linings, which configuration was hard to build as the prototype, was considered. The configuration of MPP dual chamber with double MPP linings is shown on Figure 5.20. Two solid lines in Figure 5.21 represent the MPP dual chamber silencers with double MPP454 linings with different flow conditions. It can be seen from the figure that double MPP linings improved the sound attenuation performance of the single MPP lining muffler gradually over the frequency range between 2500 Hz and 4700 Hz. The MPP dual chamber with double MPP linings has small reduction in attenuation performance compared with rigid dual chamber silencer with double MPP linings, which was suggested in Chapter 4, at the frequency region around 1600 Hz. However, the

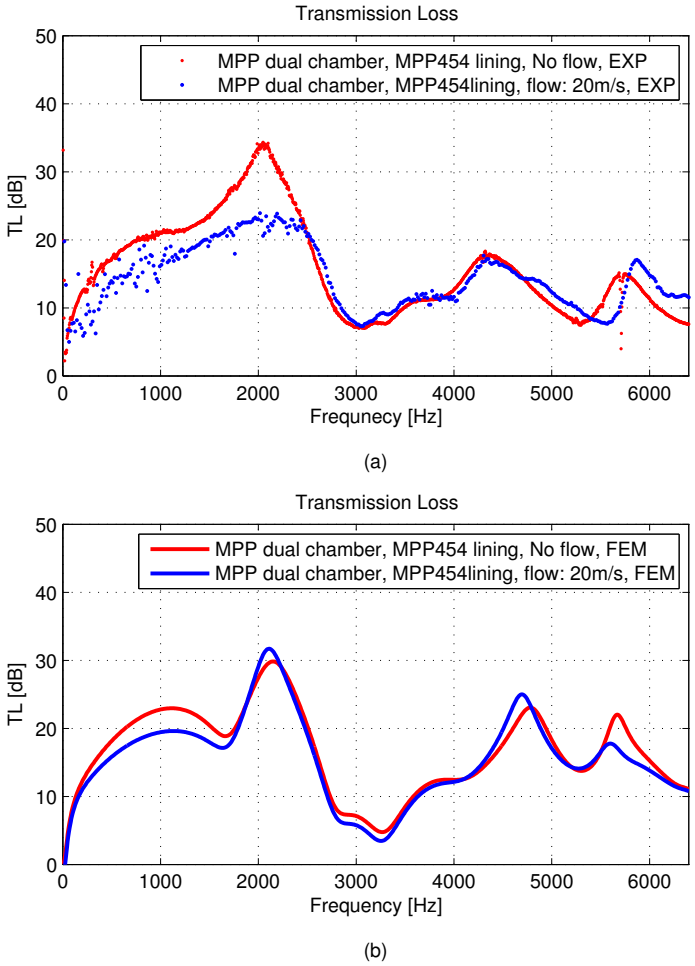

Figure 5.19. The transmission loss comparison of MPP dual silencer with and without mean flow effect. (a) Measurement results and (b) Prediction results.

overall transmission loss performance is better with the MPP divider than the rigid divider.

5.6.2 Acoustic Silencer with Inlet/Outlet Extensions

We will also take advantage of the fact that particular combinations of inlet and outlet extensions can improve the sound attenuation performance of the silencer over

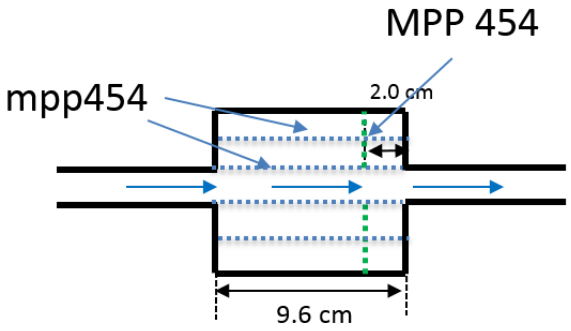

Figure 5.20. MPP dual chamber with double MPP tube linings configuration.

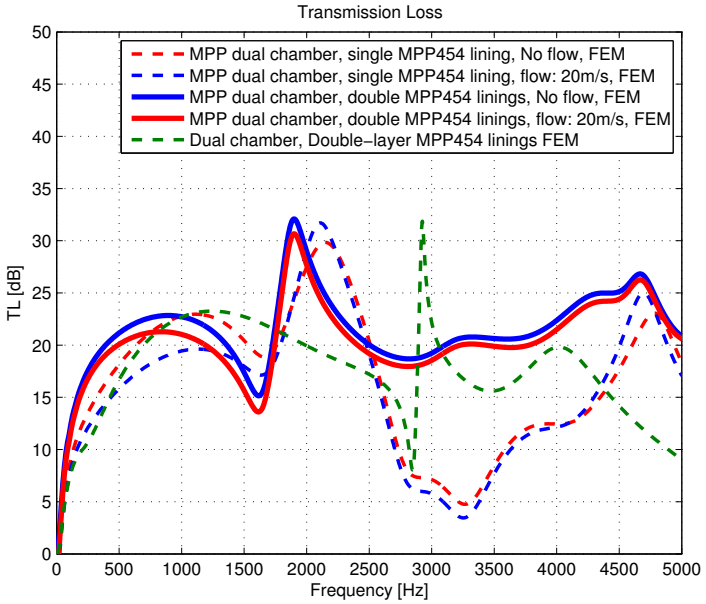

Figure 5.21. Transmission loss prediciton results for MPP dual chamber with double MPP linings.

certain frequency ranges. The inlet and outlet of the silencer were extended from the prototype muffler as shown in Figure 5.22. Four types of silencers having different combinations of MPP tube lining treatment will be considered. the properties of the MPP that was used for this study are tabulated in Table 4.1.

Figure 5.23 shows the transmission loss predictions for the four different types of silencers shown in Figure 5.22. It can be seen from the figure that the muffler with inlet and the outlet extensions but without the MPP lining treatment, which is the A type, improved the minimum transmission loss of the single chamber muffler without inlet/outlet extensions at 1700 Hz. However, the muffler type A still has a transmission loss zero at 2800 Hz.

The mufflers types B and D have relatively flat transmission loss curves in the frequency region from 0 Hz to 2500 Hz, but type B starts to lose its attenuation performance after 2500 Hz, whereas the muffler type D, which has double cylindrical MPP linings, maintains its flat transmission curve up to 5000 Hz. The transmission loss reduction in this frequency region is due to the first radial mode of the muffler, so the additional cylindrical MPP lining in the muffler type D seems to shift the radial mode to a higher frequency region.

The muffler type C, which has a single layer of cylindrical MPP lining having half the diameter of the expansion area, shows the best attenuation performance

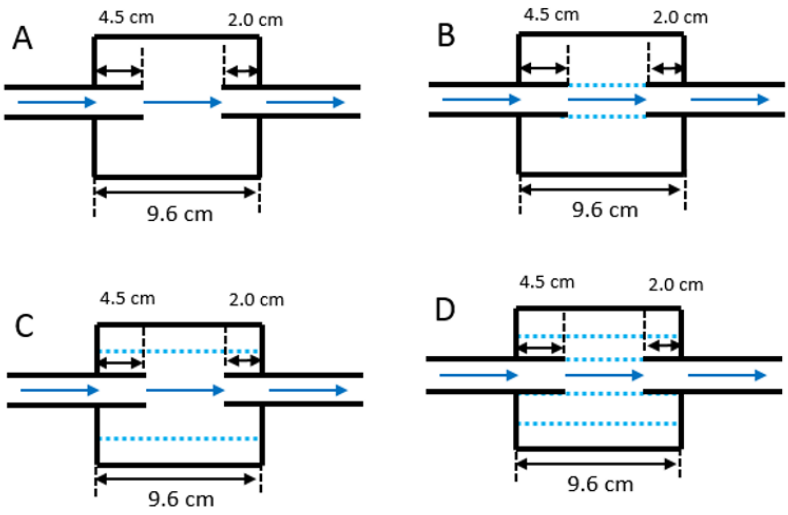

Figure 5.22. Configurations of the silencer with inlet and outlet extensions. (a) Type A: No MPP treatment, (b) Type B: Single MPP 454 Rayls tube liner, (c) Type C: Single MPP 454 Rayls tube liner in the middle, and (d) Type D: Double MPP 454 tube liners.

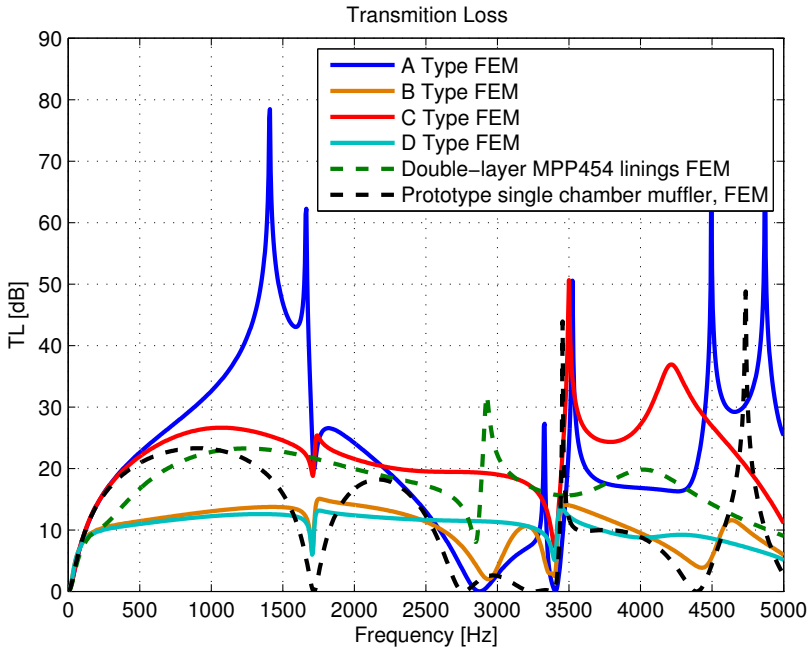

Figure 5.23. Transmission loss prediction results of inlet/outlet extended silencers with different MPP treatments.

among the four different silencer types. It can also be seen from the figure that the attenuation performance of the muffler type C is even better than the performance of a dual chamber muffler in combination with double layered cylindrical MPP lining, which was previously suggested in Chapter 4. Figure 5.24 represents transmission loss comparison between the prediction and measurement results considering mean flow effect. Both the prediction and the measurement results are again showing good agreement to each other and there are no significant losses in the sound attenuation performance of Type C muffler due to mean flow effect in this relatively low Mach number.

Figure 5.25 shows the transmission loss comparison between the MPP dual chamber silencer with double MPP linings and Type C silencer with inlet/outlet extensions. It can be seen from the figure that both types of silencer show good sound attenuation performance over the speech interference range. The type C silencer shows better performance in the low frequency region below 1800 Hz, whereas the MPP dual chamber

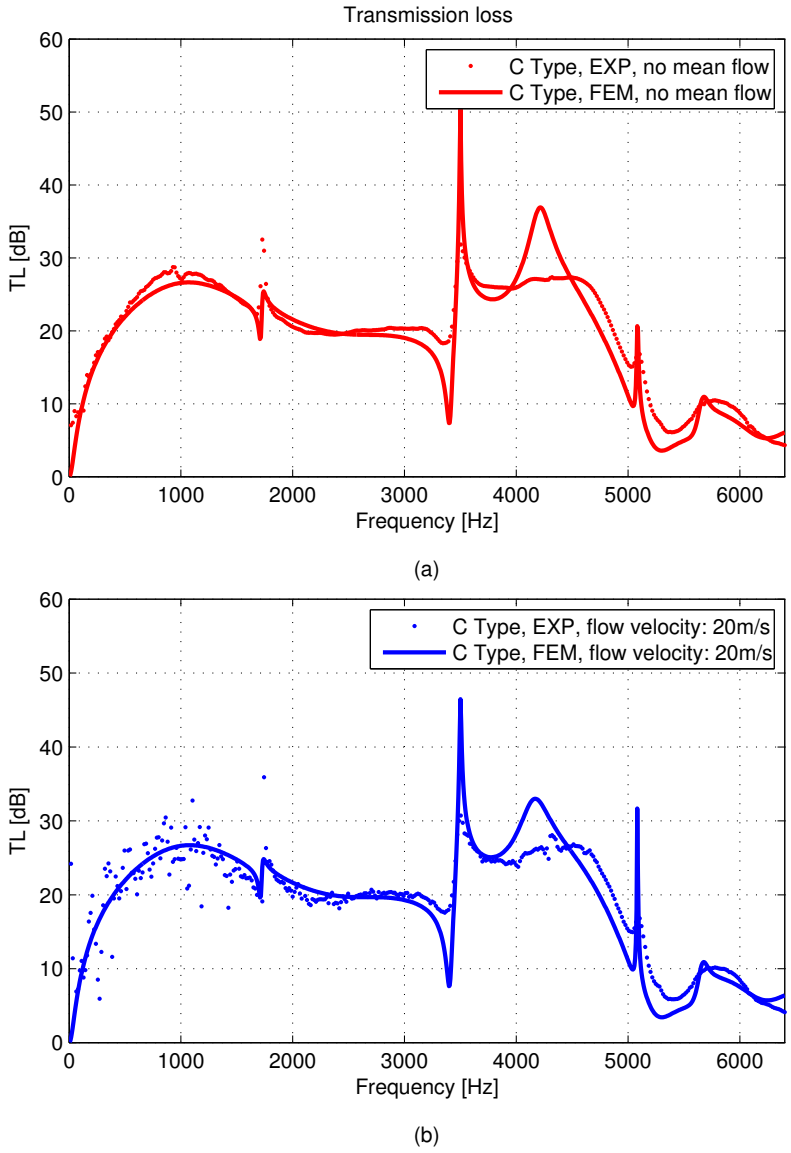

Figure 5.24. Transmission loss prediction results Type C silencer (a) with flow effect and (b) without flow effect.

with double MPP linings silencer maintains its performance up to higher frequency region above 5000 Hz.

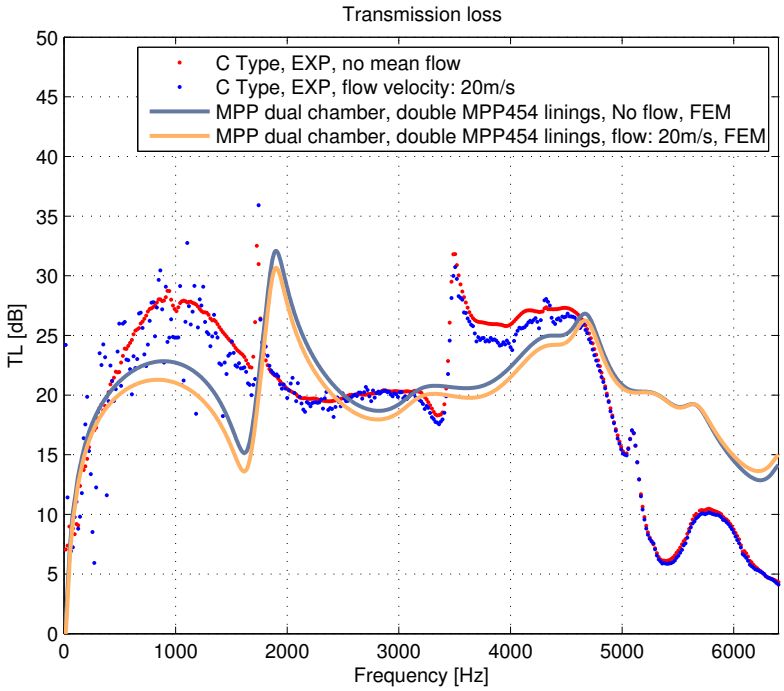

Figure 5.25. Transmission loss comparison results of MPP dual chamber silencer with double MPP linings and Type C silencer.

6. SUMMARY AND FUTURE WORK

6.1 Summary

The application of microperforated materials in the field of noise control engineering has been growing because of their sound absorbing characteristics in a wide range of frequency. Moreover, MPP's are more hygienic than conventional sound absorbing materials such as glass fiber, mineral wools, etc. In this study, MPP materials were used in fan noise control and acoustic silencer applications. Both of these applications are highly related to human involved environments, therefore the MPP is the perfect sound absorbing material in these areas. In future, more detailed studies in the application of MPP in the fan noise control and the acoustic silencer will be made.

6.2 Summary and Future Work of Fan Noise Control

6.2.1 Summary: Axial Fan Noise Control

In this research, detailed experiments on the effects of microperforated materials in the blade passage tone reduction of the 120 mm axial cooling fan were conducted. The microperforated material treatments were applied to the regular housing, in which the MPP strip only surrounds the blade tip region of the fan, and the microperforated materials were also implemented in the exteneded housing of the fan to create a duct that surrounds the flow directions of the fan as well as the blade tip region. A repeatable and fair measurement procedure was established which gave reliable results showing that the proper selection of the microperforated material for the regular housing will provide significant reductions in the blade passage tone at any operating condition of the fan. However, if the fan is built to operate under very high

pressure and low flow rate region, it is preferable to have a microperforated housing with high flow resistance.

It can also be seen from the ducted fan noise measurement that the MPP treatment as a duct will be effective in the blade passage tone attenuation compared to the unperforated ducted fan. However, it is important to decide the proper length of the duct and the flow resistance of the materials. In addition to the sound attenuation performance, flow performance of the fan inside the duct will be improved with the properly selected the MPP and the length of the duct.

6.2.2 Summary: Fan Noise Field Reconstruction

The sound fields of the axial fans with different housing materials were visualized by using the multi-reference planar Nearfield Acoustic Holography (NAH). The MPP housing materials' sound dissipation phenomena were able to be visualized by using NAH. It could be seen that the MPP can dissipate sound more efficiently than the impermeable casings as the length of the fan casing get longer on the inlet and outlet region of the fan since the sound wave can travel more inside the MPP duct so that it can have more chances to be dissipated.

6.2.3 Future Work: Structural Modifications to the Fan Casing

In the present study of fan noise, fans with different housing materials and different ducts were built as prototypes. Therefore detailed structural designs such as optimized duct length, optimized gaps between the blade-tip and the housing, bell mouth, etc. were not considered. However, those structural designs are critical in the flow motion around the fan and therefore structural design modifications and optimization should be considered in future studies.

6.2.4 Future Work: Simulation of Sound Power Level Generated by Fan with Different Perforated Housings

The sound fields of different types of axial fans were visualized in the present study by using multi-reference planar nearfield acoustic holography (NAH). In further study, the fan's sound field should be visualized with cylindrical NAH so to create the 3-D reconstructed sound field. Once the pressure field data are obtained, they will be used with the proper numerical simulation techniques either the infinite element method (IFEM) or the boundary element method (BEM) to simulate the far-field noise of the fans.

This methodology will provide other options to predict the noise radiated from the fan by simulation without using computational fluid dynamics (CFD), which requires researchers to model the actual fan and accurate mesh techniques to run the simulation and to achieve reliable prediction result.

6.3 Summary and Future Work of Acoustic Silencer Design

6.3.1 Summary: Acoustic Silencer Design without Flow Effect

A silencer focusing on acoustic attenuation over the speech range was suggested in this chapter. In designing the silencer, microperforated tube linings along with dual-chambers were employed. The dual-chamber silencer using a double-layer MPP lining showed good sound attenuation performance specifically by flattening the transmission loss over the target frequency range from 400 Hz to 4000 Hz, although the overall transmission loss was slightly reduced compared to the single-layered case. The MPP lining was also found to improve the flow performance of the silencer. In further studies, an optimized flow resistance of the MPP and various structural designs of the silencer will be suggested.

6.3.2 Summary: Acoustic Silencer Design considering Mean Flow Effect

In addition to silencer design methodology using Finite Element Model technique, silencer design considering grazing mean flow effect was considered. It was found that at the low Mach number (M=0.06) flow conditions such as were considered in this chapter, the mean flow is not a critical factor in the acoustic performance of the silencers that were suggested. At the end of this chapter comparison between the MPP dual chamber silencer with double MPP linings and a type C inlet and outlet extended silencer along with MPP lining was made and discussed. Predicted results were made using FE model, it was validated throughout the chapter that the FE model can be a good methodology to predict the acoustic performance of the silencers so this comparison can be considered as a fair comparison.

6.3.3 Future Work: Structural Design Modifications of Silencers

In the present study of acoustic silencer design, a prototype silencer was built without optimization of the structural design. Therefore structural design modifications is recommended in the future. For instance, multiple chamber silencers divided by the microperforated panels and their optimized locations will be determined. An optimization of the flow resistance of the MPP dividers and tube liners is recommended.

LIST OF REFERENCES

LIST OF REFERENCES

[1] M. E. Delany and E. N. Bazley. Acoustical properties of fibrous absorbent materials. *Applied Acoustics*, 3(2):105–116, 1970.

[2] D. Y. Maa. Theory and design of microperforated panel sound-absorbing constructions. *Scientia Sinica*, 18:55–71, February 1975.

[3] D. Y. Maa. Microperforated-panel wideband absorbers. *Noise Control Eng J.*, pages –, 1987.

[4] D. Y. Maa. Potential of microperforated panel absorber. *Journal of the Acoustical Society of America*, 104(5):2861–2866, November 1998.

[5] D. L. Johnson and J. Koplik. Theory of dynamic permeability and tortuosity in fluid-saturated porous media. *Journal of Fluid Mechanics*, 176:379–402, January 1987.

[6] Y. C. Champoux and J. F. Allard. Dynamic tortuosity and bulk modulus in air-saturated porous media. *Journal of Applied Physics*, 70(4):1975–1979, August 1991.

[7] N. Atalla and F. Sgard. Modeling of perforated plates and screens using rigid frame porous models. *Journal of Sound and Vibration*, 303(1-2):195–208, June 2007.

[8] L. Jaouen and F. X. Bécot. Acoustical characterization of perforated facings. *J Acoust Soc Am*, 129(3):1400–14006, January 2011.

[9] W. M. Gresho. The reduction of impeller-strut interaction noise on small tube-axial fans. *INTER-NOISE and NOISE-CON Congress and Conference Proceedings*, pages 1–6, June 1985.

[10] L. Huang and J. Wang. Acoustic analysis of a computer cooling fan. *The Journal of the Acoustical Society of America*, 118(4):2190, 2005.

[11] S. Lee, G. S. Lee, S. Heo, and C. Cheong. Computation of internal aeroacoustics of axial freezing fan in refrigerators. *INTER-NOISE and NOISE-CON Congress and Conference Proceedings*, pages 1–9, August 2008.

[12] A. Gregor and M. Hocevarb. Study of axial fan grilles noise and aerodynamic characteristics. *INTER-NOISE and NOISE-CON Congress and Conference Proceedings*, pages 1–9, May 2009.

[13] D. A. Quinlan. Application of active control to axial flow fans. *Noise Control Eng J.*, pages –, 1992.

[14] K. L. Gee and S. D. Sommerfeldt. A compact active control implementation for axial cooling fan noise. *Noise Control Engineering Journal*, 51(6):325, 2003.

[15] J. Schulz, W. Neise, and M. Moser. Active control of the blade passage frequency noise level of an axial fan with aeroacoustic sound sources. *Noise Control Eng. J.*, 2006.

[16] J. Thomassin, H. D. Vo, and N. W. Mureithi. The tip clearance flow resonance behind axial compressor nonsynchronous vibration. *Journal of Turbomachinery*, 133(4):041030, 2011.

[17] L. Gorny and G. H. Koopmann. Axial fan blade tone cancellation using optimally tuned quarter wavelength resonators. *Journal of Vibration and Acoustics*, 131(2):021002–021013, April 2009.

[18] D. L. Sutliff and M. G. Jones. Low-speed fan noise attenuation from a foam-metal liner. *Journal of Aircraft*, 46(4):1381–1394, July 2009.

[19] J. D. Maynard, E. G. Williams, and Y. Lee. Nearfield acosutic holography: I. theory of generalized holography and the development of nah. *J. Acoust. Soc. Am.*, 78(4), 1985.

[20] W. A. Veronesi and J. D. Maynard. Nearfield acoustic holography (nah): Ii. holographyic reconstruction algorithms and computer impelmentation. *J. Acoust. Soc. Am.*, 81(5):1307–1322, 1987.

[21] Y. J. Kim, J. S. Bolton, and H-S Kwon. Partial sound field decomposition in multireference near-field acoustical holography by using optimally located virtual references. *J. Acoust. Soc. Am.*, 115(4):1641–1652, 2004.

[22] M. Lee, J. S. Bolton, T. Yoo, H. Ido, and K. Seki. Fan noise control by enclosure modification. In *Proceedings of Internoise 2005, Rio de Janeiro, Brazil*, 2005.

[23] Y. Niu and Y. J Kim. Three-dimensional visualizations of open fan noise fields. *Noise*, 60(4):392–404, 2012.

[24] Y. J. Kim and Y. Niu. Improved statisticall optimal nearfield acosutical holography in subsonically moving fluid medium. *Journal of Sound and*, 331:3945–3960, 2012.

[25] A. Selamet and Z. L. Ji. Case Study: Acoustic attenuation performance of circular expansion chambers with extended end-inlet and side-outlet. *Noise Control Eng J*, 48(2):–, 2000.

[26] A. Selamet and Z. L. Ji. Acoustic attenuation perforamcne of circular expansion chambers with extended inlet/outlet. *Journal of Sound and Vibration*, 223(2):197–212, June 1999.

[27] C. J. Wu, X. J. Wang, and H. B. Tang. Transmission loss prediction on a single-inlet/double-outlet cylindrical expansion-chamber muffler by using the modal meshing approach. *Applied Acoustics*, 69(2):173–178, February 2008.

[28] F. D. Denia, A. Selamet, M. J. Martínez, and F. J. Fuenmayor. Sound attenuation of a circular multi-chamber hybrid muffler. *Noise Control Eng J*, 56(5):356–10, 2008.

[29] C. Liu, Z. L. Ji, and Z. Fang. Numerical analysis of acoustic attenuation and flow resistance characteristics of double expansion chamber silencers. *Noise Control Eng J*, 61(5):487–499, 2013.

[30] A. Selamet, F. D. Denia, and A. J. Besa. Acoustic behavior of circular dual-chamber mufflers. *Journal of Sound and Vibration*, 265(5):967–985, August 2003.

[31] Z. L. Ji. Boundary element analysis of a straight-through hybrid silencer. *Journal of Sound and Vibration*, 292(1-2):415–423, April 2006.

[32] I. Lee, A. Selamet, and N. T. Huff. Acoustic impedance of perforations in contact with fibrous material. *J Acoust Soc Am*, 119(5):2785, 2006.

[33] W. H. Tan and Z. M. Ripin. Analysis of exhaust muffler with micro-perforated panel. *Journal of Vibroengineering*, 15(2):558–573, 2013.

[34] S. Allam and M. Åbom. A New Type of Muffler Based on Microperforated Tubes. *J Vib Acoust*, 133(3):031005, 2011.

[35] J. S. Bolton and K. Hou. Validation of Micro-Perforated Panels Models. *INTER-NOISE and NOISE-CON Congress and Conference Proceedings*, pages –, January 2008.

[36] S. Allam and M. Åbom. Experimental characterization of acoustic liners with extended reaction. In *Proceedings of 14rh AIAA/CEAS Aeroacoustics Conference, Vancouver, BC, Canada*, 2008.

[37] A. Viswanathan and J. S. Bolton. Study of the effect of grazing flow on the performance of microperforated and perforated panels. In *Proceedings of Noise-con 2013, Devener, Co.*, 2013.

[38] International Organization for Standaridzation (ISO) 3744. Acoustics-determination of sound power levels of noise sources using sound pressure - engineering method in an essentially free field over reflecting plane, 1997.

[39] International Organization for Standaridzation (ISO) 3745. Acoustics-determination of sound power levels and sound energy levels of noise sources using sound pressure - prediction methods for anechoic rooms and hemi-anechoic rooms, 2012.

[40] International Organization for Standaridzation (ISO) 10302-1. Acoustics-measurement of airborne noise emitted and structure-borne vibration induced by small air-moving devices, part 1: Airbone noise measurment, 2011.

[41] MINEBEA DC Axial Fans 4710KL-05W-B50.

[42] E. G. Williams. *Fourier Acoustics: Sound Radiation and Nearfield Acoustical Holography*. Academic Press, 1999.

[43] H. S. Kwon, Y. Niu, and Y. J. Kim. Planar nearfield acoustical holography in moving fluid medium at subsonic and uniform velocity. *J. Acoust. Soc. Am.*, 128(4):1823 – 1832, 2010.

[44] K. U. Ingard. *Notes on sound sbsorption technology*, volume Chap. 2 pp. 2-1 to 2-35. Noise Control Foundation, Paughkeepsie, NY, 1994.

[45] *ABAQUS Documentation, verification guide.*

[46] ASTM E 2611-09. Standard test method for measurement of normal incidence sound transmission of acoustical materials based on the transfer matrix method.

[47] M. L. Munjal. *Acosutics of Ducts and Mufflers*. WILEY, 2014.

[48] *ABAQUS Benchmarks guide, 1.11.8 Acoustic analysis of a duct with mean flow.*

VITA

VITA

Seungkyu Lee was born in Suwon, Republic of Korea. He received his B.S. and M.S. in Mechanical Engineering from Hanyang University in Seoul, Republic of Korea in 2008 and 2010, respectively. He started Ph.D. program in Mechanical Engineering at Purdue University in 2011 and worked as a Research Assistant for Professor J. Stuart Bolton from 2011 to 2015. He received his Ph.D. degree from Purdue University in December 2015. In November 2015, he started his current position at Industrial Business Group of the 3M Company in Maplewood, MN, USA as a Research Acoustics Scientist.